UNIVERSITY OF CALIFORNIA

Santa Barbara

Electrochemical Enzyme Biosensors: Towards Next-Generation Diagnostics

A dissertation submitted in partial satisfaction of the requirements for the degree of Doctor of Philosophy in Biochemistry and Molecular Biology

by

Connor Alan Davis

Committee in charge:

Professor Lior Sepunaru, Co-chair

Professor Kevin Plaxco, Co-chair

Professor Herbert Waite

Professor Arnab Mukherjee

Professor Sebastian Streichan

December 2024

The dissertation of Connor Alan Davis has been approved

Professor Sebastian Streichan

Professor Arnab Mukherjee

Professor Herbert Waite

Professor Kevin Plaxco, Committee Co-Chair

Professor Lior Sepunaru, Committee Co-Chair

September 2024

ACKNOWLEDGEMENTS

There are many people whose support, friendship and love were essential to this journey. To my very first supporters, my family, who have always encouraged my want to know why and always had the highest expectations for me when they asked if I was done with the writing yet, there is never enough thanks.

To the friends who started their PhD journey at the same time as me, who provided an understanding one can only gain by such a shared experience and also many great moments of great company with food, games, exploration and silly kung-fu movies. To Lale, Jorge, Ryan, Devin, Jim, Sujaya - thank you for calming the waters when casting our boats from shore and for being yourselves in moments of both highs and lows.

To my lab mates, thank you for your questions, your discussions, and for your camaraderie. The lab only became a more enjoyable place to be as more and more of you joined. I look forward to seeing your journeys and know you will go far. Thanks for making a great place to ask and tackle any question.

To Lior Sepunaru, the mentor who saw in me much more than I saw in myself. If not for you, my journey would have been cut short. I have far too much to thank you for, but ultimately, thank you for your wisdom, for your genuine care for students, and for your patience and willingness to learn and grow from each student as much as we learn and grow for you.

To Brad, Steph, Luc and Jon, friends who are truly more akin to family, there are too many memories to thank you for, so thank you for making Santa Barbara feel like home, as will be anywhere we see each other in the future.

And finally, I thank Ivana Jordanovska (and Dule!) for unconditional support in all the highs and the lows. For pushing me to travel (and go on much needed walks!), and for reminding me that it's important to not forget to take time to live and be happy. I look forward to having much more opportunities to spend time with my pack.

And to my Grandpa Theron – I made it!

VITA OF CONNOR ALAN DAVIS

EDUCATION

Bachelor of Science in Chemical Engineering 2016
Purdue University

Doctor of Philosophy in Biomolecular Science and Engineering 2024 (Expected)
University of California, Santa Barbara

PROFESSIONAL EMPLOYMENT

Independent Researcher, Chemistry Development Team Jan-May 2021
Laxmi Therapeutic Devices – Goleta, CA

Graduate Teaching Assistant

MCDB 1B, MCDB 110, MCDB 131, CHE 180 Various 2016-2024

PUBLICATIONS

"Electrochemical Investigation of Enzyme Kinetics with an Unmediated, Unmodified Platinum Microelectrode: The Case of Glucose Oxidase" *In Submission*. (2024)

"What can electrochemistry tell us about individual enzymes?" Davis, C.; Wang, S.X.; Sepunaru, L. *Current Opinions in Electrochemistry*, 25(2021) 100643 https://doi.org/10.1016/j.coelec.2020.100643

"Does Nitrate Reductase Play a Role in Silver Nanoparticle Synthesis? Evidence for NADPH as the Sole Reducing Agent", Hiezchold, S.; Walter, A.; Davis, C.; Taylor, A.; Sepunaru, L. *ACS Sustainable Chemistry & Engineering*, 7(9) 2018 – p. 8070-8076

AWARDS

Central Continuing Fellowship 2022
UC Santa Barbara

Independent Project Funding – 2021
Conductive Polymer Enzyme Hybrid Thin-Films for Biosensing proposal
Laxmi Therapeutics

FIELDS OF STUDY

Major Field: Electrochemistry of Redox-Enzymes

Studies in Electroanalytical Descriptions of Enzyme Kinetics with Prof. Lior Sepunaru

Studies in Organic Electrochemical Transistors with Prof. Lior Sepunaru, Prof. Michael Chabinyc and Dr. Leanne Beer – Laxmi Therapeutics

ABSTRACT

Electrochemical Enzyme Biosensors:

Towards Next-Generation Diagnostics

By

Connor Alan Davis

Electrochemical biosensors offer a platform to build miniaturizable and easy to use sensing technology with high levels of accuracy and sensitivity. This has led to applications across many industries, including in the food industry, for environmental monitoring, pharmaceutical production, and healthcare. Though there are a wealth of biomolecules which can provide specificity, enzymatic electrochemical biosensors (EEBs) have thus far proved most commercially successful. The central principle of EEBs is the coupling of the enzyme reaction to a change in redox active species near an electrode which can be electrochemically quantified. The continuous glucose monitor (CGM) is the foundational example of an EEB and has enabled the benefits associated with higher frequency of use and intervention in patients with diabetes. However, as the frontiers of medicine and healthcare, there has been substantial need to improve EEBs – expanding the substrates they interact with, increasing the time for which operation is stable, pursuing lower limits of detection, etc.

In this dissertation, I describe my work which focuses on understanding how the contexts of biosensors – especially including electrode modifying materials towards reaching the needs of next generation medicine- influence the enzyme behavior and how it displays in electrochemical measurements. I first measure the reaction rates of glucose oxidase in solution to determine descriptive thermodynamic and kinetic variables, using a simple system without

using a modified electrode or external mediator via chronoamperometric measurements at a platinum microelectrode. By examining how those variables change with the reaction condition, I delineate a set of guidelines to decouple pure electrochemical effects from changes to enzyme behavior, serving to aid investigations which seek to improve EEBs. Following this, I discuss the current capabilities for electrochemistry to elucidate the behavior of single enzymes, which represents both the ultimate limit of detection in healthcare settings but also a means to further our fundamental understanding of enzymes their behavior in the presence of an electrode. Finally, I will describe some of my efforts to treat enzyme-conductive polymer mixtures as a hybrid material, measuring how the presence of enzyme alters the conductivity of thin-films of PEDOT:PSS and how PEDOT:PSS films influence enzyme kinetics. These measurements are coupled with a discussion of how conductive polymers can play a role in the future of biosensing, highlighting organic electrochemical transistors (OECTs) as transduction method for enzymes at low sensitivity limits. In total, my work aims to further the potential of EEBs in the next generation of medicine, and to provide my insights after much thought and learning about the electrochemistry behind these wonderful systems.

TABLE OF CONTENTS

1.0 Thesis aims and Outline

Aims

The aim of this research is to improve the understanding of enzymatic biosensors by studying the electrochemical response of redox enzyme reactions in several contexts. First, I examined how changes to the electrolyte such as pH and starting reactant concentrations manifested in electrochemical measurements, working to delineate between pure electrochemical influences and actual enzyme kinetic influences. These experiments are representative of the function of modern continuous glucose monitors (CGMs). Follow this, I worked to further study enzyme electrochemistry in contexts relevant to next generations of healthcare, such as at the limits of detection (single entities) and in the presence of conjugated polymer systems, a material that is meant to enhance device performances and enable new signal transduction mechanisms.

2.0 Introduction

Electrochemistry is the field of study which is concerned with the movement of electrical charges and the chemical changes of state which accompany them. An electrochemical biosensor transduces the highly specific chemical or physical interactions between biomolecules and their recognition targets to electronic signals, serving as an analytical means of detection.[1] As it provides an electronic connection to the chemical nature of a system, the evolution of electrochemistry has coincided with the revolutionary developments in the field of electronics.[2,3] Powerful and low-noise electronics, in combination with micro or nanoscale electrodes, has enabled substantial improvements to the limits of detection and range of systems probable by electrochemistry. However, the impact of these improvements has been deep but narrow, being realized in only a very few commercial examples. This is best demonstrated by the stark contrast between the first biosensor, developed in 1962 by Clark and Lyons[4] and several examples of modern continuous glucose sensors shown in **Figure 1**. Though the improved form factor has made continuous monitoring a reality, the technology is still based on analytical electrochemistry developed in the 1980s and hasn't been realized for other clinical targets.[5] As an avenue of introduction to my research, this chapter will cover the motivations for, and current status of, electrochemical biosensors to enable a forward-looking discussion of the capabilities of EEBs.

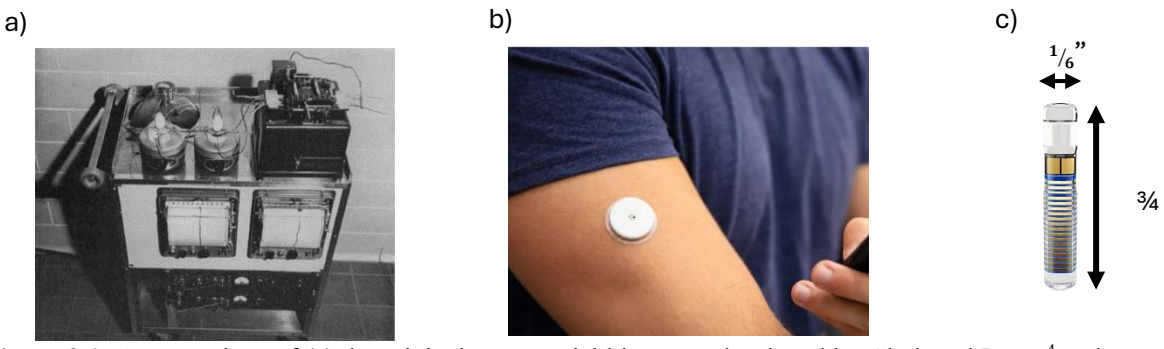

Figure 2.1: A comparison of (a) the original commercial biosensor developed by Clark and Lyons[4] and several examples of modern CGMs, including (b) the on-skin Freestyle Libre3[6] and (c) the implantable Eversense V3[7]

2.1 Motivation – Current Electrochemical Biosensors and Next Generation Health

As a point-of-care device, electrochemical biosensors are able to offer unique advantages in diagnostic applications. The points of comparison for biosensors are “gold standard” clinical methods, which include imaging, polymerase chain reaction (PCR) testing, next generation sequencing, enzyme-linked immunosorbent assays (ELISA), antimicrobial susceptibility testing and lateral flow assays.[8] Many of these methods require skilled users to complete the test and interpretation of the results and may come with hours to days of processing time before results are delivered. In some cases, such as in the diagnosis of bacterial infections, this can be detrimental to patient outcomes; in cases of sepsis, response timeliness is critical for successful intervention[9], yet the estimated portion of missed or delayed diagnosis ranges from 8.2 – 20.8% of cases.[10] In pathogen identification, the lack of rapid diagnostics contributes to current practices which lead to misuse and overprescription of antibiotics[11] – antimicrobial resistant bacteria were the direct cause of 1.27 million deaths in 2019. [12]Conversely, some methods such as lateral flow assays offer much faster time to results, at the cost of higher sensitivity limits or qualitative yes/no detection only. More broadly, given the massive cost of healthcare (of which diagnostics comprise ~10%[13]) and the economic burden on the order of hundreds of

billions of dollars from diagnostic error[14], there is clear need to improve and develop better assays for monitoring human health which are both rapid and quantitative.

In contrast, continuous glucose monitors demonstrate the benefits of electrochemical biosensing for diagnosis in dealing with chronic disease. Diabetes mellitus is a condition induced by sustained high blood sugar levels due to either autoimmune targeting of insulin producing cells (type 1) or poor pancreatic production and cellular insensitivity to insulin (type 2).[15] For the estimated 10.5% of the adult population reported to have diabetes in 2021[16], monitoring blood glucose levels is important for disease management, including for making the decision on when to use insulin. In diabetes management, the use of CGMs enabled increased frequency of glucose monitoring, which is associated with decreased hypoglycemia and increased time in desired glycemic range.[17] These devices are enable by the nature of the electrical signal produced; electrochemical biosensors are both readily miniaturized and easy to use – communication to a digital app allows users to easily understand the measurement.[1] Further, the electrical signal provides instantaneous feedback on the state of the measured system, providing fast results and high time resolution with detection limits rivaling or surpassing other gold standard methods.

Despite the clear need for improved diagnostics and evidence of success of enzymatic electrochemical biosensors in CGMs, further practical application of EEBs has been limited. The next generation of medicine is largely centered around the use of molecular diagnostics – determining health states by monitoring studying the molecular makeup of healthy and diseased tissue. Under this umbrella, personalized and precision medicine seek to incorporate molecular diagnostics to aid in treatment design and monitoring. Further, the collection of this individual data into population health datasets provides a means to improve our understanding

of disease and to move towards preventative and early detection-based diagnosis.[18] This requires a wholistic molecular view of describing disease - incorporating genetic information with other environmental factors (temperature, hydration, etc.) and other molecules determined to be an indicator of disease states termed biomarkers.[19] To meet the needs of diagnostics in healthcare, the goal of my research is to further the capabilities of EEBs. I pursued this goal – through single enzyme electrochemistry and conductive polymer films – will be further addressed in the conclusion of this introduction.

2.2 Enzymes Among Biorecognition Elements in Biosensors

A sensor is typically described as two components – a recognition element (receptor) and a transducer. The transducer element is responsible for conveying the recognition events in a useful/quantifiable output. The recognition element imparts specificity and sensitivity for the target, which are crucial requirements of any chemical sensing method. Many biological functions similarly rely on highly specific and sensitive biochemistry, and thus devices in which biomolecules serve as the receptor element are termed 'biosensors' and have been widely studied and developed to measure target concentrations.[20] **Table 2.1** lists several bioreceptors which have been demonstrated for biosensing in literature.

Given the focus of my work on enzymatic electrochemical sensors, it is important to consider the needs of next generation diagnostics and the advantages and limitations EEBs face in meeting them. One such demand is to increase the time resolution of diagnostic measurements to better assess health states- electrochemical biosensors offer the possibility to achieve this by continuous monitoring.[21] However, a key consideration in achieving this is the nature of the interaction between the receptor and target. In **Table 2.1**, the interactions have been labelled as either chemical or affinity – a chemical interaction is meant to portray that the target is

chemically transformed during the interaction, whereas affinity interactions represent typically more simple binding which is generally non-transformative binding to specific targets.

For biosensors, the means of electrochemical transduction is largely dictated by the type of interaction. For chemical interactions, the transformation of the target can be utilized to drive faradaic (charge transfer) current at an electrode. For affinity interactions, the influences on current are less direct, displaying as either a disruption to access to the electrode surface, or as non-faradaic currents, the latter being compatible with continuous *in vivo* monitoring. These types of interactions are often less sensitive than the transformative interactions, especially if e.g. a small target is captured by an antibody at the electrode surface, or very small additional charge is brought to the electrode surface when few copies of nucleic acids bind to an already covered surface. Electrochemically, this can be described as providing very little change to the impedance experienced at the electrode surface – small additions of insulating materials do not alter current flows as strongly as the presence of transferrable electrons in faradaic interactions. One strategy devised to combat the low sensitivity of affinity interactions is to add a redox probe labelled secondary or sandwich receptor which binds to the receptor/target complex.[1] Ultimately, this transduction strategy is typically not amenable to the *in vivo* and continuous nature of next generation biosensors, as the secondary receptor is typically added to the solution following binding to prevent non-specific signals. Enzyme receptors offer advantages over the other receptors by nature of their chemical interaction with their target and corresponding advantageous transduction method (which will be covered further in **Section 2.3**).

One exception to this rule (noted by a star in **Table 2.1**) are aptamer-based sensors, which utilize short (10s of bases) nucleic acid sequences which have been evolved to change

conformation upon binding to targets.[5] By covalently attaching a redox probe to the electrode bound surface aptamer, target binding can feasibly produce changes in faradaic signal. In fact, electrochemical aptamer-based biosensors (EABs) offer the most direct competition to enzymes as viable diagnostics in next generation medicine; both are amenable to continuous *in vivo* measurements and cover similar target spaces, being primarily suited for small molecule sensing.[22] What, then, separates these two bioreceptors classes? Despite impressive demonstrations, e.g. of real-time tracking of pharmaceuticals in live rat models, EABs have struggled to translate to commercial breakthroughs.[23] This is largely attributed to concerns with stability, both in the attachment to the electrode and of the DNA strand against degradation from *in vivo* sources such as enzymatic cleavage.[24] Conversely, the early success of the enzyme-based glucose monitor is partially attributed to the robustness of the glucose oxidase molecule.[25] Further, biocompatible polymer coatings can be used to mask an enzyme covered electrode[26], while other efforts are required to achieve similar stabilization for EABs[27], owing to the necessity of conformation change in the signal transduction. As academic efforts continue to develop the capabilities of biosensors using both of these receptors, the hope is that both may prove successful for the sake of human health. Due to the demonstrated success of EEBs, the remainder of this work seeks to be part of the effort on the enzyme frontier.

Table 2.1 Recognition Elements in Biosensing

Recognition Element	Target types	Interaction (*= exception to signal transduction restrictions)	Advantages	Challenges
Enzymes	Metabolites (small molecules)	Chemical	Demonstrated commercial success Access to faradaic transduction	Specificity Inhibitors
Nucleic Acids	Hybridization partner	Affinity	High specificity for nucleic acid targets unique	Degradation Sensitivity
Peptides	Peptides	Affinity*	Comparable size to target gives relatively high sensitivity for target More robust than nucleic acids	Stability on surfaces
Aptamers	Metabolites Proteins	Affinity	Evolvable target selection Viable redox labelling strategy for *in vivo* operation	Stability
Antibody Antigen	Antigen (typically proteins or peptides) Antibody	Affinity	Low limit of detection due to high affinity interaction	Poor sensitivity in signal transduction Strong interaction makes reversibility difficult for continuous monitoring *in vivo*
Microorganisms/Cells	Metabolites Antigens	Chemical Affinity	Selectivity may be achieved by natural control of uptake	Requires conditions which maintain viability Large size

2.3 Operating Principles of Electrochemical Enzymatic Biosensors

As mentioned in the previous section, enzymatic electrochemical biosensors are relatively unique among available receptors in part due to their capabilities to drive faradaic current by chemically transforming their target. This has been valuable both in diagnostic monitoring, but also in probing fundamental biological behaviors, but is limited to cases where the chemical transformations can be coupled to electrode reactions in some manner. Here, the operation of an EEB will be elaborated for context when considering their place in future diagnostic devices. **Section 2.4** will further detail how the concentration of the target can be understood from the electrochemical signal.

Of primary importance, EEBs require an enzyme which catalyze a reaction that includes charge transfer with the target of interest – so called oxidation and reduction ("redox") reactions. Due to the importance of this type of reaction in the biochemistry of life, an entire family of enzymes known as oxidoreductases have been categorized. Though just one of seven classes of enzymes recognized by the *International Union of Biochemistry and Molecular Biology*, oxidoreductases account for nearly a third (1995 of 6843) of catalogued enzymes.[28] To facilitate the redox reaction with its target, most oxidoreductases feature either metal atoms or a select number of other moieties as a cofactor in their active site.[29,30] The presence and concentration of the target can therefore be confirmed by conveying the turnover of the active site cofactor to the electrode.

The operation of EEBs can be classified into three groups, often called "generations", based upon how the enzyme reaction is transduced electrochemically (shown in **Scheme 2.1**). First generation sensors require that either the target or reaction product are redox active. The 1st generation sensors arose with the original proposal to monitor O_2 concentrations in patient's

blood by using glucose oxidase from Clark and Lyons in 1962, later commercialized by Yellow Spring Instruments in 1975. This generation is also useful in the detection of neurotransmitters, where the targets such as ascorbic acid, acetylcholine or dopamine are redox active in an accessible potential range.[31] Second generation sensors expanded upon the first by introducing an exogenous redox active species with the responsibility of transducing the chemical reaction. This affords the ability to control the concentration of the secondary reactant, as well as to select species with favorable redox chemistry. Though first conceived as a solution-based mediator, this class has expanded to include mediators which are immobilized at the electrode as well. Many of the modern CGMs are of this generation of sensor. Finally, third generation sensors use direct communication between the enzyme's active site and the electrode surface, known as direct electron transfer (DET). This form of transduction is most desirable for biosensing applications, as it removes complications arising from the secondary reactant. Third generation sensors are also the key feature of the field of study known as protein film voltammetry, which enabled direct measurement of the thermodynamic properties of the active site in enzymes.[32] However, this generation of sensor is rare, as electrical coupling falls off greatly with distances greater than 20 Å[33], requiring the enzyme to either have an active site near the edge of the protein shell, or to have a means of relaying the charge through electron transfer centers.[34] While these features are more common among enzymes of certain functions, such as in photosynthesis or in the electron transport chain, where the passage of energetic electrons is a crucial component of the encompassing function, only ~100 oxidoreductases have been determined to be capable of DET.[35]

As a model system for analysis, **Chapter 3** features a first-generation sensor system to highlight the effects of reaction conditions on the enzyme and how those propagate to

electrochemical signals. **Chapters 4** features 1st and 2nd generation systems, though some of the techniques are amenable for any generation. The efforts of others in attempting to provide means to generally engineer oxidoreductases for 3rd generation functionality will hopefully prove successful to the benefit of sensors for next-generation diagnostics and medicine.

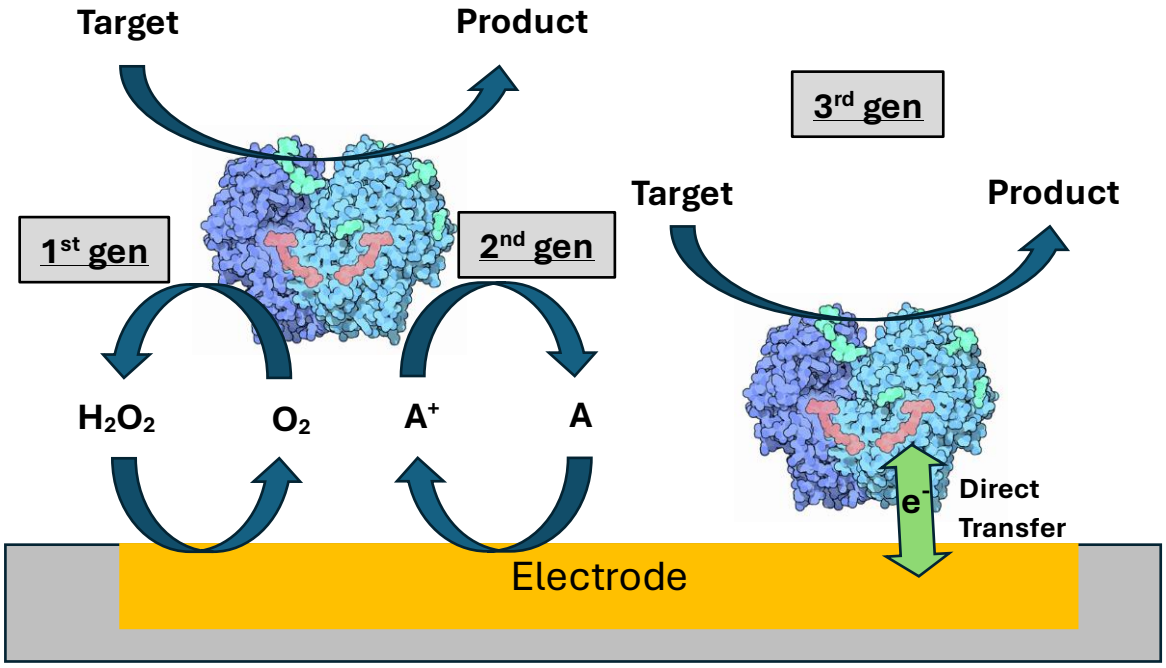

Scheme 2.1: **Generations of enzymatic electrochemical biosensors.** 1st generation sensors utilize a redox active target or product – shown in this example is oxygen and hydrogen peroxide, both of which have been used for glucose sensing using glucose oxidase. 2nd generation sensors follow the same concept as first generation sensors but introduce an exogenous redox mediator, usually to provide benefits such as higher concentrations (to enable faster reactions) and more favorable charge transfer behavior. 3rd generation sensors are considered the most desirable for biosensing, as it removes any complications associated with the second reaction by substituting it with direct electron transfer with the electrode. However, DET capable enzymes are rare, making this a tough method to regularly implement.

2.4 Electroanalytical Methods for EEBs

The purpose of the electrochemical method is to extract concentrations from measured electrical signals, i.e. that it is analytical. Because the rate of reaction at the electrode surface (and accordingly, the current) is dependent on the concentration of the species, this goal can be achieved via a few methods. Most simply, calibration curves are often determined to empirically link the concentration of the analyte and measured electrical signals under a limited range of conditions. However, closed-form solutions of general theoretical cases also exist to aid the extraction of the concentration from electrochemical measurements[36–39]. Substantial effort has been focused on either prevention or recalibration of drifting signals, which may arise during *in vivo* measurements due to biofouling, sensor degradation, or changes to the reaction environment (see **sections 3.3.2 and 3.3.3** for example), and will hamper accurate assessment of the target concentration regardless of the electrochemical method selected.

Electrochemical methods are most readily divided into potentiodynamic and potentiostatic, depending on whether the potential applied to the working electrode is held constant during a measurement. The most widely employed techniques for EEBs are cyclic voltammetry and amperometry[3] respectively. However, the last decade has also seen a significant rise in the use of sinusoidal current or potential-based ('AC') techniques, such as square-wave voltammetry (for EAB sensors especially[40]) and electrochemical impedance spectroscopy (EIS)[41]. Outside of their ability to diagnose kinetic processes on different timescales, the practical benefit of AC methods is the ability to select frequencies which minimize undesirable factors such as drift and noise. However, use of these methods places additional demands on the circuitry and power consumption of biosensing devices and may better serve as a method to surveil the "health" of the electrode in biosensors.[42]

Due to the heterogeneous nature of the electrochemical reactions (i.e. surface reactions at the electrode interface), mass transfer plays a significant role in the rates of reaction, and thereby the observed currents. Due to the benefits provided in terms of mass transfer, the use of electrodes with dimensions on the microscale (aka microelectrodes) are an important underlying part of EEBs and electrochemical sensors in general. As shown in **Figure 2.2**, the flux to a microelectrode is largely radial in character, owing both to the fact that the edge to area ratio is relatively high, and that the volume near the electrode in which the redox active species is depleted expands hemi-spherically around the electrode surface. This stands in contrast to the macroelectrode, in which the non-linear flux at the electrode edge is essentially insignificant.

In practice, the use of microelectrodes in EEBs is not only important for practical, functional reasons (minimizing pain, enabling placement into and localized measurement of tissues), but also for achieving the goals of the measurement. Phenomenologically, the superior mass transport to a microelectrode provides two major advantages – 1) the ability to rapidly respond to changes in the environment and 2) easier to interpret, steady-state current responses in both potentiostatic and dynamic measurements.[43] The second feature is highlighted in **Section 2.4.1** below in the theoretical cyclic voltammograms (CVs) shown in **Figure 2.2**, where the microelectrode CV shows a constant value regardless of overpotential (resulting in the "S") shape, as compared to the macroelectrode CV, which shows decreasing current with over potential (the classic "duck" shape). Though the solutions below discuss the classical disk electrode, the circular rod profile of wire electrodes used in several CGMs and other biosensors also benefit from similar non-linear mass transport effects.

2.4.1 Cyclic voltammetry

Cyclic voltammetry is a key electrochemical method, as scanning through voltage ensures an understanding of the redox active agent's formal potential – the voltage at which a redox species is equally likely to undergo forwards and backwards redox transformation for a certain reaction condition. An accurate understanding of the formal potential of a system is essential to ensure proper operation of potentiostatic techniques – application of an overpotential ensures maximal signal generation and operation in conditions which are theoretically described. Further, when the redox species measured by CV is the active site of an enzyme, thermodynamic information on the cofactor is directly obtained.[32]

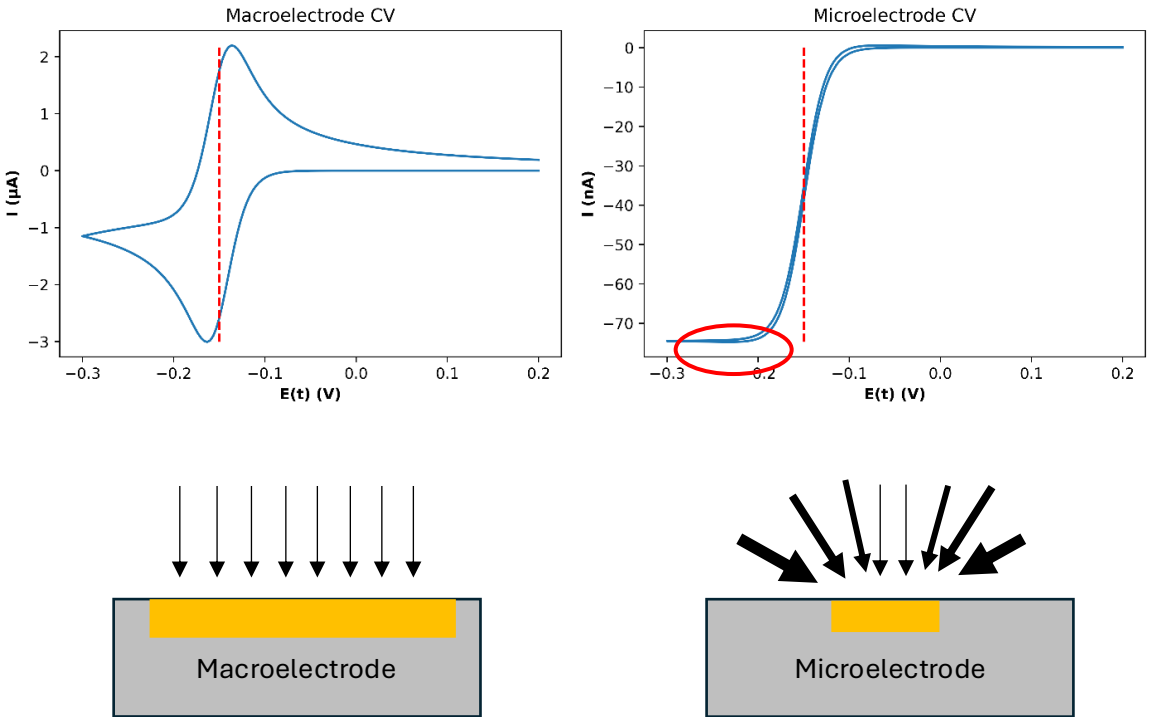

Figure 2.2 A comparison of the flux (arrows) to the surface of A) a macro or B) a microelectrode, showing the relative radial character is higher at the microelectrode. Accompanying, simulated CVs for 50 mM of a redox species at the corresponding electrodes. Vertical red dashed lines indicate the formal potential, while the circled region shows the steady state nature achieved at the microelectrode.

By nature of being a potentiodynamic technique, cyclic voltammetry offers the ability to extract some time-dependent information through altering the potential. By changing the rate at which potential is scanned (applying different "scan rates"), it is possible to determine some kinetic rate constants based upon changes in the CV response, such as for coupled chemical reactions.[44] However, the extraction of such information can be quite challenging, especially with regards to enzymatic reactions, as even the textbook examples require determination of a "kinetic-zone" space and non-trivial mathematics which vary depending on which zone the device is operating under.[44] This is because the scan rate presents an additional time constant to consider in comparison to mass transfer and homogeneous reactions. It is possible to understand the speed at which other processes occur in the reaction solution by raising or lowering the scan rate past the rate of the other processes of interest. However, an accurate assessment of how scanning the potential contributes to the measured current is required to accurately understand the kinetics of the other processes. Due to these challenges, amperometry remains the preferred electrochemical method for EEBs.[45]

2.4.2 Chronoamperometry

Chronoamperometry is potentiostatic method, measuring the current over time resulting at an electrode when applying a fixed potential with a redox active species in solution. A straightforward sensors is then achieved when the redox reaction involves a species whose concentration is in some way related to the analyte of interest. This section will introduce the classical solution to the one electron diffusion-reaction problem, which in the long-time limit, approximates to a steady state value in many conditions which are commonly designed for in biosensors. However, it is also possible to choose a set of conditions under which the current

is non-steady state but instead is a (linear) function of the enzyme's kinetics, which is the main method used in **Chapter 3**.

2.4.3 Model Amperometry Solution – Potential Step Response

For a general redox reaction, as in *Eq. 1* below, it is assumed that sufficient potential is applied such that the rate of reaction at the electrode surface is limited by mass transfer to the electrode surface.

$$O + ne^- \leftrightarrow R \qquad \textit{Eq. 1}$$

Assuming no convection of the solution, the convection-diffusion equation simplifies to Fick's second law, enabling a description of the spatial concentration profile with time (*Eq. 2* below)

$$\frac{\partial C_o(x,t)}{\partial t} = D_o \frac{\partial^2 C_o(x,t)}{\partial x^2} \qquad \textit{Eq. 2}$$

Some sensible assumptions can be made about the system to construct boundary conditions. Classically, they include: the solution is homogeneous prior to application of the potential (E*q. 3*), a semi-infinite boundary at the bulk (E*q. 4*), and that the surface concentration is zero for all non-zero times (*Eq. 5*)

$$C_o(x,0) = C_o^* \qquad \textit{Eq. 3}$$

$$\lim_{x\to\infty} C_o(x,t) = C_o^* \qquad \textit{Eq. 4}$$

$$C_o(0,t) = 0 \qquad \text{for (t >0)} \qquad \textit{Eq. 5}$$

Deriving the concentration profiles in time is ultimately important due to the fundamental relationship between current and flux at the electrode surface. This concept is represented mathematically by *Eq. 6* below and is the bedrock upon which electrochemical theory is built. This core concept stated by is *Eq.*6 is that the current density (J_0) is linked to the rate of reaction at the electrode surface ($\frac{i(t)}{nFA}$) by the flux of species to the surface ($D_o \left[\frac{\partial C_o(x,t)}{\partial x}\right]_{x=0}$).By plugging

the boundary conditions into Fick's second law which describes the flux, the necessary concentration profile can be analytically represented, allowing for the determination of current as a function of time.

$$-J_o(0,t) = \frac{i(t)}{nFA} = D_o\left[\frac{\partial C_o(x,t)}{\partial x}\right]_{x=0} \qquad Eq.\ 6$$

The solution presented in *Eq. 7* below is the classical current-concentration relationship known as the Cottrell equation. Of importance to note is the inverse relationship to the square root of time, indicating that at the infinite limit, the current will trend to zero. This is understood as arising from an ever-increasing diffusion layer, in which the concentration of the active species is depleted. Importantly, the nature and propagation of the concentration profile is dependent on the geometry of the electrode surface. The Cottrell equation considers a planar electrode, such that all diffusion is linear toward the electrode surface. In the model case of a spherical or hemi-spherical electrode, the current instead converges to a steady state value, matching the steady state current achieved by cyclic voltammetry at a microelectrode (note the lack of time dependence in *Eq. 8* below) owing to the spherical diffusion achieved with these systems behaving similarly to the hemispherical electrode, as shown in **Figure 2.2**.

$$i(t) = \frac{nFAD_O^{1/2}C_o^*}{\pi^{1/2}t^{1/2}} \quad \text{[planar]} \qquad Eq.\ 7$$

$$i(t) = 4\pi r_e DFC_o^* \quad \text{[spherical – long time limit]} \qquad Eq.\ 8$$

Figure 2.3 below shows a model chronoamperometric response of a microdisk electrode, which demonstrates a few further key features of the method: 1) the concentration dependence of the target of the measured current, 2) the initial non-steady state response, which is followed by 3) either a continually decreasing response associated with a macroelectrode OR reaching

steady state at the longer time limit associated with a microelectrode. The first feature is associated with non-faradaic currents arising from the application of a potential, followed by a more slowly decreasing region which occurs as the diffusion profile around the electrode moves towards steady state. Importantly, this feature does not contribute to continuous electrochemical measurements for EEBs after the measurement "settles" following initiation. This theoretical description of microelectrode behavior is foundational to understanding the responses observed in EEBs.

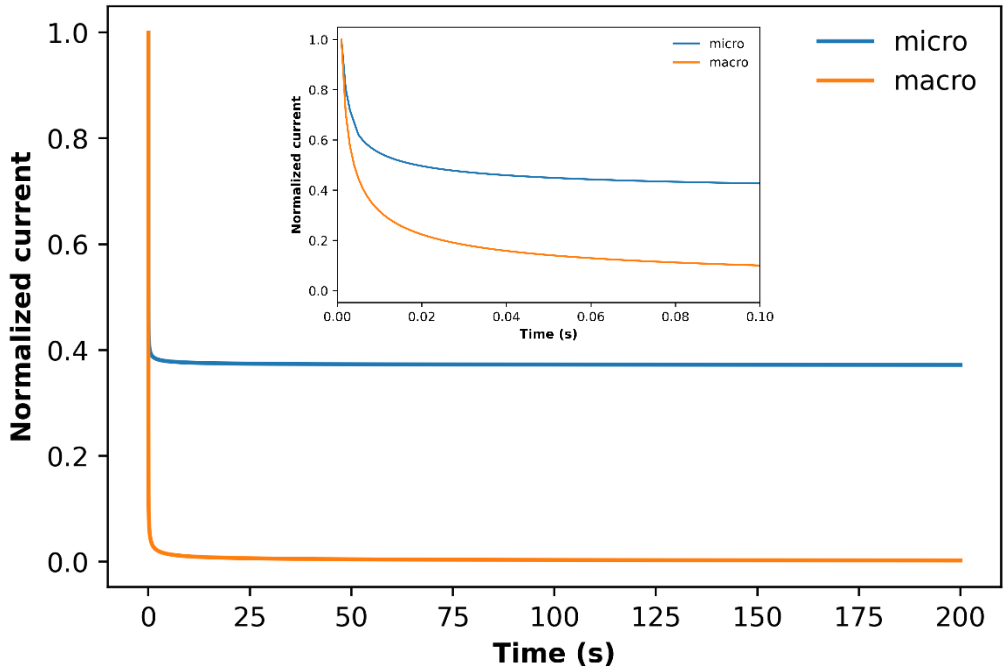

Figure 2.3 A comparison of normalized current for the theoretical response for a potential step chronoamperogram at a micro and macroelectrode disk electrode. The graph highlights the non-zero steady state current achieved at the microelectrode. The inset highlights the very initial response, where the non-faradaic and concentration profile phenomenon are the major drivers of the observed current.

2.5 Conclusion and Outlook on EEBs and Next Generation Diagnostics

Despite the clear need for improved diagnostics and evidence of success of enzymatic electrochemical biosensors in CGMs, further practical application of EEBs has been limited. In considering how EEBs can contribute to the next generation of molecular diagnostics, it is important to delineate the challenges that must be overcome and to review the methods by which research aims to meet them.

The first major initiative of next-generation medicine is to expand the use of genetic markers to understand and treat disease. In this arena, EEBs as a class are not well suited, due to the inability to determine the nucleic acid sequence as well as the challenge of, and lack of established need for reading genetic information in a continuous manner. Other methods, such as next generation sequencing, or even other electrochemical methods, such as nanopore sequencing, are already established and capable of meeting the needs of next generation medicine in this capacity.[46]

Outside of the genetic component of precision medicine, lifestyle, environmental factors and biomarkers are also incorporated into diagnosis. Electrochemical and spectroscopic methods have been developed which cover aspects of lifestyle and environmental factors – many smart devices are already capable of monitoring variables such as step counts, temperature, hydration levels, O_2 levels, etc. It is in the final diagnostic class, biomarkers, in which EEBs are suited to significantly contribute. A biomarker is any biological molecule which can be associated with the normality of biological function, or specifically associated with a condition or disease[47] – this include several types of molecules (such as RNAs, proteins, etc.) which are better suited to other receptors found in **Table 1.** There exist several categories of low-

molecular-weight biomarkers[48], including reactive oxygen and nitrogen species, volatile organic compounds, amino acid, fatty acids, carbohydrates, vitamins for some of which oxidoreductases exist towards EEB construction. In the absence of a known enzyme, genome mining and protein engineering strategies can be used to find or develop amenable enzymes for the task.[49] Biomarkers from these categories have been associated with a myriad of diseases, covering cardiovascular and neurological diseases[50], infections, cancer, arthritis and even aging.[48] Here arises the use-case of continuous monitoring in molecular diagnostics; some biomarkers are known to continually fluctuate, such as the stress hormone cortisol, and these fluctuations may be associated with ascribing disease states.[51]

In addition to the foundational need of specificity, sensitivity is another essential feature of biosensors. Continual monitoring sensors measure "non-invasive" biological media, such as sweat, tears, and interstitial fluids, to allow for longer term use of the device. Though the small molecules targets of interest for EEBs are often able to cross many biological barriers to enter these media, the resulting concentrations of the target are often much lower than in the blood or tissue of interest.[48] Additionally, an important aim of next-generation medicine is to utilize precision medicine to enable early diagnostic and prognostic screening – in this capacity, biomarkers will further tend to be in lower concentrations than in later stages of disease. When considering how EEBs can contribute to next-generation diagnostics, it's important to note that such low sensitivity is not a challenge faced by CGMs – blood glucose levels are in the 100s of micromolar to millimolar range, from which relatively large currents can be measured in biosensors.

The scope of this thesis is largely in response to this later point, examining the potential for electrochemical enzyme biosensors to operate at low concentrations relevant to precision

medicine and molecular diagnostics. **Chapter 3** covers the electrochemical response of nanomolar concentrations of glucose oxidase to examine how enzyme kinetics is influenced by reaction conditions and the electrochemical measurement. Following this, two means of addressing the sensitivity limits of EEBs are then discussed – **Chapter 4** deals with the capabilities of electrochemistry to detect singular enzyme activity, representing the ultimate limit for the receptor capabilities, and **Chapter 5** discusses conductive polymer-enzyme hybrids as a nanomaterial to enable more sensitive electrochemical measurements as well as the OECT as a potential mechanism to push the success of EEBs.

2.6 References for Chapter 2

1. Wu, J., Liu, H., Chen, W., Ma, B. & Ju, H. Device integration of electrochemical biosensors. *Nature Reviews Bioengineering* **1**, 346–360 (2023).

2. Shacham-Diamand, Y. Electrochemistry and Microelectronics, Perspective and Prospective. *Isr J Chem* **61**, 51–59 (2021).

3. Baracu, A. M. & Dinu Gugoasa, L. A. Review—Recent Advances in Microfabrication, Design and Applications of Amperometric Sensors and Biosensors. *J Electrochem Soc* **168**, 037503 (2021).

4. Clark, L. C. & Lyons, C. Electrode Systems For Continuous Monitoring In Cardiovascular Surgery. *Ann N Y Acad Sci* **102**, 29–45 (1962).

5. Sezgintürk, M. K. Introduction to commercial biosensors. in *Commercial Biosensors and Their Applications* 1–28 (Elsevier, 2020). doi:10.1016/B978-0-12-818592-6.00001-3.

6. Abbott. FreeStyle Libre 3 System: Designed with you in mind. *https://www.freestyle.abbott/us-en/products/freestyle-libre-3.html* (2024).

7. Ascensia & Senseonics. EverSense E3 Continuous Glucose Monitoring System. *https://www.eversensecgm.com/eversense-e3/* (2024).

8. Brazaca, L. C. & Sempionatto, J. R. The application of biosensors in precision medicine. in *Biosensors in Precision Medicine* 133–162 (Elsevier, 2024). doi:10.1016/B978-0-443-15380-8.00006-0.

9. Husabø, G. *et al.* Early diagnosis of sepsis in emergency departments, time to treatment, and association with mortality: An observational study. *PLoS One* **15**, e0227652 (2020).

10. Neilson, H. K. *et al.* Diagnostic Delays in Sepsis: Lessons Learned From a Retrospective Study of Canadian Medico-Legal Claims. *Crit Care Explor* **5**, e0841 (2023).

11. Avershina, E., Khezri, A. & Ahmad, R. Clinical Diagnostics of Bacterial Infections and Their Resistance to Antibiotics—Current State and Whole Genome Sequencing Implementation Perspectives. *Antibiotics* **12**, 781 (2023).

12. Murray, C. J. L. *et al.* Global burden of bacterial antimicrobial resistance in 2019: a systematic analysis. *The Lancet* **399**, 629–655 (2022).

13. Newman-Toker, D. E., McDonald, K. M. & Meltzer, D. O. How much diagnostic safety can we afford, and how should we decide? A health economics perspective. *BMJ Qual Saf* **22**, ii11–ii20 (2013).

14. Newman-Toker, D. E. *et al.* Burden of serious harms from diagnostic error in the USA. *BMJ Qual Saf* **33**, 109–120 (2024).

15. Mayo Clinic Staff. Mayo Clinic Diseases & Conditions- Diabetes. *https://www.mayoclinic.org/diseases-conditions/diabetes/symptoms-causes/syc-20371444* (2024).

16. Boyko, E. & Magliano, D. IDF Diabetes Atlas. *10thEd* (2021).

17. Miller, E. M. Using Continuous Glucose Monitoring in Clinical Practice. *Clinical Diabetes* **38**, 429–438 (2020).

18. Biosensors: from personalised medicine to population health. *EBioMedicine* **53**, 102746 (2020).

19. Brazaca, L. C. & Sempionatto, J. R. The application of biosensors in precision medicine. in *Biosensors in Precision Medicine* 133–162 (Elsevier, 2024). doi:10.1016/B978-0-443-15380-8.00006-0.

20. Kim, E. R., Joe, C., Mitchell, R. J. & Gu, M. B. Biosensors for healthcare: current and future perspectives. *Trends Biotechnol* **41**, 374–395 (2023).

21. Ghazizadeh, E., Naseri, Z., Deigner, H.-P., Rahimi, H. & Altintas, Z. Approaches of wearable and implantable biosensor towards of developing in precision medicine. *Front Med (Lausanne)* **11**, (2024).

22. Tan, X. *et al*. Progress in Nanomaterials-Based Enzyme and Aptamer Biosensor for the Detection of Organophosphorus Pesticides. *Crit Rev Anal Chem* **54**, 247–268 (2024).

23. Downs, A. M. & Plaxco, K. W. Real-Time, In Vivo Molecular Monitoring Using Electrochemical Aptamer Based Sensors: Opportunities and Challenges. *ACS Sens* **7**, 2823–2832 (2022).

24. Shaver, A. & Arroyo-Currás, N. The challenge of long-term stability for nucleic acid-based electrochemical sensors. *Curr Opin Electrochem* **32**, 100902 (2022).

25. Bauer, J. A., Zámocká, M., Majtán, J. & Bauerová-Hlinková, V. Glucose Oxidase, an Enzyme "Ferrari": Its Structure, Function, Production and Properties in the Light of Various Industrial and Biotechnological Applications. *Biomolecules* **12**, 472 (2022).

26. Ramanaviciene, A. & Plikusiene, I. Polymers in Sensor and Biosensor Design. *Polymers (Basel)* **13**, 917 (2021).

27. E. Wang, R., Wu, H., Niu, Y. & Cai, J. Improving the Stability of Aptamers by Chemical Modification. *Curr Med Chem* **18**, 4126–4138 (2011).

28. International Union of Biochemistry and Molecular Biology. *ExploreEnz: Enzyme Count*. (2024).

29. Hay Mele, B. *et al.* Oxidoreductases and metal cofactors in the functioning of the earth. *Essays Biochem* **67**, 653–670 (2023).

30. May, S. W. & Padgette, S. R. Oxidoreductase Enzymes in Biotechnology: Current Status and Future Potential. *Nat Biotechnol* **1**, 677–686 (1983).

31. Choi, H. K., Choi, J.-H. & Yoon, J. An Updated Review on Electrochemical Nanobiosensors for Neurotransmitter Detection. *Biosensors (Basel)* **13**, 892 (2023).

32. Armstrong, F. A. Some fundamental insights into biological redox catalysis from the electrochemical characteristics of enzymes attached directly to electrodes. *Electrochim Acta* **390**, 138836 (2021).

33. Winkler, J. R. & Gray, H. B. Electron Flow through Metalloproteins. *Chem Rev* **114**, 3369–3380 (2014).

34. Butt, J. N. *et al*. Voltammetric characterization of rapid and reversible binding of an exogenous thiolate ligand at a [4Fe-4S] cluster in ferredoxin III from Desulfovibrio africanus. *J Am Chem Soc* **115**, 1413–1421 (1993).

35. Shleev, S. *et al*. Oxygen Electroreduction versus Bioelectroreduction: Direct Electron Transfer Approach. *Electroanalysis* **28**, 2270–2287 (2016).

36. Rajendran, L. & Saravanakumar, K. Analytical expression of transient and steady-state catalytic current of mediated bioelectrocatalysis. *Electrochim Acta* **147**, 678–687 (2014).

37. Molina, Á., González, J., Laborda, E., Henstridge, M. C. & Compton, R. G. The transient and stationary behaviour of first-order catalytic mechanisms at disc and hemisphere electrodes. *Electrochim Acta* **56**, 7404–7410 (2011).

38. Galceran, J., Taylor, S. L. & Bartlett, P. N. Modelling the steady-state current at the inlaid disc microelectrode for homogeneous mediated enzyme catalysed reactions. *Journal of Electroanalytical Chemistry* **506**, 65–81 (2001).

39. Molina, Á., Martínez-Ortiz, F. & Laborda, E. Rigorous Analytical Solution for EC Mechanism in Normal Pulse Voltammetry at Spherical Electrodes and Microelectrodes. *Int J Electrochem Sci* **4**, 1395–1406 (2009).

40. Verrinder, E., Leung, K. K., Erdal, M. K., Sepunaru, L. & Plaxco, K. W. Comparison of voltammetric methods used in the interrogation of electrochemical aptamer-based sensors. *Sensors & Diagnostics* **3**, 95–103 (2024).

41. Magar, H. S., Hassan, R. Y. A. & Mulchandani, A. Electrochemical Impedance Spectroscopy (EIS): Principles, Construction, and Biosensing Applications. *Sensors* **21**, 6578 (2021).

42. Sharma, H. *et al*. Multimodal Simultaneous Amperometry and Electrochemical Impedance Spectroscopy Measurement for Biosensing Applications. in *2022 IEEE 19th India Council International Conference (INDICON)* 1–5 (IEEE, 2022). doi:10.1109/INDICON56171.2022.10040164.

43. Forster, R. J. Microelectrodes: new dimensions in electrochemistry. *Chem Soc Rev* **23**, 289 (1994).

44. Savéant, J. & Costentin, C. *Elements of Molecular and Biomolecular Electrochemistry*. (Wiley, 2019). doi:10.1002/9781119292364.

45. Xiao, X. & Ulstrup, J. Towards continuous potentiometric enzymatic biosensors. *Curr Opin Electrochem* **46**, 101549 (2024).

46. Morash, M., Mitchell, H., Beltran, H., Elemento, O. & Pathak, J. The Role of Next-Generation Sequencing in Precision Medicine: A Review of Outcomes in Oncology. *J Pers Med* **8**, 30 (2018).

47. National Cancer Institute: Biomarker. *https://www.cancer.gov/publications/dictionaries/cancer-terms/def/biomarker*.

48. Mollarasouli, F. & Bahrani, S. Low-molecular-weight biomarkers: types and detection strategies. in *The Detection of Biomarkers* 23–69 (Elsevier, 2022). doi:10.1016/B978-0-12-822859-3.00012-2.

49. Zhu, Z., Song, H., Wang, Y. & Zhang, Y.-H. P. Protein engineering for electrochemical biosensors. *Curr Opin Biotechnol* **76**, 102751 (2022).

50. Franco, R., Reyes-Resina, I. & Navarro, G. Dopamine in Health and Disease: Much More Than a Neurotransmitter. *Biomedicines* **9**, 109 (2021).

51. Qiu, S. *et al*. Small molecule metabolites: discovery of biomarkers and therapeutic targets. *Signal Transduct Target Ther* **8**, 132 (2023).

3. Determining Enzyme Kinetics Using an Unmodified, Unmediated Microelectrode – Electrochemical vs Enzymatic Influences of Reaction Conditions

3.1 Introduction

Studying enzyme kinetics is a central pillar of enzymology. Measuring the physical parameters that control enzymatic biochemical processes helps unravel how nature "designs" catalysts to accelerate reactions.[1–3] Quantitative analysis of the enzyme-substrate (and product) equilibrium constants and maximum reaction rates provides insight into the catalytic mechanism that places a functional context on the spatial structure of the enzyme. Furthermore, mechanistic insights enable strategies to alter or control their biochemical reaction(s), which is advantageous for various applications in bioengineering and biotechnology, such as the food industry[4,5], biomedical devices[6], pharmaceuticals[7], and biofuels.[8,9] The standard methods for studying enzyme kinetics are based on optical[10], magnetic resonance and nuclear imaging methods[11], mass spectrometry[12], and microdialysis.[13] On the other hand, electrochemistry is less commonly used.[14] Although the family of enzymes which perform redox reactions (the oxidoreductases) is large, significant design/complications accompany extending electrochemistry as an analytical method to members of the other classes. Additionally, electrochemistry is certainly competitive in terms of sensitivity (especially in concentrations relevant to enzyme behavior), specificity and electrode fouling are critical concerns in complex environments. Finally, the signal for readout being collected via heterogeneous reaction at the electrode requires accounting for mass transport and additional reaction kinetics in analytical analyses.[15] Nonetheless, methods developed by the electrochemical community have significantly addressed these points of contention, which can offer unique insights/advantages.[16–21]

The most common method to study enzyme catalysis via electrochemistry is through confinement to the electrode surface, also known as protein film voltammetry. Through electronic coupling to the enzyme's accessible active site(s), the potential applied to the working electrode uniquely offers a continuous and tunable driving force with which to measure the thermodynamic redox potential of the catalytic enzymatic center.[22,23] Resulting currents in the presence of substrate can be used to determine the thermodynamic parameter K_M and the kinetic parameter V_{max}.[24,25] In the absence of direct electron transfer, binding enzymes to the electrode surface can additionally enable methods to alter and therefore analyze mass transport, such as through use of a rotating electrode or other means of convection. The technique is also valuable for technological applications as it offers the possibility to create reusable and easily separable enzyme systems which require a relatively small amount of protein.[26,27] However, the method requires specific immobilization techniques and is limited to enzymes that maintain activity following the stress-inducing process of immobilization to a solid surface.[28–30] Further, immobilization may alter the enzyme's intrinsic kinetics[15,31-33] or even substrate scope.[34]

Another electrochemical approach uses mediators that exchange charge with the electrode surface and the diffusing enzyme's interior catalytic site. This way, the enzyme is retained in solution in its native state, and the mediator serves as a means to transduce the enzymatic redox event. This strategy facilitated the development of glucose sensors and is still commonly used as a basic architecture for second-generation electrochemical biosensor design.[35-38] The mediator scheme can provide an electron transport agent superior to the endogenous substrate (via comparatively better heterogeneous kinetics and/or by requiring lower overpotentials) and control over the rate-limiting reaction step by altering the mediator concentration.[25] Although

advantageous, the mediated scheme is more commonly applied for biosensing applications rather than analytical thermo-kinetics studies. Importantly, one must ensure that the mediator does not alter or obscure the behavior of the enzymatic chemical step of interest.[39] As a critical example, a series of electron mediators showed varying current responses with glucose oxidase in differing pHs[40], a mode of analysis which shows the complex transition of the rate-limiting step when undertaken with dioxygen as the endogenous mediator.[41]

In this work, we study the kinetics of freely diffusing glucose oxidase (GOx) enzymes using unmodified, commercially-available microelectrodes without using artificial mediators. The radial diffusion to the microelectrode enables amperometric measurements that produce a monotonic increase in current that corresponds to the accumulated enzymatic activity in the bulk solution, using nanomolar concentrations of enzyme. We contrast our kinetics and thermodynamics investigation with conventional mediated UV-Vis spectroscopy and show that the level of analytical precision is comparable. The method's strength is further emphasized once oxygen concentration is varied within the enzymatic sample. The ability to measure the oxygen concentration with the same instrumentation at any given time enables the kinetic analysis to incorporate effects arising from the secondary oxygen substrate. Further, the micro-voltammetry platform highlights the necessity of the ping-pong mechanism for describing the enzymatic reaction, commonly not implemented in glucose oxidase kinetics analysis as the *sine qua non* for mechanistic investigation.

3.2 Methods

- Chemicals:

Buffer components including Tris base, potassium chloride (KCl), sodium chloride (NaCl), Potassium phosphate monobasic (KH_2PO_4) and sodium phosphate dibasic (Na_2HPO_4), acetic acid (glacial), sodium acetate (CH_3COONa), D-glucose, 2,2′-Azino-bis(3-ethylbenzothiazoline-6-sulfonic acid) diammonium salt (ABTS as 10mg tablets) and hydrogen peroxide were purchased from Sigma Aldrich (St. Louis, MO). Enzymes including peroxidase from horseradish (Type VI, essentially salt-free, lyophilized powder, ≥250 units/mg solid) and glucose oxidase from *Aspergillus niger* (Type VII, lyophilized powder, ≥100,000 units/g solid) were also purchased from Sigma Aldrich and used as received. No contaminant catalase activity was detected by overnight incubation in 10 mM hydrogen peroxide. Solutions were created using deionized water (resistivity ≥ 18.2 MΩ). All chemicals were used as received. Glucose oxidase solutions were made fresh and kept on ice for the duration of experiments (up to a few hours). To minimize the dilution of oxygen (when added), 200 μL of GOx solution was added to a final volume of 4 mL of working solution in all electrochemical experiments. Solutions were magnetically stirred for 5 seconds at 300 rpm following the addition of GOx.

- Electrochemistry:

Experiments were performed in 1x phosphate-buffered saline (PBS) at pH 7.4- 137 mM NaCl, 2.7 mM KCl, 10 mM Na_2HPO_4, and 1.8 mM KH_2PO_4 - unless otherwise stated. For experiments with varied pH outside the buffering range of PBS, 10 mM acetate buffer and 10 mM Tris base were used – with adjustments made by KOH or H_2SO_4 as necessary. No changes in bulk pH were observed after completion of any measurement. When adding oxygen to the

solution, O_2 gas was sparged through a bubbler for at least 15 minutes to achieve saturation. Oxygen concentration was monitored by measuring reductive current directly before measuring GOx activity.

A three-electrode electrochemical cell was constructed with a 10 μm diameter platinum microelectrode (BASi MF-2005) as the working electrode, a platinum wire (CHI #115) as the counter, and a saturated calomel electrode (CHI #101) as the reference electrode. Experiments were measured inside a Faraday cage and controlled using a BioLogic SP300, including an ultra-low-current module. All potentials are referenced against SCE. The working electrode was mechanically polished with 1-, 0.3-, and 0.05-micron alumina oxide slurry and rinsed with DI H_2O. To achieve a consistent electrode surface, an oxidative treatment at 0.55 V in 150 μM H_2O_2 in 1xPBS was performed for 30 minutes after polishing (further discussed in **SI Section S3.7.1A**). The counter electrode was flame annealed for ~5 seconds prior to use. The current measured at the working electrode did not appreciably change between runs, and thus the working electrode was not polished between experiments to maintain the same surface roughness within sets of either glucose or GOx concentrations. The electrically active area of the electrode was determined electrochemically with ruthenium hexaamine and the diffusion coefficient of H_2O_2 was determined by analysis using the Randles–Sevcik equation through cyclic voltammetry (**Fig. S3.7.1B and C**). The diffusion coefficient of H_2O_2 to be 1.21 ± 0.08 x 10^{-5} cm^2/s. This is largely in agreement with other reports which have electrochemically determined the diffusion coefficient ranging from 0.8-1.6 x 10^{-5} cm^2/s.[42,43]

- Spectroscopy:

UV-Vis spectroscopy was done using a Shimadzu 1800 photo spectrometer. For electrochemical standards, H_2O_2 concentration was verified using absorbance at 240 nm with an extinction coefficient of ε_{240} = 43.6 $M^{-1}cm^{-1}$.[44] For UV-Vis based enzyme kinetics, final concentrations of 2,2′-Azino-bis(3-ethylbenzothiazoline-6-sulfonic acid) diammonium salt (ABTS) and horseradish peroxidase were ~87 μM and ~750 nM respectively. Briefly, horseradish peroxidase is used to couple H_2O_2 production to oxidation of ABTS to $ABTS^{\bullet+}$, which displays a shifted absorption peak centered around 400 nm and increased absorption in the range >500 nm. Control experiments showed the molecular extinction coefficient of ABTS to agree with manufacturer specification (ε_{420} = 34 mM^{-1}) and was used to determine the molecular extinction coefficient for the oxidized form at wavelength 720 nm was determined to be ε_{720} = 14.2 mM^{-1}. Representative spectra used to calculate the molecular extinction coefficients in the various buffers used experimentally are shown in **Fig. S3.7.2B**. The stoichiometry of H_2O_2 to $ABTS^{+\bullet}$ was taken as 1:2 following previous reports.[45]

- Kinetics analysis

All reported values are determined from a minimum of a triplicate repetition as a minimum. Fit to the Michaelis-Menten or other kinetics rate equations were confirmed with R^2 values ≥ 0.95. Error bars and reported values represent the standard deviation on the regressed parameters, which included true standard deviations in the fitting. A two-sample t-test with a pooled variance was used to determine the statistical significance of any difference in reported mean values. The null hypothesis is that the two values are the same, so p-values >0.05 indicate a failure to reject that hypothesis.

3.3 Results

3.3.1 UV-Vis vs. Electrochemistry of H_2O_2, a Secondary Product of Glucose Oxidase

Glucose oxidase catalyzes the oxidation of glucose to D-glucono- δ -lactone, followed by the re-oxidation of its active site by an electron acceptor (endogenously O_2), ultimately producing hydrogen peroxide[41,46] (**Fig. 3.1A**). It is a homodimer with an active site that utilizes FAD/$FADH_2$ as the electron acceptor/donor. The following equation describes the overall biochemical redox reaction:

$$\beta - \mathrm{D} - \mathrm{Glucose} + \mathrm{O_2} \overset{GOx}{\Longleftrightarrow} D - glucono - \delta - lactone + \mathrm{H_2O_2} \qquad (3.1)$$

Both H_2O_2 and O_2 are electrochemically active and could therefore be used in measuring GOx activity. They are commonly probed with a platinum electrode due to the relatively low potentials required for their redox chemistry.[47] The mechanism of hydrogen peroxide and oxygen reduction proceed via a non-trivial/ complex, and potentially rate-limiting, surface reaction at platinum electrodes and requires exclusion from the observed effects. Hydrogen peroxide reduction occurs in the same potential region as oxygen reduction and is often discussed as an intermediate in the two-electron pathway of the oxygen reduction reaction (ORR), the prevalence of which is determined by several variables of interest to enzymatic studies – such as pH, anion identity/concentration, and temperature.[47] It is possible to selectively monitor oxygen electrochemically via the use of an oxygen selective membrane (the Clark electrode), but the electrodes are often bulky, expensive, and/or have long response times. In addition to the reasons above, we focused our investigation on the oxidation of H_2O_2 to avoid the electrochemical depletion of O_2, which is a necessary co-substrate for glucose oxidase activity and may complicate the kinetic analysis.[48] Therefore, transforming the reaction

product (H_2O_2) to an amperometric value using electrochemistry appears to be an elegant method for studying enzyme kinetics (**Fig. 3.1A**).

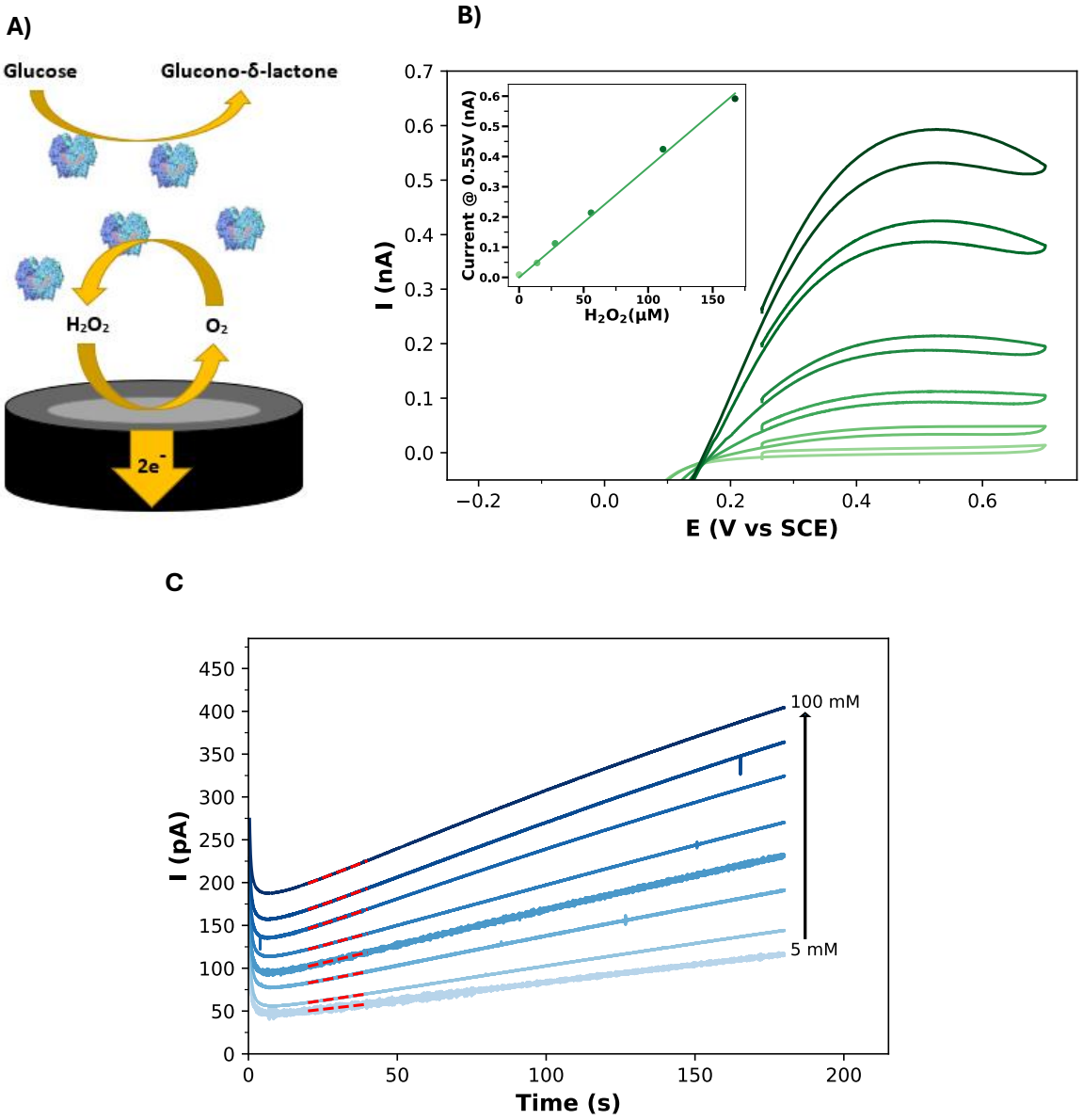

Figure 3.1. GOx activity produces a linear increase in currents when measured with a bare platinum microelectrode. A) Schematic of the homogeneous (enzymatic) and heterogeneous (electrochemical) reactions. B) Linear sweep voltammograms using bare Pt electrode (r ≈ 5 μm) of micromolar H2O2 concentrations produce steady-state currents that are linearly proportional to peroxide concentration and used to determine the diffusion coefficient (inset). Current response is linear for hydrogen peroxide standards up to ~ 500 μM; inset shows range of concentrations with relevant current values for kinetics measurements. Scan rate is 20 mV/s. C) An example set of chronoamperograms collected at 0.55 V vs SCE for solutions of 2.5 nM GOx and varying glucose concentrations (5, 7.5, 10, 15, 20, 35, 50, and 100 mM). The red dashed line indicates where initial rates fitting was done to determine enzyme kinetics.

Platinum microdisk electrodes in PBS solutions with varied H_2O_2 concentrations showed well established voltammetric signals, with steady-state currents proportional to H_2O_2 concentration (**Fig. 3.1B** and inset). The voltammograms show a current plateau above 0.45 V vs SCE; faster interfacial electron transfer is not achieved with additional electric driving force. In this regime, the system is deemed mass transport limited in which the flux of the hydrogen peroxide across a "diffusion layer"- a volume with a concentration gradient which is decreasing toward the electrode- becomes the current-limiting phenomenon. A description of the flux (including the diffusion layer profile) then allows for an analytical determination of the relationship between the current and the redox-active agent's physical characteristics, such as the diffusion coefficient and concentration. For a microdisk electrode, the gradient in the diffusion layer expands approximately hemi-spherically following a sufficient potential step to the mass transport limited region, allowing for a steady state current classically described by *eq. 3.2*.[49-52]

$$I_{ss} = 4nFDC^{*}r_e \tag{3.2}$$

Where in our reaction, n = 2 corresponds to the number of electrons transferred for H_2O_2 oxidation, F is Faraday's constant, $D_{H2O2} = 1.21 \pm 0.08 \times 10^{-5} cm^2/s$ is the empirically measured diffusion coefficient of peroxide, C^* is the bulk analyte concentration and $r_e \approx 5\mu m$ is the electrode radius.

Classically in electrochemical methods, experiments are designed such that the non-linear nature of enzyme reaction rates simplify to a well-described first order EC' mechanism, such as by using excess enzyme and/or substrate, so that the enzymatic contribution is taken as

constant in time.[104] In this work, experimental conditions are selected such that the current linearly increases with time, reflecting the catalytic production of H_2O_2 by GOx (**Fig. 3.1C**). The curves in **Fig. 3.1C** display some important characteristics, including slopes which are increasingly steep with higher glucose concentration, as well as a sustained linearity on the order of minutes. Features of pure electrochemical effects are also observed in the traces, such as initial decay due to the loss of non-faradaic current arising from rapid charge rearrangement processes at the electrode surface, which occur after applying a potential step. Further, differing y-axis intercepts for the linear portion of the curves in **Fig. 3.1C** are due to the different initial H_2O_2 concentrations resulting from the short mixing time and electrochemical cell setup before running individual concentrations of glucose.

The inclusion of an enzymatic reaction alters the diffusion equations, making the bulk concentration a function of time and adding a concentration source within the diffusion layer, which we represent as i_{enz} with the prefactor χ_{enz} in *eq. 3.3*. If the overall rate of reaction is slow compared to diffusion, the concentration gradient can be approximated as static in the diffusion layer and the change in bulk concentration can be taken as the rate limiting. Therefore, as a first approximation, we assume a pseudo steady state is achieved and take *eq. 3.2* as the form of $\chi_{enz}(t)$. Taking the time derivative of both sides of *eq. 3.4* (while allowing C* to be a function of time) and rearranging gives a direct relationship between the slope of the current and the rate of the homogeneous reaction (*eq. 3.5*). The exact contribution and form of χ_{enz} is an interesting theoretical problem and the approximation above serves as a limiting case.

$$I = I_{ss} + I_{enz} = 4nFDC^{*}r_e + i_{enz}(t) \tag{3.3}$$

$$i_{enz}(t) = \chi_{enz} C^*(t) \quad where \quad \chi_{enz} \approx 4nFDr_e \tag{3.4}$$

$$\left(\frac{1}{\chi_{enz}}\right) * \frac{dI}{dt} = \left[\frac{dC(r,t)}{dt}\right]_{enz} \tag{3.5}$$

After establishing a means to determine enzymatic reaction rates, an enzyme kinetics framework can be employed to characterize its behavior. Michaelis-Menten kinetics are often used to describe the relationship between the substrate concentration ([S]) and reaction rate (υ) of an enzyme following *eq. 3.6* below.[54] The parameter V_{max} describes a theoretical absolute maximum rate of reaction under completely saturating substrate concentrations and K_M represents a substrate concentration at which half the maximum velocity is achieved. The maximum reaction rate is a product of the enzyme concentration and the apparent catalytic rate constant (*eq. 3.7)* – which may represent contributions of one or more elementary steps in the enzyme reaction. 'Initial' reaction rates are measured shortly after mixing enzyme and substrate to abate rate-diminishing effects from influences such as inactivation, product build up, substrate depletion, etc. Hence, to validate the current-concentration relationship described above, the Michaelis parameters V_{max} and K_M were used for comparison of electrochemical chronoamperometry with the gold-standard UV-Vis using a standard ABTS based method.[55,56]

$$\nu = \frac{V_{max}\,[S]}{K_M + [S]} \tag{3.6}$$

$$V_{max} = [E]k_{cat} \tag{3.7}$$

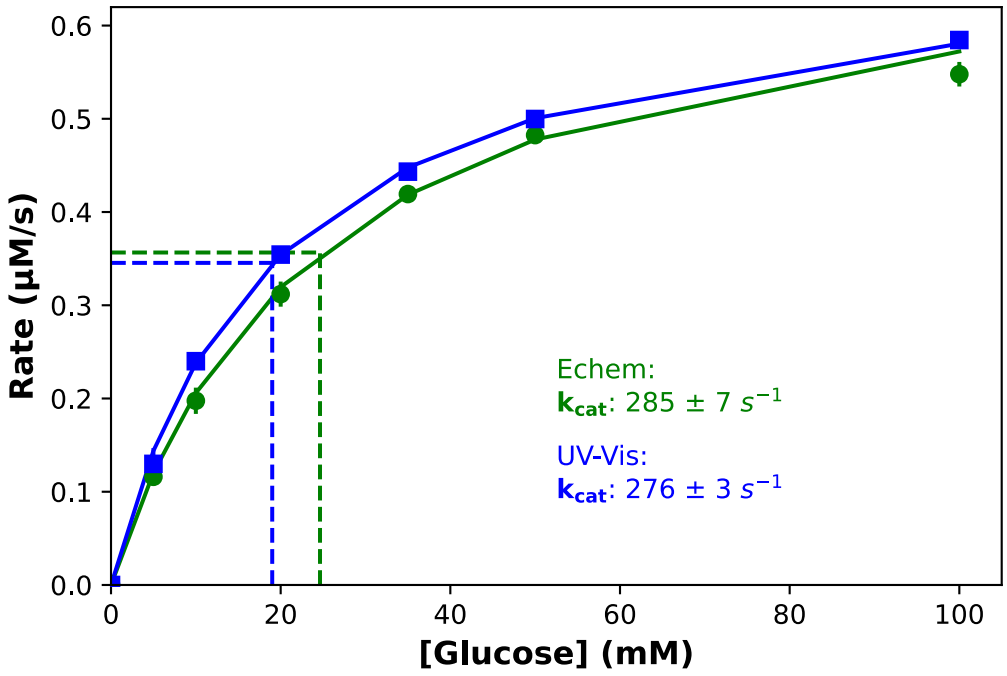

Figure 3.2: Rate analysis comparison between conventional UV-Vis and the proposed unmediated electrochemistry on a microelectrode shows agreement between the methods. Experimental data for 2.5 nM GOx has been fit with the Michaelis-Menten rate equation for the electrochemical (green circles) and UV-Vis methods (blue squares). The K_M values are 24.6 ± 1.6 and 19.3 ± 1.9 mM for Echem and UV-Vis, respectively.

As shown in **Fig. 3.2**, the two methods demonstrate GOx kinetics which are within error of each other (difference of means - $p \approx 0.13$), with k_{cat} values of 285 ± 7 s^{-1} and 276 ± 3 s^{-1}. The K_M values (marked by dashed lines in **Fig. 3.2**) are, however, not within error ($p < 0.001$), with values of 24.6 ± 1.6 and 19.0 ± 0.6 mM for Echem and UV-Vis, respectively. The Michaelis-Menten equation is known to be sensitive to the endpoint values, which may suggest that the higher error observed for higher glucose concentrations is a significant driver of the difference in the K_M values. Empirically, it appears the form of $i_{enz}(t)$ is a permissible current-concentration relationship to determine enzyme kinetics under the selected experimental

conditions. The nature of the rate limiting process is examined in the next section by altering the enzyme and oxygen concentrations, with the aim to understand if the glucose oxidation step is rate determining.[44]

3.3.2 Examining the Rate Limiting Step by Varying GOx and Oxygen Concentrations

The kinetic framework we have used to determine enzyme kinetics via electrochemistry has two major assumptions – 1) that the glucose oxidation step is the rate determining process in the enzyme reaction and 2) that the observed plateau of the kinetics is due to the substrate saturation of the enzyme (e.g. all active sites are occupied, increasing substrate concentration can't increase reaction rates). We therefore sought to find the bounds where the initial rates assumption can be applied and to then understand what processes may compete with oxidation of glucose as the rate determining step. The effect of glucose oxidase and oxygen concentration on k_{cat} and K_M offers insight into which processes may be rate limiting. In a reaction which is purely determined by the catalytic step, a change in V_{max} is expected to be directly proportional to changes in GOx concentration (as in *eq. 3.7*), giving a constant k_{cat} and indicating the rate-determining process is unchanged. If glucose oxidation is solely the rate limiting step, manipulation of the oxygen concentration should show no influence on reaction rates.

The relationship between V_{max} and GOx concentration is presented in **Fig. 3.3A**. The expected linear trend (blue dashed line in **Fig. 3.3A**) between V_{max} and GOx concentration was observed up to 5 nM GOx, marked by the green region on the figure**.** Adjacent to this region, V_{max} deviates from linearity, but the observed K_M values remain similar to those in the linear response region (**Fig. 3.3B**), up to the measured value of 10 nM. As opposed to measurements collected at concentrations in the linear region, the chronoamperograms in the transition region do not maintain a constant slope, but rates determined by fitting the very initial part of the curve still maintain similar K_M values. Example chronoamperograms displaying this behavior

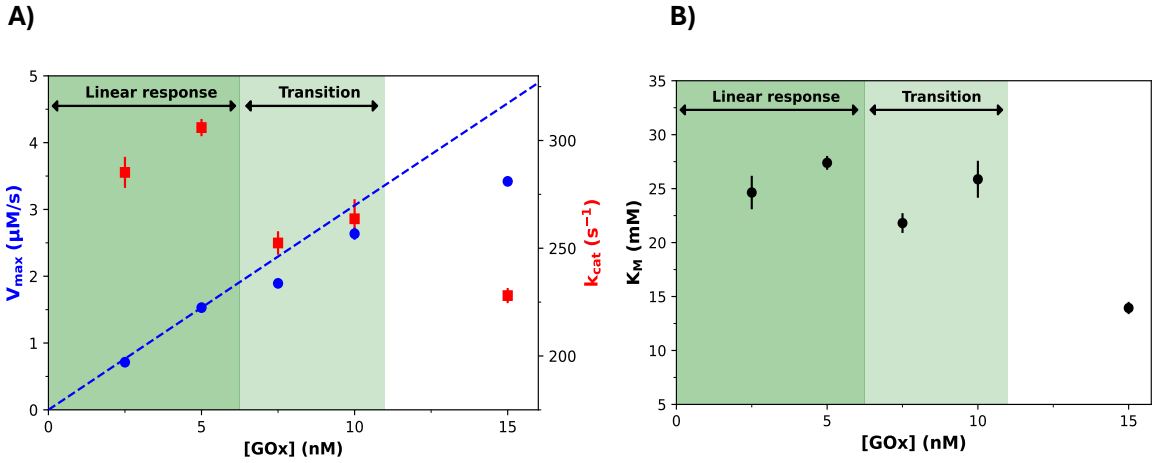

Figure 3.3: **The trends of Vmax and K_M determined by electrochemistry with increasing GOx concentration offer insight into the boundary under which glucose oxidation is the rate limiting step.** Values are determined from fit to Michaelis-Menten kinetics model. A) Maximum rate (blue circles) and k_{cat} (red squares) as well as B) K_M as a function of GOx concentration show kinetics which are decreasing with measurement time, but when initial rates are collected, the results approach the previous trendline. This is evidenced by the retention of a similar K_M value across the two zones in B) – see **Fig. S3.3** and **S3.4**.

are shown in **Fig. S3.3A**. The continuity of the K_M value into the transition region is likely a consequence of the loss of linearity occurring more significantly at the highest glucose concentrations for these GOx concentrations. Due to overall slower reaction rates for low glucose concentrations, the shape of the kinetics curve is largely maintained with the increasing

enzyme concentration. Outside of the transition region, even the apparently linear or fastest time period of data collection still leads to kinetics with significantly decreased K_M values - indicating that the saturation of the enzyme turnover is being influenced by other kinetic processes.

To understand the driving force for the deviation from the linear response in GOx concentration, we investigated the influence of oxygen on the observed kinetics. Since re-oxidation of the FAD cofactor is required for multiple turnovers with glucose oxidase, a more precise description of the GOx behavior is to use the sequential ping-pong mechanism. [41,57-59] As opposed to the mechanism comprised of two kinetic steps (*eq. 3.8* below) used in deriving the Michaelis Menten rate equation, the ping-pong mechanism further considers the kinetic steps of the reoxidation of GOx's active site, as detailed in *eq. 3.9* below. The ping-pong rate equation is shown in *eq. 3.10*.

$$E + A \underset{k_{-1}}{\overset{k_1}{\leftrightharpoons}} EA \overset{k_2}{\rightarrow} E + P \tag{3.8}$$

$$E + A \underset{k_{-1}}{\overset{k_1}{\leftrightharpoons}} EA \overset{k_2}{\rightarrow} E^* + P \rightarrow E^* + B \underset{k_{-3}}{\overset{k_3}{\leftrightharpoons}} E^*B \overset{k_4}{\rightarrow} E + Q \tag{3.9}$$

Where E = GOx, A = glucose, P = D-glucono-δ-lactone, E^* is the reduced form of GOx
B is O_2 and Q is H_2O_2

$$\nu = \frac{V_{max}[O_2][G]}{K_{M,O_2}[G] + K_{M,G}[O_2] + [O_2][G]} \tag{3.10}$$

It is evident from the solubility of oxygen at ambient conditions (~0.24 mM)[60,61] and the Michaelis constant for oxygen (values reported 0.2 - 0.51 mM)[62-66] that oxygen is not greatly in excess and may influence the GOx reaction kinetics, especially from increased consumption with elevated GOx concentration as in **Fig 3.3A**. The relative sensitivity of the enzyme kinetics to dissolved oxygen concentration under the ping-pong framework is shown in **Fig. S3.4**.

Therefore, the extent to which the reoxidation of the active site of GOx contributes as a limiting step was investigated by two means- 1) decreasing the oxygen concentration by delaying the start time of collecting the current in the electrochemical method and 2) performing both electrochemical and UV-Vis methods under O_2 saturated conditions. In the first case, delaying the start of the chronoamperometric measurements until 60 seconds after the addition of glucose oxidase substantially ($p < 0.001$) reduced the measured maximum velocity (**Fig. 3.4A**). The reaction rates for higher glucose concentrations more greatly deviate than lower concentrations owing to the greater oxygen consumptions at the higher substrate concentrations. This manifests as a decrease in the K_M value. When the measurements are repeated under saturated O_2, the agreement between the two methods is restored even with the 60 second delay. Under these conditions, the maximum velocity substantially increased for both electrochemistry and UV-Vis, as seen in **Fig. 3.4A**, giving k_{cat} values within error ($p = 0.40$) at 433 ± 24.0 and 447 ± 10.4 s^{-1} respectively. To directly address the influence of oxygen concentration on the limit to which initial rates experiments could be achieved, the enzyme-concentration dependence experiment conducted in **Fig. 3.3** was replicated under saturated oxygen conditions. As is shown in **Fig. 3.4B**, an extended linear response and transition zone is observed, with the previous transition region now being fully encompassed in the linear response. The amount of non-linearity observed in the chronoamperogram at 15nM GOx and

100mM glucose is seen to be three times lower for the saturated oxygen experiment (**Fig. S3.5B**)

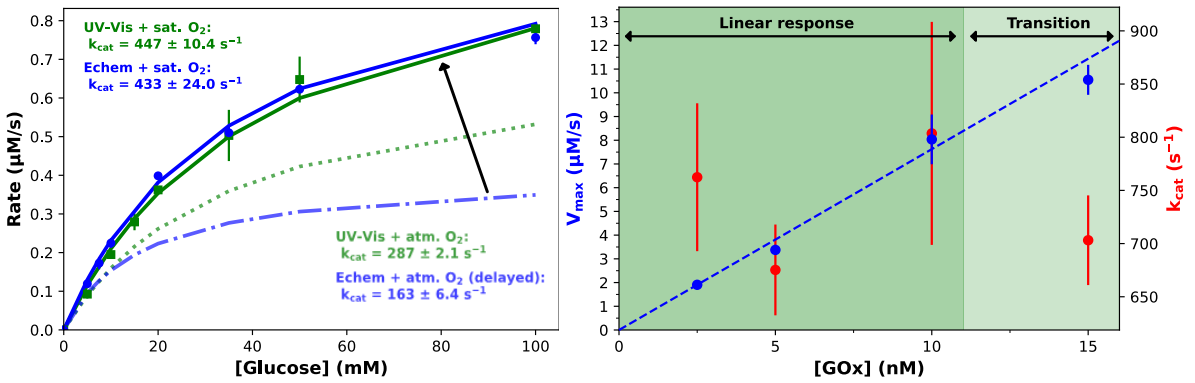

Figure 3.4: **Manipulation of oxygen concentration in the electrochemical method suggests its role as a rate limiting process for higher GOx concentrations.** A) Echem with a 60 second delay in data collection (blue dash-dot) and UV-Vis (green dotted) show kinetics results which do not align (especially at high glucose concentrations). UV-Vis (green squares) and Echem (blue circles) converge under elevated oxygen (dotted lines show ambient data presented previously). B) The dependence of V_{max} (blue circles) and k_{cat} (red squares) on GOx concentration repeated under saturated O_2 shows an extended linear range in comparison to **Fig. 3.3A**.

Ultimately, these results suggest that the upper limit of the electrochemical method involves an aspect of the re-oxidation step. By increasing GOx concentration and thereby the overall reaction rates, the second half reaction becomes non-negligible in the limiting kinetic process. Due to the agreement between the electrochemical and UV-Vis and the influence of oxygen over the linear nature of the response, this result suggests that the different transport of H_2O_2 in heterogeneous (to the electrode) vs homogeneous (in bulk by absorbance) systems does not serve as a limiting step in measuring the enzyme kinetics. Generally, under the conditions suggested by this method, where the overall rate of reactions is slow enough to give the sustained linearly increasing current, we believe this interpretation should allow generalizable

use to other enzyme systems. Following this insight, we next examine the operational bounds of this method with regards to buffer/pH and compare it to UV-Vis results.

3.3.3 Influence of Chloride and pH on Current Responses – Enzyme Sensitivity and Heterogeneous Effects

Investigating the behavior of enzymes under various pH conditions can aid the understanding of reaction mechanisms and enable protein engineering and other strategies to enhance performance in application settings.[67,68] For glucose oxidase, early work by Nakamura and Ogura[69] and Gibson, Swoboda and Massey[63] led to the proposal of the fundamental kinetic steps now understood as the ping-pong mechanism discussed in the previous section. Following work considered the effects of pH[41,48,59], chloride[70], and inhibitors[71] on GOx kinetics, enabling the suggestion of which active site residues are important to the enzymatic reaction based upon their ionizable behavior. These proposals came well before the structure of GOx was determined[72] or molecular docking studies[73] could validate the identities of the residues involved.

Here, we have assessed the capabilities of the chronoamperometric method to similarly resolve reaction conditions that influence enzyme behavior by examining the effect of changing the pH. To decouple any influences of buffer conditions on measured kinetics arising from electrochemical changes alone, a series of hydrogen peroxide standards were collected via cyclic voltammetry. The values of the peak currents remained linear with peroxide concentration for currents relevant to enzyme kinetics measurements (**Fig. 3.5A**). However, the slopes of the current-concentration dependence showed significant differences. To maintain the conditions needed to use the framework of *eq. 3.2* to parse the difference in slopes, the

potential at which the currents were observed was shifted as needed to be in the diffusion-limited response region (**Table S3.5** lists the potentials used for each buffer).

Through this lens, the influence of the buffer on the current-concentration relationship can be understood to represent changes to both the diffusion coefficient of peroxide in the different buffers, and to changes in the electro-active area of the working electrode (also serving as surrogate for changes to the heterogeneous reaction kinetics). Previous work examining the causes of the concentration-saturating nature of the hydrogen peroxide oxidation reaction on platinum electrodes established the involvement of a surface adsorbed reaction.[42] The number of available surface sites were determined to be activated by the presence of phosphate[74], and competed for by chloride.[75] These phenomena are reflected in the slopes in **Fig. 3.5A**; peroxide in Tris buffer and the addition of chloride to acetate buffer both showed decreased slopes. Acetate buffer in the absence of chloride showed higher responsiveness than PBS- it may be that the equilibrium of the surface species at pH 5 more greatly benefits from the lack of chloride as compared to the presence of phosphate in PBS, especially for the relatively low concentrations of peroxide relative to the saturating point (~1 mM). Extending the potential window significantly restores peroxide sensitivity from ~1.5 pA/μM to the presented value for acetate KCl (as expected[75]) while Tris buffer does not show the same potential shift (**Fig. S3.5**).[73]

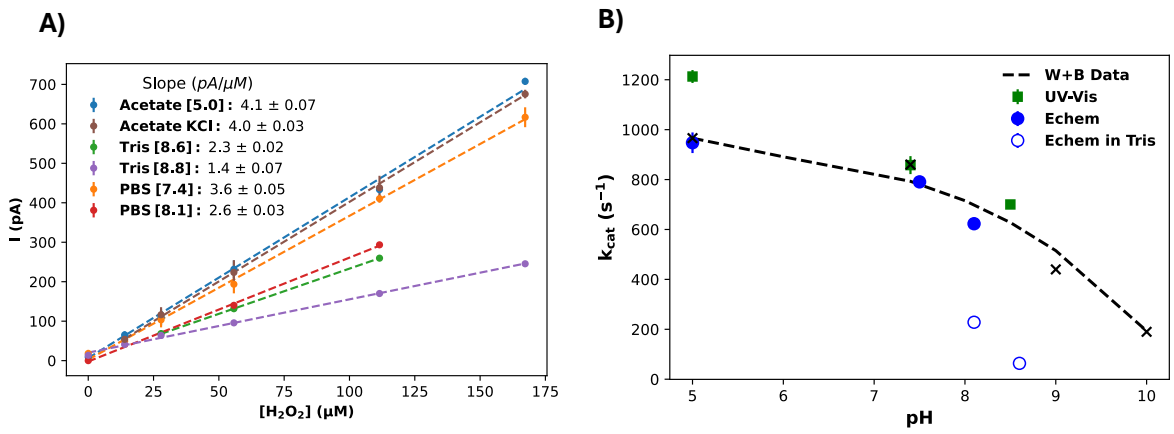

Figure 3.5: Comparison of the effects of pH on the measured kinetics of GOx by Echem and UV-Vis show some agreement between the trends in pH but also raise potential limitations when compared to previous literature. A) The electrochemical sensitivity (pA/μM) to H_2O_2 decreases as pH increases. Bracketed values in the legend indicate the measured pH value for the buffer. Changes in the sensitivity can be understood to represent any pH-based changes to diffusivity of peroxide as well as effective changes to the active electrode area (whether physical or due to changes in the mechanism of the surface reaction). B) The value of kcat determined by electrochemistry (blue circles) and UV-Vis (green squares) agree with the values published by Weibel and Bright[41] (black trendline and x's) for pHs 7.4 and 5. The open circles are measurements performed in Tris buffer. Deviations at higher pH were investigated by considering the electrochemical response to peroxide alone.

The results of **Fig. 3.5A** were therefore applied as an adjustment factor to electrochemical measurements of GOx activity to isolate the influences of the buffer on the enzyme behavior - all results were "normalized" to the pH 7.4 results. Changes in the potential at which peak currents occurred, as determined from the peroxide standards, were applied in the chronoamperometric measurements for the corresponding buffer. The results in **Fig. 3.5B** show enzyme kinetics collected at a variety of pHs, as well as a comparison to both UV-Vis measurements and the pH dependence of k_{cat} published by Weibel and Bright.[41] As the referenced work uses a kinetic framework with a two-step reaction and considers the infinite limit for glucose and oxygen concentrations, k_{cat} values were determined by fitting to the ping-pong mechanism. Increasing pH showed a substantial reduction in activity which is more

significant at higher values. At pH 5, 7.5, and 8.1, both the electrochemical method and UV-Vis method agree with the values determined by Weibel and Bright.[92] However, at higher pH the electrochemical measurements deviates from the UV-Vis results and the reference trend, marked by the open circles on **Fig. 3.5B**. While this method readily replicates the results of pH investigations under some of the conditions, it highlights the necessity of accounting for the underlying electrochemistry.

3.4. Discussion

Electrochemical systems involving enzymes stand to be a major contributor to the next generation of technological development by way of biosensing, biofuel cells, and electrocatalytic synthesis. At the heart of these developments are the selectivity and kinetic performance of the enzyme. Accordingly, it is important to understand the mechanisms by which such systems are hampered. Along this line- platinum electrodes and glucose oxidase used in combination were the genesis of the modern wave of biosensor research; many technological developments and experimental strategies have been employed to improve upon the original design by Lyons and Clark.[76] A common example relevant to this work is the use of flux restricting membranes in modern continuous glucose sensors, serving to lower the reaction rate and reduce oxygen consumption.[77] Our work in **Section 3.3.2** addresses this topic by demonstrating how such influences on the reaction mechanism arise in measured chronoamperograms and in reactant concentration dependencies. Though O_2 was previously known as a participant in the GOx reaction cycle, the deviation from expected linear increases in rates matching increases in enzyme concentration provides a means to diagnose the presence of such complications when extended to other systems.

Another common improvement is the use of external mediators to enhance electron transfer rates and to provide co-substrates at concentrations not subject to depletion by the enzyme turnover. Significant work has been done to theoretically describe the electrochemical response of a mediated bioelectrocatalytic system. Typically, enzyme activity is taken to be so high that the electrochemical response is independent of its kinetics.[68] Two of the foundational assumptions common in these analyses do not hold for the system we described here. First is the practice of taking the redox-active species which transduces the reaction to the electrode to be zero at the start of the measurement. In our method oxygen- serving as the co-substrate/mediator- is non-zero in the bulk, as it is necessary for catalytic turnover in the absence of other artificial co-substrates. There is necessarily a non-constant driving force for flux from the bulk arising from the enzymatic reaction, complicating the insights from the current which depend on established concentration profiles arising from this typical assumption. Secondly, the ambient dissolved oxygen concentration (~0.24 mM) is very near to the GOx binding constant (values reported 0.2 - 0.51 mM), opposed to analyses using mediator concentrations either far greater or lesser than the Michaelis constant. While this precluded the use of the analytical work done before, working under these conditions was essential to determining reaction kinetics and gaining insights based around pH and chloride influence on GOx behavior. Due to these reaction conditions, significant consumption may challenge the use of steady state kinetics (e.g. the concentrations of the enzyme intermediates being constant)- by using appropriately small concentrations of enzyme, the consumption rate of O_2 is minimized.

The observations of the influence of pH on the electrochemically determined GOx kinetics suggest that extra diligence must be used when looking at how electrochemical enzyme sensors

or reactors work in different operating conditions. For instance, further work could be done to incorporate phosphate into e.g. Tris for higher pHs to understand if there are still electrochemical influences in the deviation from the kinetics determined by UV-Vis. Additionally, minimal reaction rates are required to ensure the current-concentration relationship is valid. The evoked steady state response in *eq.* 3.2 (e.g. Cottrellian behavior) is a long-time limit approximation – the current collected for initial rates measurements have not fully come to a true steady state, but the rate of decay (<0.1 pA/s) is negligible. However, at the slower reaction rates encountered at higher pH, background decay of current is on the same order of magnitude as the observed enzymatic current slopes (See **Fig S3.6**). Higher enzyme concentrations might be viable at this pH to minimize this source of error. This otherwise may represent a lower limit to the use of the long-term limit of the current-concentration relationship (*eq. 4*). Our results in **Section 3.3.3** demonstrate how the heterogeneous electron transfer alone may significantly influence measured kinetics and must be accounted for. In comparison to systems which use external mediators, the use of the endogenous electron acceptor minimizes the possibility that the resulting insights into pH effects on enzymatic kinetics is instead a function of an exogenous mediators' pH sensitivities. More broadly stated, an accurate knowledge of the current-concentration relationship is essential to making bon-fide insight into enzyme kinetics electrochemically.

Although our results suggest that mass transport between the bulk and electrode surface do not hinder the observed enzyme kinetics, operating conditions can be selected which produce reaction systems that behave otherwise. Recently, Szczepanczyk *et Al.* also performed a comparison between oxygen electrode chronoamperometry and spectrophotometry for measuring catalase activity.[46] They observe a significantly lower activity value for the UV-Vis

based method. This is understood to be a difference in mass transport of peroxide to the catalase active site and/or oxygen transport to the electrode, since the disparity in activity diminishes when increasing catalase concentration or when removing stirring from the electrochemical method. In addition to examining the limiting processes in the activity readout, altering substrate and enzyme concentrations can validate that the assumptions used in the enzyme kinetics model hold. As a summary of the results discussed in the case of glucose oxidase, we offer the following guidelines for implementing this method with other enzyme systems.

Guidelines for assessing enzyme kinetic parameters using the electrochemical method:

1) Characterize the electrochemical reaction of the redox active species.
    a. Ensure stable electrode behavior over a duration relevant to kinetics measurement (on the order of 10s of seconds, ideally).
    b. Determine linear response region of current depending on redox species concentration, if any limits exist.
    c. Determine electrode size and diffusion coefficient in the system of interest using cyclic voltammetry, as described in **SI Section 3.1.**
2) Select working conditions which produce reaction rates within electrochemical and initial rates considerations.
    a. Select enzyme concentrations which:
        i. Give sustained linear positive slopes
        ii. Are substantial compared to baseline decay processes (<1%)
        iii. Do not lead to significant changes to reactant concentrations.
    b. Select substrate concentrations which:

i. Vary at least an order of magnitude below the K_M value, and to a value above the K_M where saturation is evident.

3) Measure enzyme kinetics, making sure to collect rate data as near to introduction point of the reagent as possible.
4) Ensure any cofactors or co-reactants are not controlling the observed kinetics.
    a. Calculate deviations from linear chronoamperometric responses as in **SI Section 3.3** to validate the selected working conditions.
    b. Comparison to UV-Vis or other spectroscopy may serve as supporting proof of observed reaction rates.
5) Repeat the above considerations when changing reaction conditions such as buffer, pH, etc.
    a. Empirical adjustment factors can be applied to the kinetics analysis, accounting for changes to current-concentration relationship when still within appropriate (as in S**ection 3.3.3** and **SI Section 3.5**)

3.5. Conclusion

In this work, we have presented an electrochemical method for exploring enzyme kinetics based on initial rates. The new method relies on an unmediated analyte radial diffusion to a bare, microelectrode, which offers the advantage of creating a relatively straightforward electrochemical monitoring technique of the enzyme's physical properties such as k_{cat} and K_M. This approach not only facilitates the investigation of key enzymatic descriptors across different systems relevant to enzymology, biosensors, and biosynthesis, but also provides guidelines for achieving reliable results. The glucose/glucose oxidase system was employed to compare the method with standard UV-Vis techniques, enabling empirical corrections to the

electrochemical data. These comparisons suggest that the empirical form of the current-concentration relationship holds under our experimental conditions and that mass transport to the electrode does not obscure the observed kinetics. We further explored the influence of co-substrate and enzyme concentrations to define the conditions under which the catalytic reaction remains rate-limiting within the initial rates framework. Loss of linearity in measuring the reaction rates, combined with sensitivity to the O_2 co-reactant was observed for the higher reaction rates achieved at high glucose and enzyme concentrations. This suggests that part of the oxidative half-reaction begins to contribute to the rate determining process and serves as a boundary to where our method can be used accurately. By applying empirical corrections to the current-concentration relationship, we aligned the electrochemical data with previously described effects of pH and chloride on enzyme kinetics. This highlights the method's dependence on baseline current levels—and consequently overall reaction rates—and underscores the importance of using the natural co-substrate to fully capture both electrochemical and enzymatic behavior.

3.6. References for Chapter 3

1. Robinson, P. K. Enzymes: principles and biotechnological applications. *Essays Biochem* **59**, 1–41 (2015).

2. Cornish-Bowden, A. *Fundamentals of Enzyme Kinetics*. (Wiley-Blackwell, 2013).

3. Bisswanger, H. *Enzyme Kinetics: Principles and Methods*. (Wiley-VCH, 2017).

4. Kapoor, S., Rafiq, A. & Sharma, S. Protein engineering and its applications in food industry. *Crit Rev Food Sci Nutr* **57**, 2321–2329 (2017).

5. Fernandes, P. Enzymes in Food Processing: A Condensed Overview on Strategies for Better Biocatalysts. *Enzyme Res* **2010**, 1–19 (2010).

6. Rocchitta, G. *et al.* Enzyme Biosensors for Biomedical Applications: Strategies for Safeguarding Analytical Performances in Biological Fluids. *Sensors (Basel)* **16**, 780 (2016).

7. Sun, H., Zhang, H., Ang, E. L. & Zhao, H. Biocatalysis for the synthesis of pharmaceuticals and pharmaceutical intermediates. *Bioorg Med Chem* **26**, 1275–1284 (2018).

8. Liew, W. H., Hassim, M. H. & Ng, D. K. S. Review of evolution, technology and sustainability assessments of biofuel production. *J Clean Prod* **71**, 11–29 (2014).

9. Pellis, A., Cantone, S., Ebert, C. & Gardossi, L. Evolving biocatalysis to meet bioeconomy challenges and opportunities. *N Biotechnol* **40**, 154–169 (2018).

10. Ye, D. *et al*. Bioorthogonal cyclization-mediated in situ self-assembly of small-molecule probes for imaging caspase activity in vivo. *Nat Chem* **6**, 519–526 (2014).

11. Li, Z. *et al*. Creatine Kinase, a Magnetic Resonance-Detectable Marker Gene for Quantification of Liver-Directed Gene Transfer. *Hum Gene Ther* **16**, 1429–1438 (2005).

12. Bivehed, E., Strömvall, R., Bergquist, J., Bakalkin, G. & Andersson, M. Region-specific bioconversion of dynorphin neuropeptide detected by in situ histochemistry and MALDI imaging mass spectrometry. *Peptides (N.Y.)* **87**, 20–27 (2017).

13. Dube, S. *et al*. 11β-Hydroxysteroid Dehydrogenase Types 1 and 2 Activity in Subcutaneous Adipose Tissue in Humans: Implications in Obesity and Diabetes. *J Clin Endocrinol Metab* **100**, E70–E76 (2015).

14. Armstrong, F. A. Some fundamental insights into biological redox catalysis from the electrochemical characteristics of enzymes attached directly to electrodes. *Electrochim Acta* **390**, 138836 (2021).

15. Neira, H. D. & Herr, A. E. Kinetic Analysis of Enzymes Immobilized in Porous Film Arrays. *Anal Chem* **89**, 10311–10320 (2017).

16. Martin, D. J., McCarthy, B. D., Rountree, E. S. & Dempsey, J. L. Qualitative extension of the EC' Zone Diagram to a molecular catalyst for a multi-electron, multi-substrate electrochemical reaction. *Dalton Transactions* **45**, 9970–9976 (2016).

17. Savéant, J. & Costentin, C. *Elements of Molecular and Biomolecular Electrochemistry*. (Wiley, 2006). doi:10.1002/9781119292364.

18. Hirst, J. Elucidating the mechanisms of coupled electron transfer and catalytic reactions by protein film voltammetry. *Biochimica et Biophysica Acta (BBA) - Bioenergetics* **1757**, 225–239 (2006).

19. Merrouch, M., Hadj-Saïd, J., Léger, C., Dementin, S. & Fourmond, V. Reliable estimation of the kinetic parameters of redox enzymes by taking into account mass transport towards rotating electrodes in protein film voltammetry experiments. *Electrochim Acta* **245**, 1059–1064 (2017).

20. Armstrong, F. A., Heering, H. A. & Hirst, J. Reaction of complex metalloproteins studied by protein-film voltammetry. *Chem Soc Rev* **26**, 169 (1997).

21. Gulaboski, R., Mirčeski, V., Bogeski, I. & Hoth, M. Protein film voltammetry: electrochemical enzymatic spectroscopy. A review on recent progress. *Journal of Solid State Electrochemistry* **16**, 2315–2328 (2012).

22. Jenner, L. P. *et al.* Heme ligation and redox chemistry in two bacterial thiosulfate dehydrogenase (TsdA) enzymes. *Journal of Biological Chemistry* **294**, 18002–18014 (2019).

23. Armstrong, F. A. Insights from protein film voltammetry into mechanisms of complex biological electron-transfer reactions. *Journal of the Chemical Society, Dalton Transactions* 661–671 (2002) doi:10.1039/b108359g.

24. Léger, C. *et al.* Enzyme Electrokinetics: Using Protein Film Voltammetry To Investigate Redox Enzymes and Their Mechanisms. *Biochemistry* **42**, 8653–8662 (2003).

25. Bedendi, G. *et al.* Enzymatic and Microbial Electrochemistry: Approaches and Methods. *ACS Measurement Science Au* **2**, 517–541 (2022).

26. Bolivar, J. M., Woodley, J. M. & Fernandez-Lafuente, R. Is enzyme immobilization a mature discipline? Some critical considerations to capitalize on the benefits of immobilization. *Chem Soc Rev* **51**, 6251–6290 (2022).

27. Basso, A. & Serban, S. Industrial applications of immobilized enzymes—A review. *Molecular Catalysis* **479**, 110607 (2019).

28. Shang, W., Nuffer, J. H., Dordick, J. S. & Siegel, R. W. Unfolding of Ribonuclease A on Silica Nanoparticle Surfaces. *Nano Lett* **7**, 1991–1995 (2007).

29. You, C.-C., De, M., Han, G. & Rotello, V. M. Tunable Inhibition and Denaturation of α-Chymotrypsin with Amino Acid-Functionalized Gold Nanoparticles. *J Am Chem Soc* **127**, 12873–12881 (2005).

30. Edwards, R. A. & Huber, R. E. Surface denaturation of proteins: the thermal inactivation of β-galactosidase (Escherichia coli) on wall–liquid surfaces. *Biochemistry and Cell Biology* **70**, 63–69 (1992).

31. Hu, J., Li, S. & Liu, B. Properties of immobilized pepsin on Modified PMMA microspheres. *Biotechnol J* **1**, 75–79 (2006).

32. Cho, Y. K. & Bailey, J. E. Immobilization of enzymes on activated carbon: Properties of immobilized glucoamylase, glucose oxidase, and gluconolactonase. *Biotechnol Bioeng* **20**, 1651–1665 (1978).

33. Khan, M. R. Immobilized enzymes: a comprehensive review. *Bull Natl Res Cent* **45**, 1–13 (2021).

34. Subrizi, F. *et al.* Carbon Nanotubes as Activating Tyrosinase Supports for the Selective Synthesis of Catechols. *ACS Catal* **4**, 810–822 (2014).

35. Wang, J. Electrochemical Glucose Biosensors. *Chem Rev* **108**, 814–825 (2008).

36. Hammond, J. L., Formisano, N., Estrela, P., Carrara, S. & Tkac, J. Electrochemical biosensors and nanobiosensors. *Essays Biochem* **60**, 69–80 (2016).

37. Mehrvar, M. & Abdi, M. Recent Developments, Characteristics, and Potential Applications of Electrochemical Biosensors. *Analytical Sciences* **20**, 1113–1126 (2004).

38. Cass, A. E. G. *et al*. Ferrocene-mediated enzyme electrode for amperometric determination of glucose. *Anal Chem* **56**, 667–671 (1984).

39. Persson, B. & Gorton, L. A comparative study of some 3,7-diaminophenoxazine derivatives and related compounds for electrocatalytic oxidation of NADH. *J Electroanal Chem Interfacial Electrochem* **292**, 115–138 (1990).

40. Bourdillon, C., Demaille, C., Moiroux, J. & Saveant, J. M. New insights into the enzymic catalysis of the oxidation of glucose by native and recombinant glucose oxidase mediated by electrochemically generated one-electron redox cosubstrates. *J Am Chem Soc* **115**, 1–10 (1993).

41. Weibel, M. K. & Bright, H. J. The Glucose Oxidase Mechanism: Interpretation of the pH Dependence. *Journal of Biological Chemistry* **246**, 2734–2744 (1971).

42. Hall, S. B., Khudaish, E. A. & Hart, A. L. Electrochemical oxidation of hydrogen peroxide at platinum electrodes. Part 1. An adsorption-controlled mechanism. *Electrochim Acta* **43**, 579–588 (1998).

43. Prabhu, V. G., Zarapkar, L. R. & Dhaneshwar, R. G. Electrochemical studies of hydrogen peroxide at a platinum disc electrode. *Electrochim Acta* **26**, 725–729 (1981).

44. Wheeler, C. R., Salzman, J. A., Elsayed, N. M., Omaye, S. T. & Korte, D. W. Automated assays for superoxide dismutase, catalase, glutathione peroxidase, and glutathione reductase activity. *Anal Biochem* **184**, 193–199 (1990).

45. Zhang, Y., Tsitkov, S. & Hess, H. Proximity does not contribute to activity enhancement in the glucose oxidase–horseradish peroxidase cascade. *Nat Commun* **7**, 13982 (2016).

46. Bauer, J. A., Zámocká, M., Majtán, J. & Bauerová-Hlinková, V. Glucose Oxidase, an Enzyme “Ferrari”: Its Structure, Function, Production and Properties in the Light of Various Industrial and Biotechnological Applications. *Biomolecules* **12**, 472 (2022).

47. Katsounaros, I. *et al*. Hydrogen peroxide electrochemistry on platinum: towards understanding the oxygen reduction reaction mechanism. *Physical Chemistry Chemical Physics* **14**, 7384–7391 (2012).

48. Wohlfahrt, G., Trivić, S., Zeremski, J., Peričin, D. & Leskovac, V. The chemical mechanism of action of glucose oxidase from Aspergillus niger. *Mol Cell Biochem* **260**, 69–83 (2004).

49. Compton, R. & Banks, C. *Understanding Voltammetry*. (World Scientific, 2018).

50. Shoup, D. & Szabo, A. Chronoamperometric current at finite disk electrodes. *J Electroanal Chem Interfacial Electrochem* **140**, 237–245 (1982).

51. Hepel, T. & Osteryoung, J. Chronoamperometric transients at the stationary disk microelectrode. *J Phys Chem* **86**, 1406–1411 (1982).

52. Zhaohui, L., Zhenbin, J. & Dengping, G. Chronoamperometry for the determination of some electrode parameters using microelectrodes. *J Electroanal Chem Interfacial Electrochem* **259**, 39–47 (1989).

53. Bartlett, P. N. & Pratt, K. F. E. A study of the kinetics of the reaction between ferrocene monocarboxylic acid and glucose oxidase using the rotating-disc electrode. *Journal of Electroanalytical Chemistry* **397**, 53–60 (1995).

54. Johnson, K. A. & Goody, R. S. The Original Michaelis Constant: Translation of the 1913 Michaelis–Menten Paper. *Biochemistry* **50**, 8264–8269 (2011).

55. Sigma-Aldrich. *Enzymatic Assay of Peroxidase (EC 1.11.1.7) 2,2'-Azino-Bis(3-Ethylbenzthiazoline-6-Sulfonic Acid) as a Substrate*.

56. Bankar, S. B., Bule, M. V., Singhal, R. S. & Ananthanarayan, L. Glucose oxidase — An overview. *Biotechnol Adv* **27**, 489–501 (2009).

57. Roth, J. P. & Klinman, J. P. Catalysis of electron transfer during activation of O2 by the flavoprotein glucose oxidase. *Proceedings of the National Academy of Sciences* **100**, 62–67 (2003).

58. Su, Q. & Klinman, J. P. Nature of Oxygen Activation in Glucose Oxidase from Aspergillus niger: The Importance of Electrostatic Stabilization in Superoxide Formation. *Biochemistry* **38**, 8572–8581 (1999).

59. Bright, H. J. & Appleby, M. The pH Dependence of the Individual Steps in the Glucose Oxidase Reaction. *Journal of Biological Chemistry* **244**, 3625–3634 (1969).

60. Xing, W. *et al.* Oxygen Solubility, Diffusion Coefficient, and Solution Viscosity. in *Rotating Electrode Methods and Oxygen Reduction Electrocatalysts* (eds. Xing, W., Yin, G. & Zhang, J.) 1–31 (Elsevier, 2014). doi:10.1016/B978-0-444-63278-4.00001-X.

61. Ringborg, R. H., Toftgaard Pedersen, A. & Woodley, J. M. Automated Determination of Oxygen-Dependent Enzyme Kinetics in a Tube-in-Tube Flow Reactor. *ChemCatChem* **9**, 3285–3288 (2017).

62. Toftgaard Pedersen, A. *et al.* Characterization of a continuous agitated cell reactor for oxygen dependent biocatalysis. *Biotechnol Bioeng* **114**, 1222–1230 (2017).

63. Gibson, Q. H., Swoboda, B. E. P. & Massey, V. Kinetics and Mechanism of Action of Glucose Oxidase. *Journal of Biological Chemistry* **239**, 3927–3934 (1964).

64. Lindeque, R. M. & Woodley, J. M. The Effect of Dissolved Oxygen on Kinetics during Continuous Biocatalytic Oxidations. *Org Process Res Dev* **24**, 2055–2063 (2020).

65. Nakamura, S., Hayashi, S. & Koga, K. Effect of periodate oxidation on the structure and properties of glucose oxidase. *Biochimica et Biophysica Acta (BBA) - Enzymology* **445**, 294–308 (1976).

66. Yasukawa, T., Goto, K. & Mizutani, F. Determination of the Apparent Michaelis Constant of Glucose Oxidase Immobilized on a Microelectrode with Respect to Oxygen. *Electroanalysis* **22**, 927–930 (2010).

67. Mu, Q. *et al*. Thermostability improvement of the glucose oxidase from Aspergillus niger for efficient gluconic acid production via computational design. *Int J Biol Macromol* **136**, 1060–1068 (2019).

68. Padilla-Martínez, S. G., Martínez-Jothar, L., Sampedro, J. G., Tristan, F. & Pérez, E. Enhanced thermal stability and pH behavior of glucose oxidase on electrostatic interaction with polyethylenimine. *Int J Biol Macromol* **75**, 453–459 (2015).

69. Nakamura, T. & Ogura, Y. Kinetic Studies on the Action of Glucose Oxidase. *J Biochem* **52**, 214–220 (1962).

70. Rogers, M. J. & Brandt, K. G. Interaction of halide ions with *Aspergillus niger* glucose oxidase. *Biochemistry* **10**, 4630–4635 (1971).

71. Rogers, M. J. & Brandt, K. G. Multiple Inhibition Analysis of *Aspergillus niger* Glucose Oxidase by D-Glucal and Halide Ions. *Biochemistry* **10**, 4636–4641 (1971).

72. Hecht, H. J., Kalisz, H. M., Hendle, J., Schmid, R. D. & Schomburg, D. Crystal structure of glucose oxidase from Aspergillus niger refined at 2.3 Å reslution. *J Mol Biol* **229**, 153–172 (1993).

73. Meyer, M., Wohlfahrt, G., Knäblein, J. & Schomburg, D. Aspects of the mechanism of catalysis of glucose oxidase: A docking, molecular mechanics and quantum chemical study. *J Comput Aided Mol Des* **12**, 425–440 (1998).

74. Hall, S. B., Khudaish, E. A. & Hart, A. L. Electrochemical oxidation of hydrogen peroxide at platinum electrodes. Part IV: phosphate buffer dependence. *Electrochim Acta* **44**, 4573–4582 (1999).

75. Hall, S. B., Khudaish, E. A. & Hart, A. L. Electrochemical oxidation of hydrogen peroxide at platinum electrodes. Part V: inhibition by chloride. *Electrochim Acta* **45**, 3573–3579 (2000).

76. Clark, L. C. & Lyons, C. Electrode Systems For Continuous Monitoring In Cardiovascular Surgery. *Ann N Y Acad Sci* **102**, 29–45 (1962).

77. Wu, M. *et al*. Tailored diffusion limiting membrane for microneedle glucose sensors with wide linear range. *Talanta* **273**, 125933 (2024).

3.7 Supplemental Figures and Methods

Section S3.7.1. Electrochemical Determination of Parameters in the Current-Concentration Relationship for H_2O_2 on a Platinum Microelectrode

The current observed in the diffusion limited regime (where the current plateaus with respect to applied overpotential) depends upon several physical constants, such as the size of the electrode, the temperature of the solution[128], the diffusion coefficient of the species, etc. For a microelectrode, the current concentration relationship takes the form of *eq. S3.1* below (also *eq. 3.3.2* in the main body)

$$I_{ss} = 4nFDC^{*}r_e \tag{S3.1}$$

Where n = 2 corresponds to the number of electrons transferred for H_2O_2 oxidation, F is Faraday's constant, $D_{H2O2} = 1.21 \pm 0.08 \times 10^{-5}$ cm^2/s is the diffusion coefficient, C* is the bulk analyte concentration and $r_e \approx 5$ μm is the electrode radius.

- Electrochemical Pretreatment of Platinum Working Electrode

Typically, electrochemical pretreatments of platinum electrodes are undertaken in acidic (commonly H_2SO_4) conditions to alter the amount of platinum oxide present, with the goal of maximizing its reactivity towards e.g. oxygen or peroxide.[129] Initially, the possibility of electrochemical behavior shifts due to peroxide affecting the electrode surface was investigated by a long, constant application of the working voltage in a representative concentrations of peroxide (data not shown). Cyclic voltammetry in PBS alone showed two feature changes after the oxidative treatment in peroxide - (1) the reductive current from oxygen behaved more in an expected steady state fashion (blue curve) and (2) there was loss of some small oxidation features in the potential range of interest for peroxide oxidation. This treatment was therefore adopted as a matter of pre-treatment for all experiments. The figure below shows an example

CV at a scan rate of 20 mV/s displaying such behavior (ii. shows a zoom in on the oxidative part).

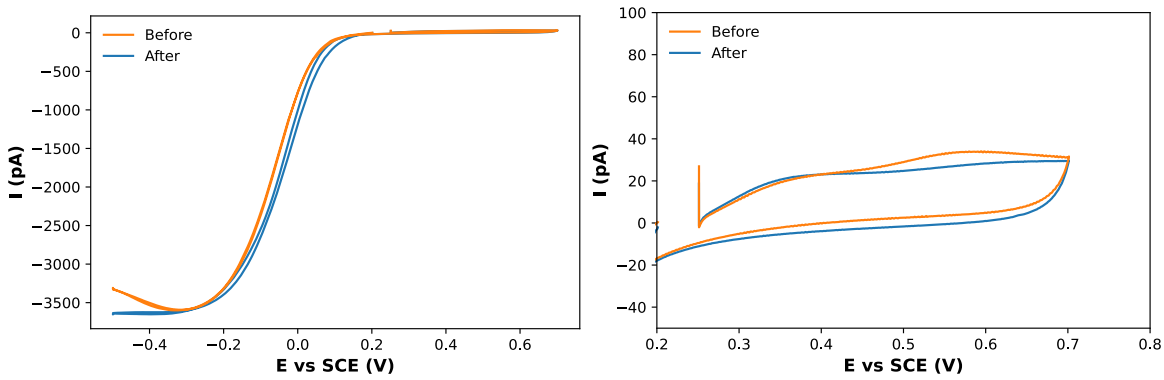

Figure S 3.7.1A Cyclic voltammograms of PBS @20 mV/s before (orange) and after (blue) oxidative treatment in 150 µM H_2O_2. ii. shows a zoom in on the positive potential region to show small features.

- The Diffusion Coefficient of Hydrogen Peroxide

The diffusion coefficient for H_2O_2 was determined by the relationship between the steady state current and the peroxide concentration using *eq. S1* above. The peroxide concentration was determined empirically prior to use in the electrochemical experiments by measuring the differential absorbance at 240 nm and ε240 = 43.6 mM^{-1} cm^{-1} for the absorptivity.[95] **Figure S3.7.1B** below shows the steady state values collected from cyclic voltammetry measurements at 20 mV/s in PBS over an even broader range than what is presented in **Fig. 3.7.1B** and are a representative example of the standards collected. The linear relationship gives an indication that *eq. S1* is a valid form to assume – hydrogen peroxide has been noted to deviate from this linear behavior at concentrations above ~1-2 mM.[129] The value of I_{SS}/C^* was established from a triplicate measurement and was used to determine the diffusion coefficient to be 1.21 ± 0.08 x 10^{-5} cm^2/s. This is largely in agreement with other reports which have electrochemically determined the diffusion coefficient ranging from 0.8-1.6 x 10^{-5} cm^2/s. [93,94]

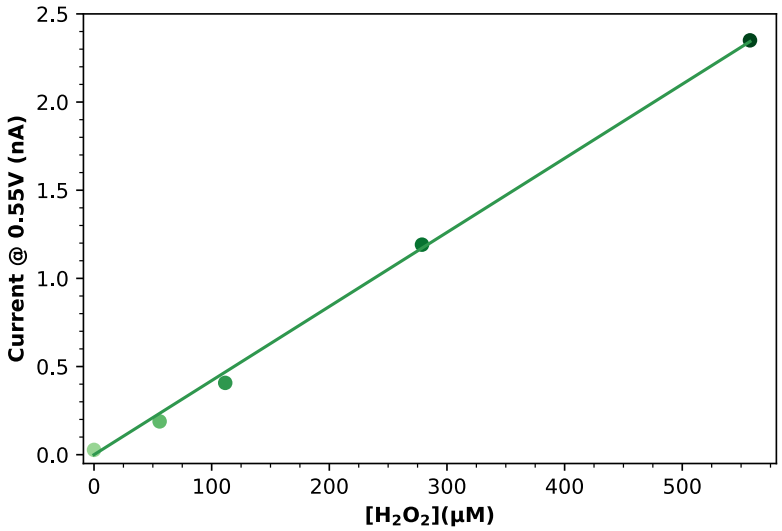

Figure S 3.7.1B Steady state currents collected from cyclic voltammograms at 20 mV/s of varying concentrations of H_2O_2 shows a linear response in concentration.

- Platinum Microelectrode Electroactive Area

By using a redox agent of known concentration and diffusion coefficient, it is possible to use the same relationship (*eq S3.1*) to instead determine the electroactive electrode radius. When an electrode with dimensions on the microscale are used, cyclic voltammetry measurements yield 's' shaped curves with steady state values instead of the classic 'duck shape'. The steady state value is the same as *eq S3.1*. To determine the electrode size, cyclic voltammetry measurements were made with a scan rate of 10 mV/s in solutions of 10 mM Ruthenium hexamine in 100 mM KCl. All solutions were degassed with argon for at least 20 minutes prior to measurement to prevent oxygen reduction from contributing to the measured current. Representative CVs are shown in i), while in ii) CVs collected after the peroxide pretreatment and further after the same electrode was used for several GOx kinetics measurements shows that the electrode size is stable during the experiments. We used a value of 8.43×10^{-10} m^2/s for the diffusion coefficient, based on the report by *Y. Wang et Al.*[130] From this analysis, the electroactive radius of the working electrode was determined to be 4.15 ± 0.07 μm, as compared to the 5 μm geometric radius from the product literature.

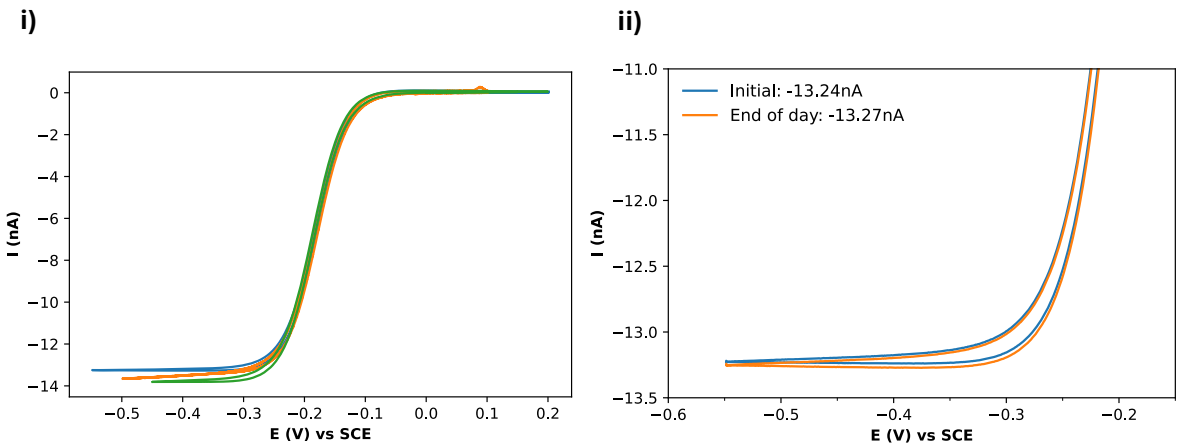

Figure S3.7.1C: Cyclic voltammograms of 10 mM Ruthenium Hexaamine at 10 mV/s for electrode sizing. I) Triplicate measurement used to determine a working electrode radius of 4.15 ± 0.07 µm. ii) Measurement of the electrode size after peroxide pretreatment compared with after use in measuring GOx kinetics.

Section S3.7.2. UV-Vis spectra for ABTS assay

Spectra are shown for ABTS before (dashed greens) and after (solid reds) oxidation via horseradish peroxidase and hydrogen peroxide. The extinction coefficient at 340nm for the unreacted ABTS was 37.3 $mM^{-1}cm^{-1}$, which agrees with a previously reported value of 36 $mM^{-1}cm^{-1}$.[131,132] Initial determination of the extinction coefficient at 405nm of the oxidized form of ABTS was low compared to reported values (29.3 vs 36 $mM^{-1}cm^{-1}$). Using the absorbance value at 340nm in the reacted spectrum to quantify unreacted ABTS gave a corrected extinction coefficient which then agreed with the literature value. This same correction was then applied to the extinction coefficient at 720 nm, which was used to determine reaction rates in UV-Vis kinetics experiments.

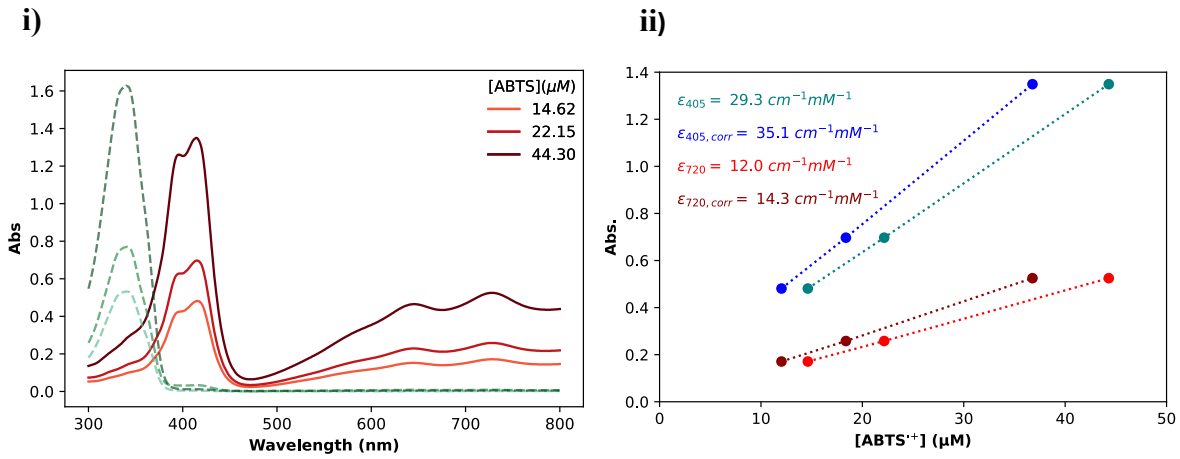

Figure S 3.7.2A: **UV-Vis measurements of ABTS for determination of the extinction coefficient.** i) Spectra of ABTS (green dotted lines) and $ABTS^{\bullet+}$ (solid red lines). ii) Slopes of absorbance in concentration for determination of the extinction coefficient at 405 (blue) and 720 nm (red). Corrected slopes are presented accounting for unreacted ABTS.

The absorbance spectra of ABTS and the oxidized form in different buffers is presented below. The accompanying **Table S3.7.2** contains the calculated values of the extinction coefficient as well as the value corrected for unreacted ABTS in parenthesis.

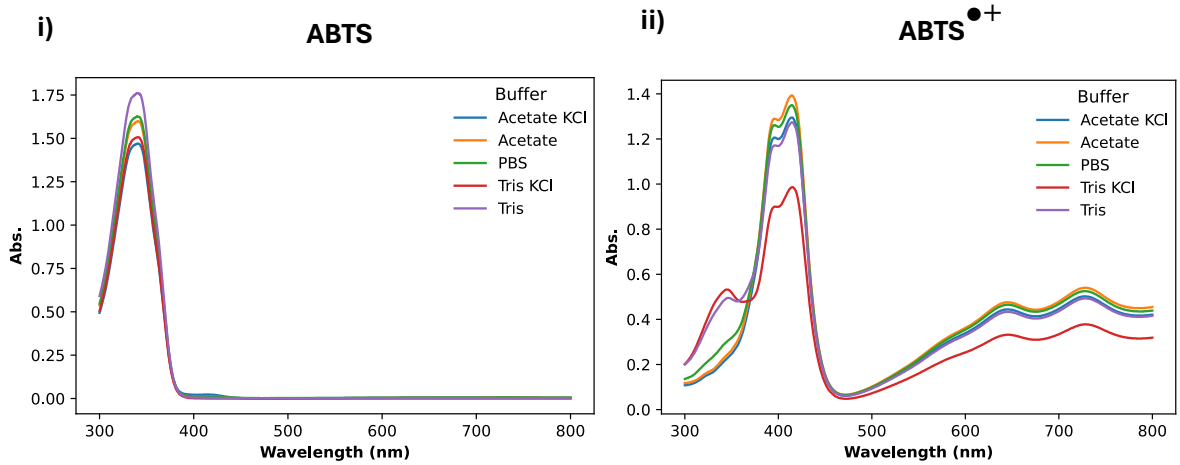

Figure S3.7.2B: **UV-Vis measurements of i) ABTS and ii) $ABTS^{\bullet+}$ for determination of the extinction coefficient in different buffers.**

- Table S3.7.2 – Extinction Coefficients of ABTS in Various Buffers

	ε_{405} (mM^{-1})	ε_{415} (mM^{-1})	ε_{720} (mM^{-1})
Acetate	29.0 (33.3)	30.3 (34.8)	12.1 (13.9)
Acetate KCl	26.7 (30.9)	27.8 (32.1)	11.1 (12.8)
Tris	26.3 (35.9)	27.7 (37.7)	11.0 (15.0)
Tris KCl	16.3 (29.7)	17.2 (31.2)	6.9 (12.6)
PBS	28.1 (33.8)	29.3 (35.2)	11.8 (14.2)

Section S3.7.3. Chronoamperograms show loss of linearity at higher concentrations of GOx and glucose

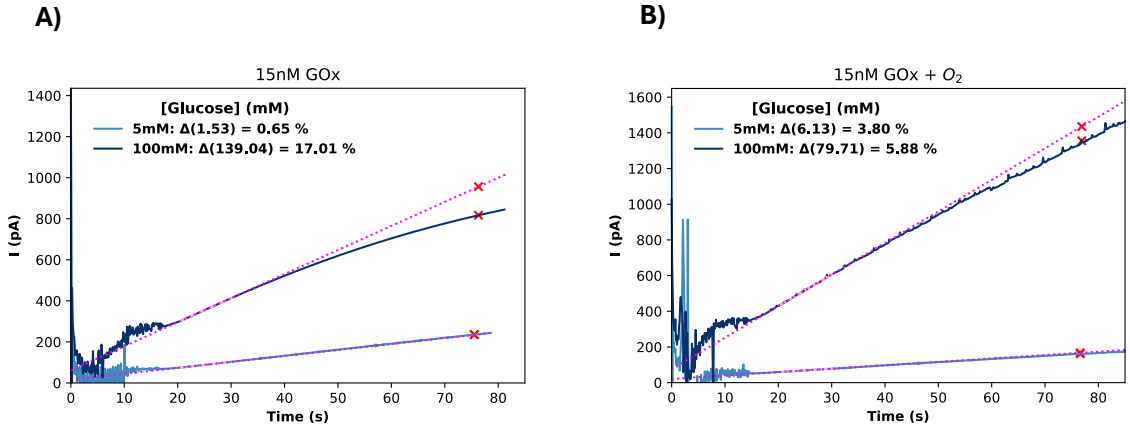

Figure S3.7.3: Linearity analysis of chronoamperograms for 15 nM GOx A) with and B) without saturating oxygen.

The figures above present a comparison of the linearity observed in the chronoamperometric measurements for a relatively high glucose oxidase concentration with and without saturated

oxygen. The pink dotted line shows the extension of the linear fit (the period of 20-30 seconds post GOx injection) used to determine initial rates for fitting to the enzyme kinetic equations in the main text. The red x's mark the point used to calculate the deviation between the linear fit and the experimental observations at 75 seconds post injection. In the case of ambient oxygen conditions, a 17% error is observed between the two at 100 mM glucose, while under saturated oxygen, the deviation is smaller (~6%). For both conditions, the error for low glucose concentrations is minimal.

Section S3.7.4. Analysis via the ping pong mechanism of the influence of the oxygen concentration on the Michaelis constant for glucose.

Section 3.3.2 analyzes the influence of oxygen concentration on the observed kinetics at different concentrations of enzyme. As is pointed out, the reoxdiation of the active site in glucose oxidase can quickly become influential in the rate determining process at higher reaction rates (achieved by higher enzyme concentrations). One way this is evident is through examination of the K_M value for glucose – when oxygen begins to contribute as a rate determining process, the K_M value for glucose shifts. This is displayed in **Fig. S3.7.4**, which shows the shift in K_M as a function of the oxygen concentration. At values of $[O_2]$ significantly above the K_M value for oxygen, there is little to no influence (the flat region). Near the K_M oxygen concentration, the shift factor changes rapidly. A short derivation of the form used to arrive at this shift factor is detailed below.

The ping-pong kinetic equation is:

$$\nu = \frac{V_{max}[G][O_2]}{K_{M,G}[O_2] + K_{M,O_2}[G] + [G][O_2]}$$

As Michaelis constants are defined as concentrations at which half of V_{max} is achieved, substitute in $V_{max}/2$ for v. By diving both sides by $V_{max}/2$ and some algebraic rearrangement, we arrive at

$$K_{M,G} = [G](1 - \frac{K_{M,O_2}}{[O_2]})$$

The factor in the parenthesis is then the shift in the glucose concentration that would be determined as the K_M value for glucose using only the Michaelis Menten equation and is plotted below for $K_{M,O2}$ = 0.48 mM. When $[O_2]$ is less than $K_{M,O2}$ the factor becomes negative, representing that achieving half of the true Vmax is not possible due to oxygen limitation.

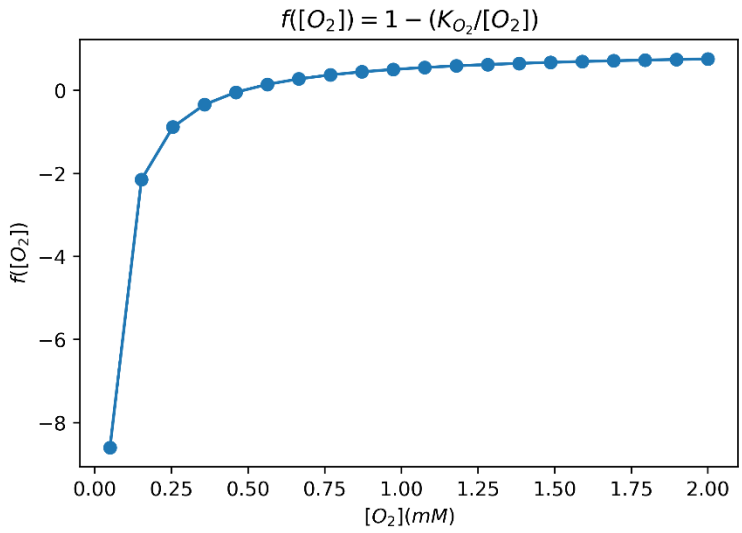

Figure S3.7.4 The influence of oxygen concentration on the observed K_M for glucose demonstrates a strong dependence in physiological conditions. The figure presents a shift factor based upon analysis of the ping-pong kinetic equation.

Section S3.7.5. Cyclic Voltammograms of H_2O_2 in different buffers shows changes in steady state current and formal potential

Cyclic voltammograms of 12.5 and 50 µM H_2O_2 at a scan rate of 20 mV/s in A) Acetate pH 5 ± 100mM KCl and B) Tris pH 8.6 show current plateaus which can be used to understand the difference in how the electrochemistry is affected by the pH and/or buffer change in **Fig. S3.7.5** below. These CVs were used to select the appropriate applied potential for measurement of glucose oxidase kinetics in main text **Fig. 3.7.5A**. A shift in the plateau potential compared to PBS is demonstrated in acetate buffer and even more so in acetate KCl. No such shift is evident in Tris buffer.

Table S3.7.5: The following potentials were used for each buffer in generating **Fig. 3.5A**:

Acetate	Acetate KCl	PBS	PBS 8.1	Tris 8.6	Tris 8.8
0.65V	0.75V	0.55V	0.6V	0.55V	0.55V

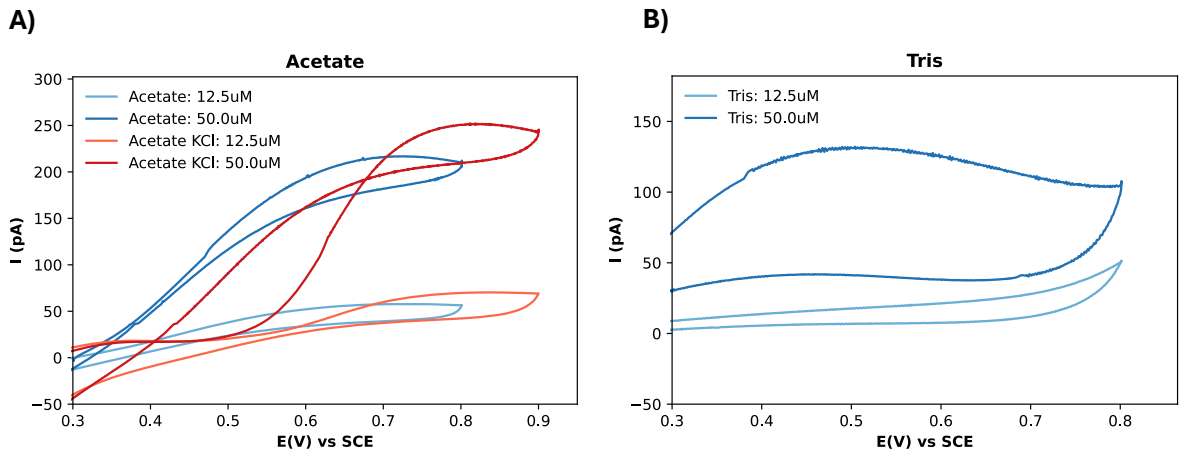

Figure S3.7.5 Oxidative portion of cyclic voltammograms for H_2O_2 in different buffers.

Section S3.7.6. – Chronoamperograms at pH 8.8 show current slopes which are comparable to negative decay of control peroxide measurements

The figure below shows a comparison between the data collected to attempt to assess GOx activity in high pH (in Tris buffer pH 8.8) compared to that for the H_2O_2 controls measured to account for changes in the current-concentration relationship. As is evident, the magnitude of the baseline decay is no longer negligible at the small reaction rates/slopes observed here, making accurate assessment of the reaction rate prone to substantial error.

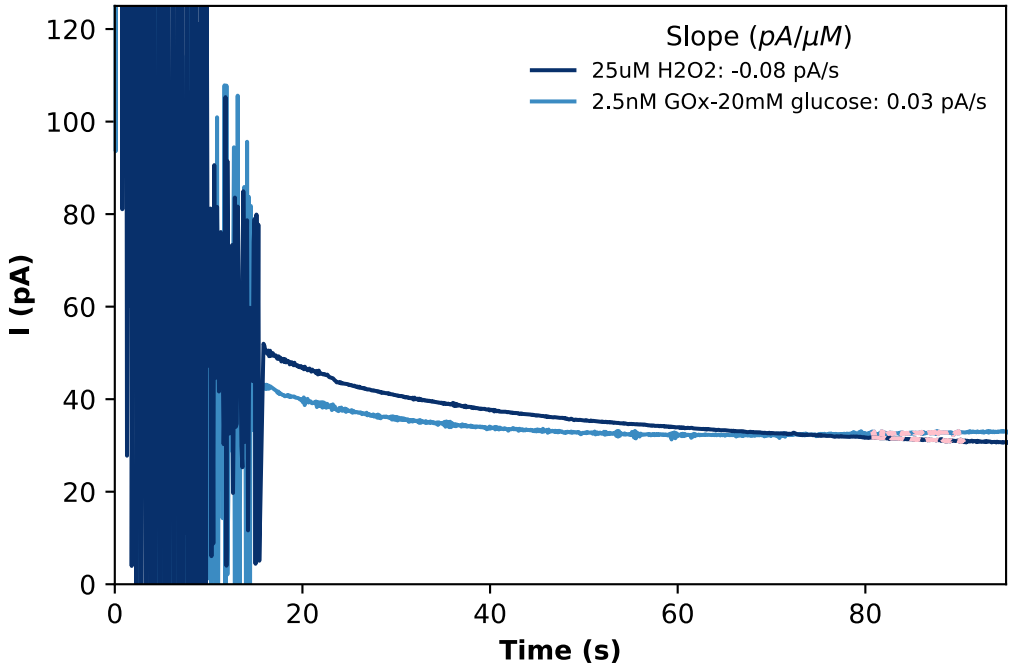

Figure S3.7.6 Comparison of decreasing current for peroxide standard (dark blue) to observed GOx kinetics (light blue) in Tris buffer pH 8.8 shows that the values are of the same magnitude.

References

1. Hall, S. B., Khudaish, E. A. & Hart, A. L. Electrochemical oxidation of hydrogen peroxide at platinum electrodes. Part III: Effect of temperature. *Electrochim Acta* **44**, 2455–2462 (1999).

2. Zhang, Y. & Wilson, G. S. Electrochemical oxidation of H2O2 on Pt and Pt + Ir electrodes in physiological buffer and its applicability to H2O2-based biosensors. *Journal of Electroanalytical Chemistry* **345**, 253–271 (1993).

3. Wheeler, C. R., Salzman, J. A., Elsayed, N. M., Omaye, S. T. & Korte, D. W. Automated assays for superoxide dismutase, catalase, glutathione peroxidase, and glutathione reductase activity. *Anal Biochem* **184**, 193–199 (1990).

4. Hall, S. B., Khudaish, E. A. & Hart, A. L. Electrochemical oxidation of hydrogen peroxide at platinum electrodes. Part 1. An adsorption-controlled mechanism. *Electrochim Acta* **43**, 579–588 (1998).

5. Prabhu, V. G., Zarapkar, L. R. & Dhaneshwar, R. G. Electrochemical studies of hydrogen peroxide at a platinum disc electrode. *Electrochim Acta* **26**, 725–729 (1981).

6. Wang, Y., Limon-Petersen, J. G. & Compton, R. G. Measurement of the diffusion coefficients of [Ru(NH3)6]3+ and [Ru(NH3)6]2+ in aqueous solution using microelectrode double potential step chronoamperometry. *Journal of Electroanalytical Chemistry* **652**, 13–17 (2011).

7. Arnao, M. B., Acosta, M., del Rio, J. A. & García-Cánovas, F. Inactivation of peroxidase by hydrogen peroxide and its protection by a reductant agent. *Biochimica et Biophysica Acta (BBA) - Protein Structure and Molecular Enzymology* **1038**, 85–89 (1990).

8. Ji, F. *et al*. Excited state electronic structures and photochemistry of different oxidation states of 2,2'-azino-bis-(3-ethylbenzothiazoline-6-sulfonic acid) (ABTS). *Spectrochim Acta A Mol Biomol Spectrosc* **253**, 119503 (2021).

4. Understanding Protein/Enzyme Electron Transport or Activity at the Ultimate Level of Detection Using Electrochemistry

4.1 How Does Electrochemistry Interface with Single Enzymes?

4.1.1 Single Enzyme Overview

Enzymes are the biological reaction machinery which enables the chemistry of life as we know it. Understanding the capabilities and mechanisms by which they catalyze reactions with high specificity in mild aqueous conditions has implications ranging from fundamental biology to applications such as industrial chemical synthesis [1], molecular bioelectronics [2], and drug development [3]. The growth of structural and molecular biology techniques alongside ensemble-based characterization methods allowed further insights into how these macromolecules achieve specificity and catalytic capabilities. Results from these techniques established that protein structures arrange steric and electrostatic factors for substrate binding [4] and influence the free energies of reaction pathways. [5*] A key discussion in enzymology is the role of dynamics in catalytic behavior. [6**] The nonstatic nature of enzymes and the influence of structural dynamics have both been recognized in allosteric regulation of protein activity [7], in substrate/product flux [8], and in charge transport mechanisms [9], but the mechanisms and influences of dynamics on the catalytic function in enzymes have been widely debated. [6**] Both thermodynamic changes in the stochastic sampling of conformational population distributions (stochastic dynamics) and coherent structural fluctuations have been questioned regarding their real impact on the catalytic chemical step. [10]

Ensemble-based measurements are inherently limited in addressing dynamics as they represent an averaging of all of the states of the molecules measured. In contrast, single-molecule methods are capable of delivering new insights regarding rare populations, multiple pathways, hidden intermediates, heterogeneity, and stochastic processes in biology. [11-13] As such, they

are contenders to address outstanding debates regarding enzymes. Imaging methods provide atomic-scale structural information via transmission electron microscopy and in vivo localization and conformational fluctuations via methods including single-molecule Förster resonance energy transfer and super-resolution microscopy. [13,14] Force methods such as optical trapping and atomic force microscopy (AFM) have provided a means to measure the energetics of protein folding. [15] Electroanalytical techniques — including those discussed herein — function in physiologically relevant conditions, offering superior spatial and sufficient temporal resolution to the aforementioned methods. [16-18] These methods circumvent the challenges associated with label- and amplification-based methods. [19-21]

Our core question, then, is to what extent can electrochemical single-entity methods contribute to the pursuit of fundamental understanding of enzymes? Armstrong et al. [22] started the field of protein film voltammetry (PFV) building on the original polarographic measurements of proteins in the lab of J. Heyrovsky [23] and sought to characterize the kinetics and thermodynamics of a monolayer of enzymes immobilized at an electrode surface. Observations from PFV drove interest in the mechanisms of charge transport within proteins, as summarized by Winkler and Gray. [24] Perhaps one of the most important observations from these studies was the direct electron transfer (ET) between redox centers and the electrode across long distances (>2 nm) through hitherto-presumed insulating peptide matrices. [25] To further understand this phenomenon, a host of techniques and architectures were developed to electrochemically address single entities following the initial observation of a single redox molecule via cycling in a nanogap Fox and Bard. [26] Fundamental to these methods is the use of a sensing apparatus and/or reaction volumes of comparable size to the entities being measured to achieve necessary signal-to-noise ratios. [27,28*] Among these techniques, nano-

impact electrochemistry (NIE) stands out because of the method's ability to probe the entity either while immobilized or freely diffusing in solution. [29] Also NIE, which is essentially a combination of chronoamperometry and micro/nano electrodes, mitigates the electrode's capacitance contribution. In addition, electrochemical scanning tunneling microscopy (EC-STM) and conductive atomic force microscopy have demonstrated single-molecule protein conductance measurement regardless of the redox behavior. [30,31] The capabilities of single-molecule electrochemical techniques to provide insight into the relationship between molecular structure and dynamics to catalytic rates and protein conductivity hint at these methods' potential contribution to the leading discussions in the enzyme behavior.

The goal of this minireview is to illuminate the frontiers, capabilities, and limitations of electrochemistry in understanding enzymatic behavior at the single-molecule level. The literature from the previous 2–3 years is highlighted which first discusses the capabilities of NIE to measure fundamental properties of enzyme behavior. We then discuss EC-STM developments to comment on its capabilities in understanding the environment's influence on experimental results, electronic properties' contributions to catalytic mechanisms, and protein dynamics. This work stands apart from other recent reviews centered on electrode architectures or electrochemical techniques to address single (bio)molecules by instead focusing on the molecular understanding electrochemistry can provide. By delineating the needs and capabilities of electrochemistry in these efforts, we hope to unite electrochemists with electrical engineers, nanotechnologists, and biologists to push these limits. Perspectives on future directions in single-enzyme electrochemical investigations are provided.

4.2 Single-Enzyme Electrochemistry Methods

4.2.1 Nano-impact Electrochemistry (NIE) for Single Enzyme Catalysis

The field of single-enzyme catalysis predominantly aims to unravel static and dynamic disorder contributions to the substrate turnover frequency, with a long-term debate on its relation to conformational changes. [32] With the advancement in low-noise electronic instrumentation, electrochemists are attempting to provide an orthogonal approach based on charge rather than photons to detect and investigate a single enzyme in operando. Lemay's seminal work by Hoeben et al. [33] demonstrated that the catalytic reaction of less than 50 immobilized hydrogenase enzymes can be observed voltammetrically with nanoelectrodes. Concurrently, Bard [34] pointed out that going down to a single-enzyme resolution would require experimental schemes that deviated from conventional PFV, which itself is limited by capacitance contribution. In 2016, Sekretaryova et al. [35] demonstrated the statement's validity using NIE, measuring the transient current response of a single laccase enzyme colliding and adsorbing onto a gold microelectrode held at a sufficiently reductive potential (Figure 4.1a).[36] The current spikes represent direct electrical communication between the electrode and the buried redox center. The spike magnitudes were used to calculate the turnover frequency (k_{cat}). Typically, discrete irreversible adsorption of an electroactive catalyst on a microelectrode produces a steady-state current corresponding to a continuous substrate turnover.[37] However, in this case, current signals decay on a millisecond timescale. The authors' interpretation was that the current decay is caused by partial denaturation or structural changes of the enzyme implying that chronoamperometric methods are sensitive to protein conformational changes. The methods are also capable of studying ET relevant to catalytic mechanisms. This was achieved by altering the overpotential, thus prohibiting unnatural intermolecular ET from

being the rate-limiting step. In the same year, Han et al. [38] reported on the electrochemistry of single horseradish peroxidase catalyzing hydrogen peroxide reduction while entrapped in a bilayer lipid–modified electrode. The authors observed a steady-state current lasting up to 80 s that was interpreted as the continuous catalytic activity of the peroxidase toward hydrogen peroxide without noticeable deactivation. In addition, the authors pointed out that the plateau current is turbulent (~50 fA amplitude) and significantly higher than the inherent noise of the instrument (~10 fA). They suggested that NIE might correlate current fluctuations with the dynamic activity of individual enzymes.

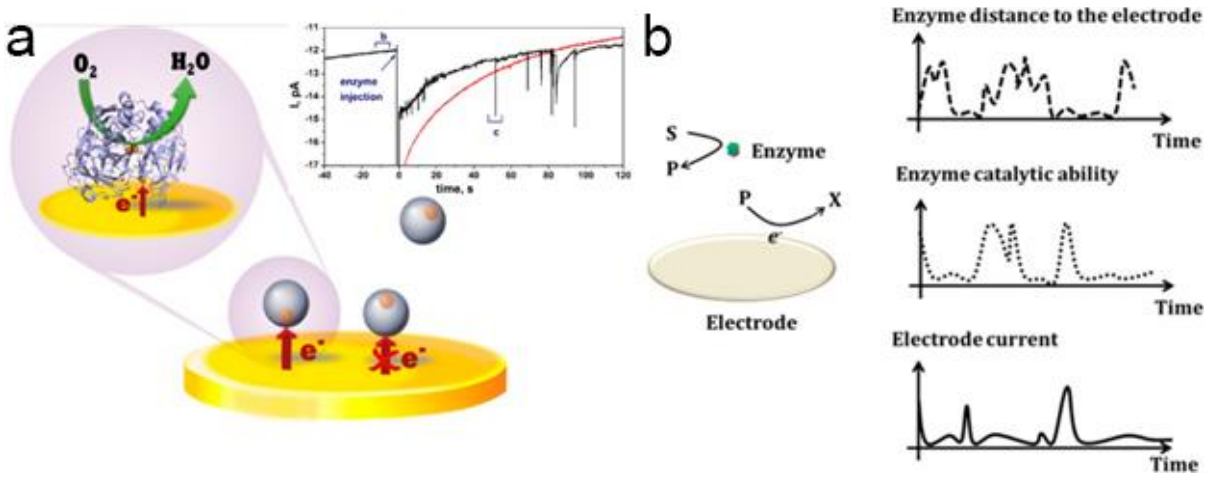

Figure 4.1 Possible routes for electrochemical detection of single enzymes via NIE. (a) An individual enzyme (here, laccase) is adsorbed onto a microelectrode and directly exchanges charge while in proper spatial orientation. Without the enzyme's substrate (oxygen) in solution, the chronoamperogram decays monotonically (inset, red curve) in contrast to current spikes seen when the solution contains atmospheric oxygen (inset, black curve). (b) Random walks of a freely diffusing enzyme can cause an intimate electrochemical coupling between the electroactive product of the diffusing enzyme and a microelectrode. The current output depends on the spatial location of the diffusing enzyme with respect to the electrode and its catalytic activity. Adapted from the study by Sekretaryova et al. [35] and Lin et al. [39]. with permission.

In contrast, Lin et al. [39, 40], Kätelhön et al. [41], and Jiang et al. [42*] have focused on the catalytic

response arising from a freely diffusing catalase enzyme near a microelectrode active toward catalysis of the enzyme's product; the enzyme does not adsorb onto the electrode. Catalase represents an extreme case of a highly efficient enzyme with an average turnover frequency on the order of 105 s^{-1} [43]. Experimental and theoretical investigations indicate that the current output depends upon the enzyme's catalytic activity and distance from the electrode (**Figure 4.1b**). Intriguingly, even at such rapid catalytic rates, the expected current induced by the enzyme's product should theoretically be below the limit of detection (see **Figure 4.2a**). In parallel, Jiang et al. [42*] observed an increase in the frequency of impacting catalase enzymes while experimental conditions were kept identical and only the substrate (hydrogen peroxide) concentration was increased. Further corroborated by fluorescence correlation spectroscopy diffusion measurements, the authors concluded that substrate-induced increase in enzyme diffusion could be the physical origin of the observation [44]. In all experiments, unexpectedly large current transients (on the order of tens of pA) were observed (**Figure 4.2b**). In fact, all reports of single-enzyme electrochemistry so far produced currents of at least 1 pA which corresponds to a pseudo–first-order rate constant of kcat ≈ 107 s^{-1}. It was further hypothesized in the case of catalase that this could be due to the reduction of oxygen bubbles created during enzyme catalysis [41] or by fluctuation in the enzyme's catalytic activity. [39**] Besides featuring unique phenomena of NIE, it is worth noting the technique's limits. The methods illustrated in Figure 1 require certain structural and chemical properties; the former being an accessible redox center, the latter being the redox-active substrate or products. In addition, **Figure 4.3C** illustrates the severity of NIE's current limitations; the average kcat of most enzymes varies between 10^{-1} to 10^{-3} s^{-1} [45] which cannot be detected electrochemically with state-of-the-art instrumentation [46]. This stems from the shot noise due to instrumentation background signals

which dictates the baseline noise level, masking catalytic events occurring in the normal range of enzyme activity. [47] Thus, NIE is unable to provide the resolution to rival optical spectroscopy. Nonetheless, the potential for label-free detection of freely diffusing enzymes justifies the quest to continue improving NIE electronic resolution.

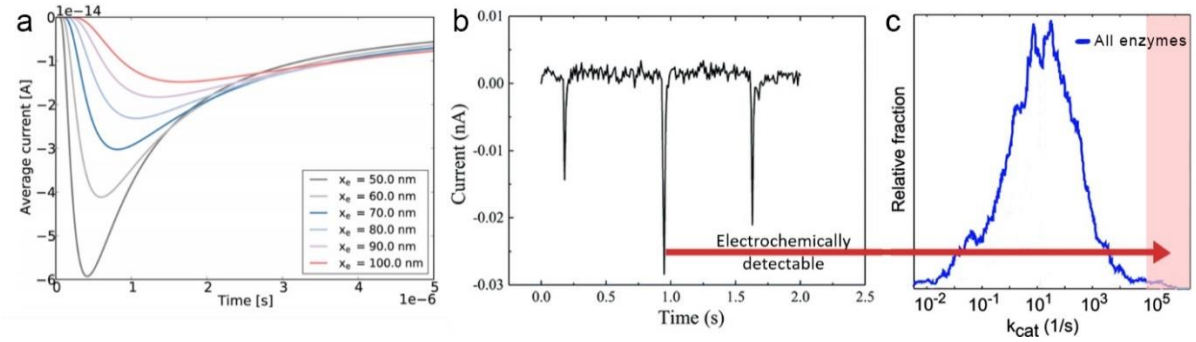

Figure 4.2 Most enzymes cannot be detected individually using NIE. (a) Simulated average current produced by a freely diffusing enzyme that produces an electroactive product at distance X_e from the electrode surface, as a function of time. The diffusion coefficient of the product is set to $D_p = 10^{-9}$ m^2 s^{-1}. (b) Experimental current transients observed by the Jiang et al. [42], on the order of tens of pA. (c) The turnover frequencies of most enzymes (~60%) are in the range of 1–100 s−1. Adapted from the study by Kätelhön et al. [41], Jiang et al. [42], and Bar-Even et al. [45]. with permission. NIE, nano-impact electrochemistry.

4.2.2 EC-STM for Conductance of Fixed Single Enzymes

Ensemble-based scientific efforts have uncovered much about protein layer conductance, including, but not limited to, the fundamental mechanisms, its dependence upon environment and set-up (e.g. electrode material [48], temperature [49,50], the type and number of chemical contacts with electrodes [51,52]) and upon protein composition (e.g. chirality [53,54], nature of the redox site [55-57]).

Moving from ensemble to individual enzyme studies requires techniques using nanoscale probes such as EC-STM. The entity of interest is wired between the probe tip and the conductive surface (an electrode), with potentiostatic control over both. The inclusion of reference and counter electrodes forms the electrochemical cell (**Figure 4.3a**). [58,59] Current passing through the protein from the tip is measured, providing insights on enzyme electronic structure and heterogeneity. There is a similar technique—cAFM—but here we emphasize the literature using EC-STM.

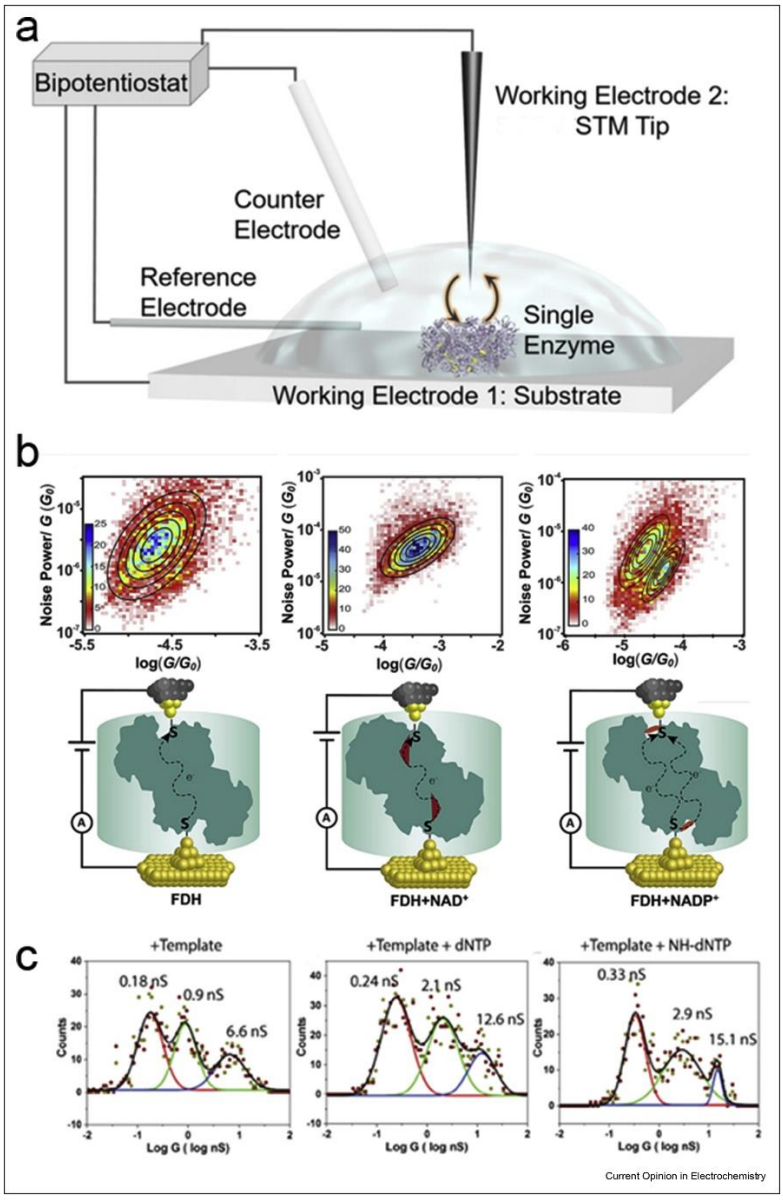

Figure 4.3 Scanning tunneling microscopy can provide insight into the conductance pathways in a single enzyme. (a) An extended technique for STM, transforming the conductive surface and STM tip into working electrodes. With the addition of counter and reference electrodes, the end result is a tiny electrochemical cell. The tip is chemically wired to the enzyme. (b) Flicker noise analysis of (left to right) FDH, FDH-NAD+, FDH-NADP+, with corresponding schematics in the second row. The noise scales with average conductance. (c) Conductance distributions of Φ26 polymerase bound with either a DNA template, a DNA template with nucleotide triphosphate (dNTP), or a DNA template with nonhydrolyzable dNTP. Adapted from. the study by Kornienko et al. [58], Zhuang et al. [70**] and Zhang et al. [72**] with permission. FDH, formate dehydrogenase; STM, scanning tunneling microscopy.

Serving as a theoretical basis to understand protein conductance via EC-STM, the works of Nathanael et al. [60], Teo et al. [61], and Futera et al. [62*] examined the fundamental process of ET in proteins, which has predominantly two mechanisms: a stepping-stone, charge hopping process and a single-step, superexchange process [63,64]. Nathanael et al. [60] studied the nature of long-range ET in peptides, focusing on the stabilizing effects amide-neighboring groups have on the radicals/radical cations needed for charge hopping. The authors demonstrated that even amino acids with high redox potentials, phenylalanine for example, phenylalanine, can act as a relay station with the assistance of this effect. Teo et al. [61] further pointed out that protein ET is restricted to tunneling among redox-active cofactors and, under strongly oxidizing conditions, a few privileged amino-acid side chains. Futera et al. [62*] focused on the single-step conduction process; they applied a gate voltage to a multiheme cytochrome sandwiched between two Au (111) electrodes, which then exhibited off-resonant coherent ET across a 3 nm junction. Simulation and theory ascribe the ET to bringing the Fermi levels of the protein and the electrode into better alignment, allowing valence band orbitals to delocalize.

To accurately understand the nature of conductance changes in EC-STM results, the effect of experimental set-ups should be taken into account. Ruiz et al. [65] investigated two experimental EC-STM modes to investigate ET in azurin, comparing the wild type to one with a cysteine point mutation. Conductance measurements of 'dynamic tapping' (The protein-modified STM tip is oscillated at various distances from the electrode surface) and static 'blinking' (spontaneous bridging of protein between fixed electrodes) modes were largely in agreement, although conductance in the dynamic mode was slightly smaller, which they suggested was due to protein stretching. Furthermore, by examining the conductance dependence on an applied gate voltage and temperature, they concluded that a change in ET mechanism occurred

with the engineered cysteine mutation. Computational studies suggest that a change in orbital localization as a result of the mutation is responsible for the change in behavior. Similarly, Zhang et al. [66*] investigated the influence of the contacts between proteins and electrodes at the single-bioentity level and observed conductances on the order of nanosiemens. They concluded that at least one strongly bonded contact is required for observable current, but the nature of the second contact (covalent linkage or complexation) contributed minimally to current readings. Of note, they demonstrate that even redox-inactive proteins can act as conductors and that the conduction is independent of the distance between electrodes. The latter observation is in line with macroscale conductance measurements showing that conductance via proteins with lengths above 2 nm are relatively similar, regardless of the protein measured [30].

Beyond the contributions from the experimental set-up, biologically relevant parameters that influence conductance include changes in protein composition and conformation. Zheng et al.'s observations in hemoglobin, superoxide dismutase, and bovine serum albumin showed a correlation between conductance and secondary structure using EC-STM and cAFM. [9] They concluded that the α-domain shows higher conductance than the β-domain and that bovine serum albumin conductance has an 'exponential-like' relation with its α-helical content. [9,67] Artés et al. [68,69] noted the contribution of azurin's redox site to its conductance, recording current fluctuations as a result of switching events between the metallic center's Cu(I) and Cu(II) states under electrochemical control. Zhuang et al. [70**] discovered that the binding of formate dehydrogenase (FDH) to a charged coenzyme (NAD+)–boosted charge transport by ~2100% and mediated a distinct ET pathway, corresponding to bioactivity. Thus, the authors correlated single-enzyme conductance with its activity. Using EC-STM, Zhang et al. [71]

measured the conductance changes of an electrochemically inert protein (αVβ3 extracellular domain of integrin) upon peptide ligand binding. They additionally observed Φ26 DNA polymerase activity, recording unique conductance distributions for different conformational populations induced by adding substrate (Figure 4.3c). This was the first case of direct electrical measurement of single-enzyme conductance during natural catalysis in electrochemical conditions [72**]. These studies highlighted here demonstrate the burgeoning application of EC-STM in single proteins (and particularly enzymes) characterization.

4.3 Conclusions and Recommendations

In this minireview, we first discussed chronoamperometric investigations of enzymes with NIE, noting results which display deviation in measured currents from theoretical values and ascribe them to fluctuations in enzyme behavior and experimental conditions. Factors which influence NIE measurements, such as enzyme stability at the interface, are also discussed. We note that the nano-impacts technique is currently insufficient to use as a tool to investigate catalysis arising from the vast majority of enzymes at a single level because of electronic resolution limitation. We then described contemporary single-molecule ET research, focusing largely on EC-STM and the experimental factors which influence measurements, including the electronic structure of the bridging material as dictated by protein structure and sequence, and the nature of the contacts. Highlighted studies note the influence of protein structure on observed conductance, including for redox-inactive proteins. This culminates with the first demonstration by Lindsay et al. in which conductance fluctuations serve as direct electrical measurement of conformational change during natural enzymatic catalysis [72].

This raises a compelling question regarding single-enzyme conductance: can enzyme conductance and/or ET pathways be used to unravel catalytic mechanisms? In the case of redox-active enzymes, conductance shows a correlation to ET kinetics, orbital alignment, and redox potential, which can, for instance, determine the local potential of the redox site and show its sensitivity to electron-donating groups. [73,74] The charge transport mechanism may be governed by the applied potential and permits control over local electronic structure relaxation during charge injection. However, it is not always clear which path electrons take, and, in the case of redox-inactive enzymes, a logical path for electron transport or localization is not inherently obvious. [75] In tandem with developing theory [74], further work will be required to link conductivity to catalytically contributing elements within the enzyme — contemporary discussion of which centers around the active site's local electric field. [76] If protein conductance measurements are to be used as more than a direct readout of conformational dynamics, we must evaluate whether they also provide information on the local electric field. Intuitively, electrochemistry provides a solid ground for investigating electric field effects. However, reports thus far have focused on the ET rate and mechanisms between a protein and an electrode [77,78] and have yet to explore the possibility of being used to alter electric fields.

How do we further elucidate the intricacies of enzyme dynamics? Combinations with spectroscopic techniques represent the possibility to simultaneously obtain a wealth of information about a system. Of exceptional interest are developments in spectroscopic methods, such as nano-IR [79] and Stark–Lo Surdo spectroscopy [80] which can provide high-resolution secondary structure details or map local electric fields, respectively. Of additional interest are nanopore techniques, which measures changes in ionic currents through ~ nanometer openings which are sensitive to targets entering the pore. We suggest that nanopores

may find use as nexuses for long (~10s of seconds), oriented interactions with enzymes in controllable environments which do not require direct contact with probes and allow interfacing with other measurement techniques. [12,81]

As the understanding of enzyme catalysis approaches a point of potential coalescence around electric field descriptions [76], we call for the field, which fundamentally unifies chemistry and electricity, to join the foray forward in concert with enzymologists, spectroscopists, and theorists.

4.4 References for Chapter 4

1. a) H. Chen, F. Dong, S.D. Minteer The progress and outlook of bioelectrocatalysis for the production of chemicals, fuels and materials *Nat Catal.*, 3 (2020), pp. 225-244, 10.1038/s41929-019-0408-2 b) A. Katranidis, Jörg Fitter Single-molecule techniques and cell-free protein synthesis: a perfect marriage *Anal Chem*, 91 (2019), pp. 2570-2576, 10.1021/acs.analchem.8b03855
2. W. Zhou, X. Dai, C.M. Lieber: Advances in nanowire bioelectronics *Rep Prog Phys*, 80 (2017), Article 016701, 10.1088/0034-4885/80/1/016701
3. A.Y. Chen, R.N. Adamek, B.L. Dick, C.V. Credille, C.N. Morrison, S.M. Cohen: Targeting metalloenzymes for therapeutic intervention *Chem Rev*, 119 (2018), pp. 1323-1455, 10.1021/2Facs.chemrev.8b00201
4. E. Persch, O. Dumele, F. Diederich Molecular recognition in chemical and biological systems *Angew Chem Int Ed*, 54 (2015), pp. 3290-3327, 10.1002/anie.201408487
5. [**]G. Jindal, A. Warshel Misunderstanding the preorganization concept can lead to confusions about the origin of enzyme catalysis *Proteins*, 85 (2017), pp. 2157-2161, 10.1002/2Fprot.25381

• • Reviews leading arguments about the nature of enzyme catalysis discussing preorganization as the central concept.

6. [*] F.M. Menger, F. Nome Interaction vs preorganization in enzyme catalysis. A dispute that calls for resolution *ACS Chem Biol*, 14 (2019), pp. 1386-1392, 10.1021/acschembio.8b01029

• • Counter-discussion to Warshel's 2017 review defending the merit of spatiotemporal effects in catalysis.

7. E. Guarnera, I.N. Berezovsky Allosteric sites: remote control in regulation of protein activity *Curr Opin Struct Biol*, 37 (2016), pp. 1-8, 10.1016/j.sbi.2015.10.004

8. C. Narayanan, D.N. Bernard, N. Doucet: Role of conformational motions in enzyme function: selected methodologies and case studies *Catalysts*, 6 (2016), p. 81, 10.3390/catal6060081
9. X.Y. Zhang, J. Shao, S.X. Jiang, B. Wang, Y. Zheng Structure-dependent electrical conductivity of protein: its differences between alpha-domain and beta-domain structures *Nanotechnology*, 26 (2015), p. 125702, 10.1088/0957-4484/26/12/125702
10. a) I. Tuñón, D. Laage, J.T. Hynes: Are there dynamical effects in enzyme catalysis? Some thoughts concerning the enzymatic chemical step *Arch Biochem Biophys*, 582 (2015), pp. 42-55, 10.1016/j.abb.2015.06.004 b) R.P. Bora, A. Warshel: Perspective: defining and quantifying the role of dynamics in enzyme catalysis *J Chem Phys*, 144 (2016), p. 180901, 10.1063/1.4947037
11. K. Gaus, J.J. Gooding: Single-molecule sensors: challenges and opportunities for quantitative analysis *Angew Chem Int Ed*, 55 (2016), pp. 11354-11366, 10.1002/anie.201600495
12. Y. Ying, Y. Long: Nanopore-based single-biomolecule interfaces: from information to knowledge *J Am Chem Soc*, 141 (2019), pp. 15720-15729, 10.1021/jacs.8b11970
13. T. Ha: Single-molecule methods leap ahead *Nat Methods*, 10 (2014), pp. 1015-1018, 10.1038/nmeth.3107
14. C. Cremer, U. Birk Perspectives in super-resolved fluorescence microscopy: what comes next? *Front Physiol*, 4 (2016), p. 11, 10.3389/fphy.2016.00011
15. J. Schönfelder, D. De Sancho, R. Perez-Jimenez: The power of force: insights into the protein folding process using single-molecule force spectroscopy *J Mol Biol*, 428 (2016), pp. 4245-4257, 10.1016/j.jmb.2016.09.006
16. M. Zhou, J.E. Dick, A.J. Bard: Electrodeposition of isolated platinum atoms and clusters on bismuth—characterization and electrocatalysis *J Am Chem Soc*, 139 (2017), pp. 17677-17682, 10.1021/jacs.7b10646
17. I.M. Derrington, J.M. Craig, E. Stava, A.H. Laszlo, B.C. Ross, H. Brinkerhoff, I.C. Nova, K. Doering, B.I. Tickman, M. Ronaghi, J.G. Mandell, K.L. Gunderson, J.H. Gundlach: Subangstrom single-molecule measurements of motor proteins using a nanopore *Nat Biotechnol*, 33 (2015), pp. 1073-1075, 10.1038/2Fnbt.3357
18. J. Li, Z. Peng, E. Wang: Tackling grand challenges of the 21st century with electroanalytical chemistry *J Am Chem Soc*, 140 (2018), pp. 10629-10638, 10.1021/jacs.8b01302
19. D. Aird, M.G. Ross, W. Chen, M. Danielsson, R. Fennell, C. Russ, D.B. Jaffe, C. Nusbaum, A. Gnirke Analyzing and minimizing PCR amplification bias in Illumina sequencing libraries *Genome Biol*, 12 (2011), p. R18, 10.1186/gb-2011-12-2-r18
20. D.G. Rawale, K. Thakur, S.R. Adusumalli, V. Rai: Chemical methods for selective labeling of proteins *Eur J Org Chem*, 40 (2019), pp. 6749-6763, 10.1002/ejoc.201900801
21. M.K. Quinn, N. Gnan, S. James, A. Ninarello, F. Sciortino, E. Zaccarelli, J.J. McManus: How fluorescent labelling alters the solution behaviour of proteins *Phys Chem Chem Phys*, 46 (2015), pp. 31177-31187, 10.1039/C5CP04463D
22. F.A. Armstrong, H.A. Heering, J. Hirst: Reactions of complex metalloproteins studied by protein-film voltammetry *Chem Soc Rev*, 26 (1997), pp. 169-179, 10.1039/CS9972600169
23. M. Heyrovsky: Early polarographic studies on proteins *Electroanalysis*, 16 (2004), pp. 1067-1073, 10.1002/elan.200403008

24. J.R. Winkler, H.B. Gray Electron flow through metalloproteins *Chem Rev*, 114 (2014), pp. 3369-3380, 10.1021/cr4004715
25. a) H.B. Gray, J.R. Winkler: Electron tunneling through proteins *Q Rev Biophys*, 36 (2003), pp. 341-372, 10.1017/S0033583503003913 b) V. Fourmond, C. Léger: Protein electrochemistry: questions and answers Biophotoelectrochemistry: from bioelectrochemistry to biophotovoltaics (2016), pp. 1-41, 10.1007/10_2015_5016
26. F.F. Fan, A.J. Bard: Electrochemical detection of single molecules Science, 267 (1995), pp. 871-874, 10.1126/science.267.5199.871
27. S. Lu, Y. Peng, Y. Ying, Y. Long: Electrochemical sensing at a confined space *Anal Chem*, 92 (2020), pp. 5621-5644, 10.1021/acs.analchem.0c00931
28. R.R. Nazmutdinov, T.T. Zinkicheva, S.A. Shermukhamedov, J. Zhang, J. Ulstrup: Electrochemistry of single molecules and biomolecules, molecular scale nanostructures, and low-dimensional systems *Curr. Opin. Electrochem.*, 7 (2018), pp. 179-187, 10.1016/j.coelec.2017.11.013

• • Wide review covering applications of EC-STM by an expert in the field.

29. J. Zhang, Y. Zhou: Nano-impact electrochemistry: analysis of single bioentities *Trends Anal Chem*, 123 (2020), p. 115768, 10.1016/j.trac.2019.115768
30. N. Amdursky, D. Marchak, L. Sepunaru, I. Pecht, M. Sheves, D. Cahen: Electronic transport via proteins *Adv Mater*, 26 (2014), pp. 7142-7161, 10.1002/adma.201402304
31. C.D. Bostick, S. Mukhopadhyay, I. Pecht, M. Sheves, D. Cahen, D. Lederman: Protein bioelectronics: a review of what we do and do not know *Rep Prog Phys*, 81 (2018), Article 026601, 10.1088/1361-6633/aa85f2
32. a) S.C.L. Kamerlin, A. Warshel: At the dawn of the 21st century: is dynamics the missing link for understanding enzyme catalysis? *Proteins*, 78 (2010), pp. 1339-1375, 10.1002/2Fprot.22654 b)K.A. Henzler-Wildman, M. Lei, V. Thai, S.J. Kerns, M. Karplus, D. Kern: A hierarchy of timescales in protein dynamics is linked to enzyme catalysis *Nature*, 450 (2007), pp. 913-916, 10.1038/nature06407 c) T.G. Terentyeva, H. Engelkamp, A.E. Rowan, T. Komatsuzaki, J. Hofkens, C. Li, K. Blank: Dynamic disorder in single-enzyme experiments: facts and artifacts *ACS Nano*, 6 (2012), pp. 346-354, 10.1021/nn203669r
33. F.J.M. Hoeben, S. Meijer, C. Dekker, S.P.J. Albracht, H.A. Heering, S.G. Lemay: Toward single-enzyme molecule electrochemistry: [NiFe]-Hydrogenase protein film voltammetry at nanoelectrodes *ACS Nano*, 2 (2008), pp. 2497-2504, 10.1021/nn800518d
34. A.J. Bard: Toward single enzyme molecule electrochemistry *ACS Nano*, 2 (2008), pp. 2437-2440, 10.1021/nn800801z
35. A.N. Sekretaryova, M.Y. Vagin, A.P.F. Turner, M. Eriksson: Electrocatalytic currents from single enzyme molecules *J Am Chem Soc*, 138 (2016), pp. 2504-2507, 10.1021/jacs.5b13149
36. S.V. Sokolov, S. Eloul, E. Kätelhön, C. Batchelor-McAuley, R.G. Compton: Electrode-particle impacts: a users guide *Phys Chem Chem Phys*, 19 (2017), pp. 28-43, 10.1039/C6CP07788A
37. A.J. Bard, H. Zhou, S.J. Kwon: Electrochemistry of single nanoparticles via electrocatalytic amplification *Isr J Chem*, 50 (2010), 10.1002/ijch.201000014

38. L. Han, W. Wang, J. Nsabimana, J. Yan, B. Ren, D. Zhan: Single molecular catalysis of a redox enzyme on nanoelectrodes *Faraday Discuss*, 193 (2016), pp. 133-139, 10.1039/C6FD00061D
39. C. Lin, L. Sepunaru, E. Kätelhön, R.G. Compton: Electrochemistry of single enzymes: fluctuations of catalase activities *J Phys Chem Lett*, 9 (2018), pp. 2814-2817, 10.1021/acs.jpclett.8b01199

• • Theoretical discussion on the observations of catalase nano-impact electrochemistry and the experimental deviation from expected values.

40. C. Lin, E. Kätelhön, L. Sepunaru, R.G. Compton: Understanding single enzyme activity via the nano-impact technique *Chem Sci*, 8 (2017), pp. 6423-6432, 10.1039/C7SC02084H
41. E. Kätelhön, L. Sepunaru, A.A. Karyakin, R.G. Compton: Can nanoimpacts detect single-enzyme activity? Theoretical considerations and an experimental study of catalase impacts *ACS Catal*, 6 (2016), pp. 8313-8320, 10.1021/acscatal.6b02633
42. [*] L. Jiang, I. Santiago, J. Foord: Observation of nanoimpact events of catalase on diamond ultramicroelectrodes by direct electron transfer *Chem Commun*, 53 (2017), pp. 8332-8335, 10.1039/C7CC04085G

• • Fluorescence correlation spectroscopy diffusion measurements corroborate increase in collision frequency of catalase nano-impact electrochemistry.

43. R.F. Beers Jr., I.W. Sizer: A spectrophotometric method for measuring the breakdown of hydrogen peroxide by catalase *J Biol Chem*, 195 (1952), pp. 133-140
44. C. Riedel, R. Gabizon, C.A.M. Wilson, K. Hamadani, K. Tsekouras, S. Marqusee, S. Pressé, C. Bustamante: The heat released during catalytic turnover enhances the diffusion of an enzyme Nature, 517 (2015), pp. 227-230, 10.1038/nature14043
45. A. Bar-Even, E. Noor, Y. Savir, W. Liebermeister, D. Davidi, D.S. Tawfik, R. Milo: The moderately efficient enzyme: Evolutionary and physicochemical trends shaping enzyme parameters *Biochemistry*, 50 (2011), pp. 4402-4410, 10.1021/bi2002289
46. J. Yao, K.D. Gillis: Quantification of noise sources for amperometric measurement of quantal exocytosis using microelectrodes *Analyst*, 137 (2012), pp. 2674-2681, 10.1039/C2AN35157A
47. R. Gao, M.A. Edwards, J.M. Harris, H.S. White: Shot noise sets the limit of quantification in electrochemical measurements *Curr. Opin. Electrochem.*, 22 (2020), pp. 170-177, 10.1016/j.coelec.2020.05.010
48. L. Zhang, K.P. Kepp, J. Ulstrup, J. Zhang: Redox potentials and electronic states of iron porphyrin IX adsorbed on single crystal gold electrode surfaces *Langmuir*, 34 (2018), pp. 3610-3618, 10.1021/acs.langmuir.8b00163
49. L. Sepunaru, I. Pecht, M. Sheves, D. Cahen: Solid-state electron transport across azurin: from a temperature-independent to a temperature-activated mechanism *J Am Chem Soc*, 133 (2011), pp. 2421-2423, 10.1021/ja109989f
50. N. Amdursky, D. Ferber, I. Pecht, M. Sheves, D. Cahen: Redox activity distinguishes solid-state electron transport from solution-based electron transfer in a natural and

artificial protein: cytochrome C and hemin-doped human serum albumin *Phys Chem Chem Phys*, 15 (2013), pp. 17142-17149, 10.1039/C3CP52885E
51. M.W. Shinwari, M.J. Deen, E.B. Starikov, G. Cuniberti: Electrical conductance in biological molecules *Adv Funct Mater*, 20 (2010), pp. 1865-1883, 10.1002/adfm.200902066
52. J.A. Fereiro, G. Porat, T. Bendikov, I. Pecht, M. Sheves, D. Cahen: Protein electronics: chemical Modulation of contacts control energy level Alignment in gold-azurin-gold junctions *J Am Chem Soc*, 140 (2018), pp. 13317-13326, 10.1021/jacs.8b07742
53. V. Kiran, S.R. Cohen, R. Naaman: Structure dependent spin selectivity in electron transport through oligopeptides *J Chem Phys*, 146 (2017), Article 092302, 10.1063/1.4966237
54. R. Naaman, Y. Paltiel, D.H. Waldeck: Chiral molecules and the spin selectivity effect *J Phys Chem Lett*, 11 (2020), pp. 3660-3666, 10.1021/acs.jpclett.0c00474
55. D.N. Axford, J.J. Davis: Electron flux through apo-and holoferritin *Nanotechnology*, 18 (2007), p. 145502, 10.1088/0957-4484/18/14/145502
56. W. Li, L. Sepunaru, N. Amdursky, S.R. Cohen, I. Pecht, M. Sheves, D. Cahen: Temperature and force dependence of nanoscale electron transport via the Cu protein azurin *ACS Nano*, 6 (2012), pp. 10816-10824, 10.1021/nn3041705
57. K.S. Kumar, R.R. Pasula, S. Lim, C.A. Nijhuis: Long-range tunneling processes across ferritin-based junctions *Adv Mater*, 28 (2015), pp. 1824-1830, 10.1002/adma.201504402
58. N. Kornienko, K.H. Ly, W.E. Robinson, N. Heidary, J.Z. Zhang, E. Reisner: Advancing techniques for investigating the enzyme-electrode interface *Acc Chem Res*, 52 (2019), pp. 1439-1448, 10.1021/acs.accounts.9b00087
59. A.K. Yagati, J. Min, J. Choi Electrochemical scanning tunneling microscopy (ECSTM) – from theory to future applications *Surface and Corrosion Science* M. Aliofkhazraei (Ed.), Modern electrochemical methods in nano, vol. 3 (2014), pp. 55-81, 10.5772/57236
60. J.G. Nathanael, L.F. Gamon, M. Cordes, P.R. Rablen, T. Bally, K.M. Fromm, B. Giese, U. Wille: Amide neighbouring-group effects in peptides: phenylalanine as relay amino acid in long-distance electron transfer Chembiochem, 19 (2018), pp. 922-926, 10.1002/cbic.201800098
61. R.D. Teo, R. Wang, E.R. Smithwick, A. Migliore, M.J. Therien, D.N. Beratan: Mapping hole hopping escape routes in proteins *Proc Natl Acad Sci USA*, 116 (2019), pp. 15811-15816, 10.1073/pnas.1906394116
62. [*] Z. Futera, I. Ide, B. Kayser, K. Garg, X. Jiang, J.H. van Wonderen, J.N. Butt, H. Ishii, I. Pecht, M. Sheves, D. Cahen, J. Blumberger: Off-resonant coherent electron transport over three nanometers in multi-heme protein bioelectronic junctions *arXiv* (2020) https://arxiv.org/abs/2007.10384

• • Dominant ET pathway for multi-redox-center proteins is a single-step, superexchange process as opposed to charge hopping using amino acid side-chains as stepping stones.

63. N.L. Ing, M.Y. El-Naggar, A.I. Hochbaum: Going the distance: long-range conductivity in protein and peptide bioelectronic materials *J Phys Chem B*, 122 (2018), pp. 10403-10423, 10.1021/acs.jpcb.8b07431
64. D.N. Beratan: Why are DNA and protein electron transfer so different? *Annu Rev Phys Chem*, 70 (2019), pp. 71-97, 10.1146/annurev-physchem-042018-052353

65. M.P. Ruiz, A.C. Aragonès, N. Camarero, J.G. Vilhena, M. Ortega, L.A. Zotti, R. Pérez, J.C. Cuevas, P. Gorostiza, I. Díez-Pérez: Bioengineering a single-protein junction *J Am Chem Soc*, 139 (2017), pp. 15337-15346, 10.1021/jacs.7b06130
66. [*] B. Zhang, W. Song, P. Pang, H. Lai, Q. Chen, P. Zhang, S. Lindsay: Role of contacts in long-range protein conductance *Proc Natl Acad Sci USA*, 116 (2019), pp. 5886-5891, 10.1073/pnas.1819674116

• • Notes the importance of a single covalent contact for EC-STM measurements as well as the benevolence to secondary contact.

67. J. Yu, Y. Chen, L. Xiong, X. Zhang, Y. Zheng: Conductance changes in bovine serum albumin caused by drug-binding triggered structural transitions *Materials*, 12 (2019), p. 1022, 10.3390/ma12071022
68. J.M. Artés, M. López-Martínez, I. Díez-Pérez, F. Sanz, P. Gorostiza: Conductance switching in single wired redox proteins *Small*, 10 (2014), pp. 2537-2541, 10.1002/smll.201303753
69. J.M. Artés, I. Díez-Pérez, Pau Gorostiza: Transistor-like behavior of single metalloprotein junctions *Nano Lett*, 12 (2012), pp. 2679-2684, 10.1021/nl2028969
70. [**] X. Zhuang, A. Zhang, S. Qiu, C. Tang, S. Zhao, H. Li, Y. Zhang, Y. Wang, B. Wang, B. Fang, W. Hong: Coenzyme coupling boosts charge transport through single bioactive enzyme junctions *iScience*, 23 (2020), p. 101001, 10.1016/2Fj.isci.2020.101001

• • Binding of charged coenzymes changes ET pathway and strongly enhances conductance.

71. B. Zhang, W. Song, P. Pang, Y. Zhao, P. Zhang, I. Csabai, G. Vattay, S. Lindsay: Observation of giant conductance fluctuations in a protein *Nano Futures*, 1 (2017), Article 035002, 10.1088/2399-1984/aa8f91
72. [**] B. Zhang, H. Deng, S. Mukherjee, W. Song, X. Wang, S. Lindsay Engineering an enzyme for direct electrical monitoring of activity *ACS Nano*, 14 (2020), pp. 1360-1368, 10.1021/acsnano.9b06875

• • Direct electrical measurement of conformational changes induced by substrate-binding and enzymatic behavior.

73. M. Hromadová, F. Vavrek: Electrochemical electron transfer and its relation to charge transport in single molecule junctions *Curr Opin Electrochem*., 19 (2020), pp. 63-70, 10.1016/j.coelec.2019.10.008
74. D.V. Matyushov: Dynamical effects in protein electrochemistry *J Phys Chem B*, 123 (2019), pp. 7290-7301, 10.1021/acs.jpcb.9b04516
75. L. Sepunaru, N. Friedman, I. Pecht, M. Sheves, D. Cahen: Temperature-Dependent solid-state electron transport through bacteriorhodopsin: experimental evidence for multiple transport paths through proteins *J Am Chem Soc*, 134 (2012), pp. 4169-4176, 10.1021/ja2097139
76. S.D. Fried, S.G. Boxer: Electric fields and enzyme catalysis *Annu Rev Biochem*, 86 (2017), pp. 387-415, 10.1146/annurev-biochem-061516-044432

77. B. Jin, G. Wang, D. Millo, P. Hildebrandt, X. Xia: Electric-field control of the pH-dependent redox process of cytochrome c immobilized on a gold electrode *J Phys Chem C*, 116 (2012), pp. 13038-13044, 10.1021/jp303740e
78. L. Filali, Y. Brahmi, J.D. Sib, Y. Bouizem, D. Benlakehal, K. Zellama, N. Lemée, A. Bouhekka, F. Kail, A. Kebab, L. Chahed: Local surface electric field's effect on adsorbed proteins' orientation *Surfaces*, 2 (2019), pp. 415-431, 10.3390/surfaces2020030
79. F.S. Ruggeri, B. Mannini, R. Schmid, M. Vendruscolo, T.P.J. Knowles: Single molecule secondary structure determination of proteins through infrared absorption nanospectroscopy *Nat Commun*, (2020), p. 2945, 10.1038/s41467-020-16728-1
80. I. Zoi, D. Antoniou, S.D. Schwartz: Electric fields and fast protein dynamics in enzymes *J Phys Chem Lett*, 8 (2017), pp. 6165-6170, 10.1021/acs.jpclett.7b02989
81. V. Van Meervelt, M. Soskine, S. Singh, G.K. Shuurman-Wolters, H.J. Wijma, B. Poolman, G. Maglia: Real-time conformational changes and controlled orientation of native proteins inside a protein nanoreactor *J Am Chem Soc*, 139 (2017), pp. 18640-18646, 10.1021/jacs.7b10106

5.0 Conclusions and Next Steps Perspective: Conductive Polymers as a Key Nanomaterial for EEBs

This chapter, as a means of concluding, represents a space for a collection of my work which I thoroughly enjoyed, but which never coalesced into publication. As the work is not peer-reviewed, I offer the following as a semi-formal prospectus on the intersection between conductive polymers and biosensors from the view of an electrochemist.

First and foremost, conductive polymers sit among a crowded field of conductivity enhancing materials used to modify electrodes with the aim of creating biosensors which push the limits of sensitivity.[133] Though the mechanism by which this is achieved may vary depending on the bioreceptor of choice, the general sentiment is that the nanomaterials "improve the charge transfer to the electrode". It is important to note that these claims are always deserving of a discerning eye, as the excitement surrounding such a notion as achieving the lowest sensitivity possible is often newsworthy. Foils to these claims have come from efforts to seriously ascribe mechanistic understanding to the achievements; as an example, a paper published by Bartlett and Al-Lolage[134] thoroughly knocked down many claims that nanomaterials such as carbon nanotubes enabled direct electrical conduction between glucose oxidase and electrodes, one of the high bars to aim for in EEBs- the so called third generation sensor. The author dispelled many claims which were largely built upon a body of work which was self-supporting; claims of observations similar to what had been published was taken as evidence enough that DET had been accomplished. Instead, Barlett and Al-Lolange[134] et al showed that simple contaminants, such as metal ions or imperfections in commercial enzyme preparations gave the same signal as were claimed to be DET. Another common error was the failure to ascribe

changes in measured signal to changes in the available surface area at the electrode when modified with these nanomaterials.

Among the nanomaterials which I considered when seeking to push forward EEBs, conductive polymers caught my attention owing to the maturity of the field in its own right – they had been successful used in developing devices such as solar cells, organic light-emitting diodes and had also enabled the development of novel electrochemical transistors which will be covered later in this chapter. As a word of both wisdom and excitement for potential future PhD students, the field of conductive polymers is highly interdisciplinary, involving nanofabrication methods, synthetic chemists designing novel polymers in combination with chemical, material and electrical engineers who seek to understand the conduction mechanisms of the devices engineered with the polymers. I don't recommend attempting to enter this field in the manner which I did – late into a PhD when there was never enough time to absorb all the field had to offer. I do, however, encourage electrochemists to join this field, as it offers fascinating systems in which charge transfer is occurring, and their insight may greatly benefit the development of the field towards the realization of electrochemical biosensors.

My original research proposal in this field was to utilize conductive polymers in place of, or in concert with, the polymers typically applied to biosensors to either encapsulate or protect enzymes. Owing to the importance of being able to calibrate and understand the failure modes of EEBs, the core concept was to monitor the conductive properties of an enzyme-containing film in conductive polymer in order to associate changes in the film's impedance with changes to sensor performance. This ultimately shifted my focus from generating organic electrochemical transistors towards treating the films as a hybrid material and attempting to characterize its properties. Films which contain at the minimum a conductive polymer and

enzyme will be referred to as conductive polymer-enzyme hybrids (CPEHs). After an introduction to conductive polymers and OECTs, I will share my attempts to find additives which were both compatible with film performance (conductive properties, integrity, and adhesion) and supportive of enzymes (aiding dispersion in the film, protecting or even enhancing the enzymatic activity).

5.1 Conductive polymers use in biosensing

Conductive polymers are a group of organic polymers which behave possess electrical conductivity ranging from semiconducting to metallic. These properties arise from the long conjugation bond networks featured along the polymer repeating units.[135] The conductivity of the polymer is generally enhanced by the addition of a doping agent which serves to either partially oxidize (p-type) or reduce (n-type) the delocalized electron bands, enabling conductivity of electrons or holes as desired. N-type doping of conductive polymers is an area of focus in recent literature, as it enables a "turn-on" type of signal in OECT devices. A couple of the most well-known conductive polymers are shown in **Figure 5.1** below. Most popular among these for biomedical applications is PEDOT:PSS, due to its high conductivity, biocompatibility and processability/availability in aqueous forms.[136] Compared to other organic soluble or processed polymers, this is an advantage for formulations with biological materials, but also comes with the incorporation of the poly-sulfonate styrene (PSS) counter-ion to enable its solubility. When thin-films are created using PEDOT:PSS, a granular core-shell structure is formed with the PSS serving as an insulator.[137] Several strategies are commonly employed to both further dope the system and to change the structure of the conductive grains, creating orders of magnitude increases in the conductivity of the film. Among these methods, such as treatment with strong acids such as H_2SO_4 acids, solvent

additives such as DMSO, methanol and ethylene glycol, and thermal treatment, can produce films with conductivities on the order of ~1000 S/cm.[137] However, when attempting to create a CPEH, these methods are not viable due to their incompatibility with maintaining active enzymes. Part of my work in this topic was to find biocompatible additives which could also benefit the electrical properties of PEDOT:PSS.

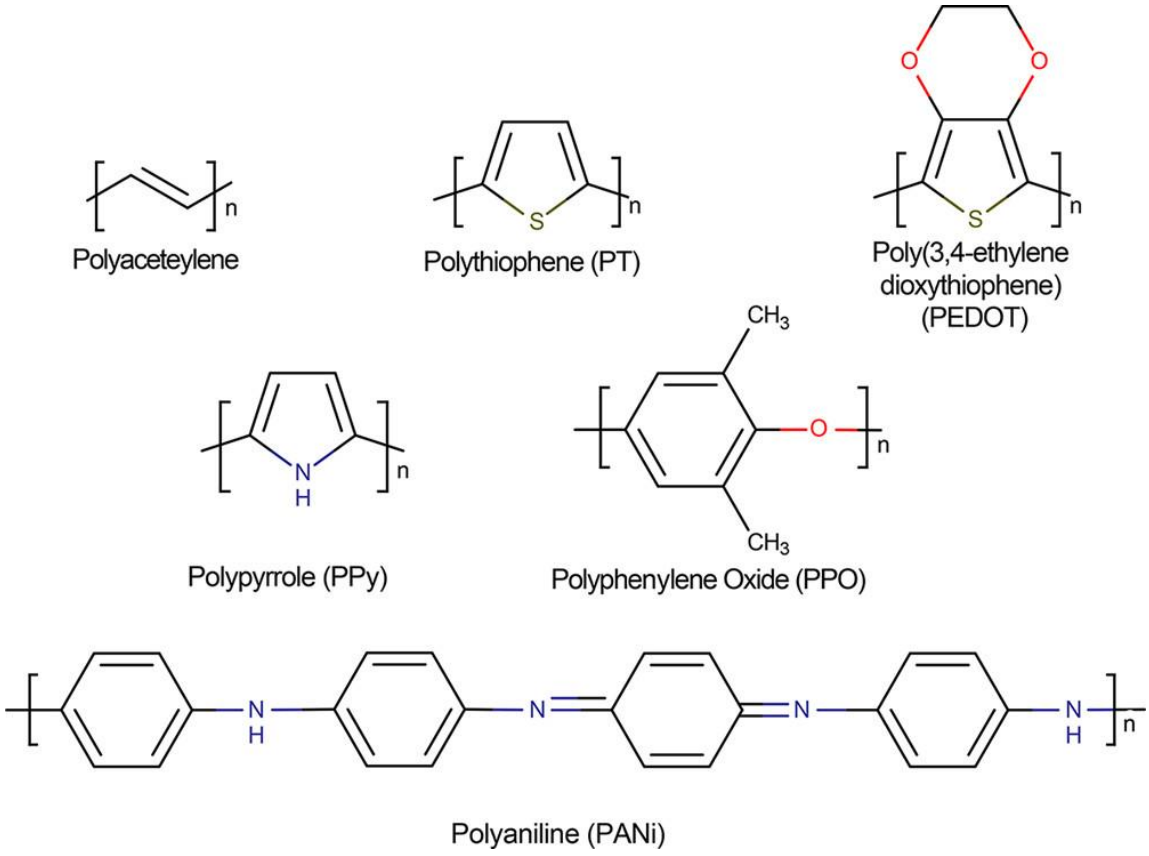

Figure 5.1 Several of the most used conductive polymers in biomedical applications. Figure is sourced from a review article on the subject by T. Nezakati *et Al.*[138]

In the field of biosensing, there are two methods by which conductive polymers are used – as an electrode modifying material in conventional sensors, and in OECT based sensors.[135] In the

realm of conventional EEBs, the purpose of the conductive polymer is the pursuit of 3rd generation biosensors, where the presence of a conducting medium (the conductive polymer) is thought to enable contact with the active site of the electrode by nature of it not being a rigid electrode surface.[139] However, a recent review highlights several amperometric glucose sensors made with various conductive polymers do not show significantly enhanced limits of detection compared to other modification methods.[139]

By comparison, organic electrochemical transistors are a very attractive alternative for pursuing electrochemical biosensing diagnostics. OECTs function as a mixed ionic-electronic conductor, where injection of counter ions from the electrolyte modulates the mobility of electrical charge along a conductive polymer channel between two electrodes.[140] As compared with other thin-film transistors, OECTs offer larger conductivity changes because whereas field effect transistors (FETs) only influence electric fields at the surface of the conductive channel, the whole volume of the conductive path is able to participate in OECTs, since small ions are readily injected into the conductive channel.[141] This comes at the cost of slower response times in comparison[141], but which are still amenable to continual sensing applications. A schematic of an OECT is shown in **Figure 5.2** below. Note that **Figure 5.2a** presents the enzyme in the conductive channel, which is aligned with my goal to study CPEHs, but is not necessarily the method of operation for current OECT-based biosensors, where the enzyme tends to be immobilized at the gate electrode. The figure of merit for OECTs is the transconductance (often labelled g_m in literature), which describes the relative change in the source-drain current with changes in the potential between the gate and channel (I_D and V_G respectively in the lower graphs for **Figure 5.2b** and **c**).

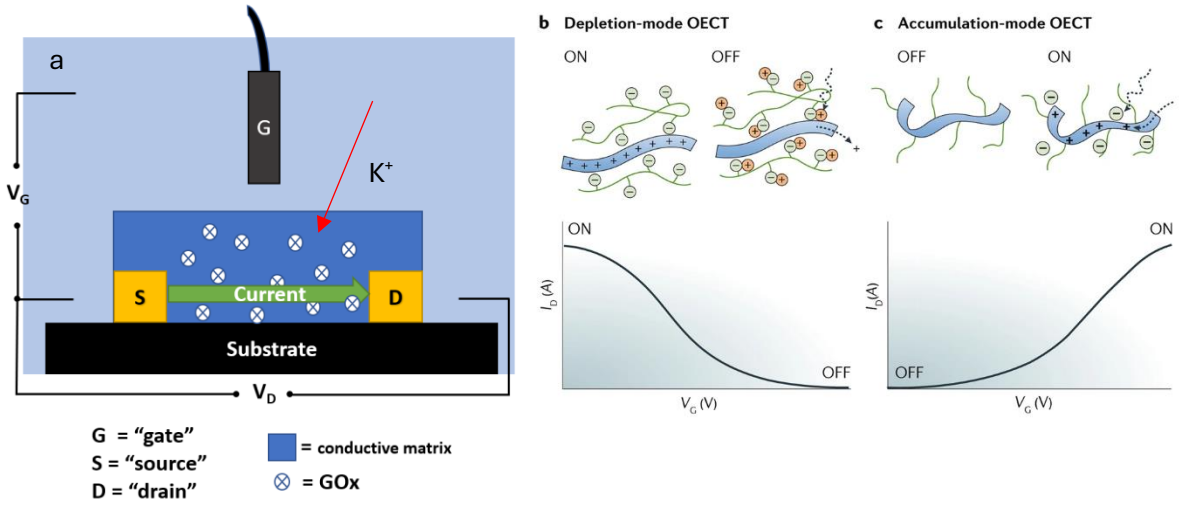

Figure 5.2 A schematic of an OECT is shown with the bioreceptor incorporated in the conductive path between the source and drain electrode. B) and C) demonstrate the operation of an OECT in depletion ("turn-off") and accumulation ("turn-on") modes. B and C are reproduced with permission from Rivnay, J., Inal, S., Salleo, A. *et al.* Organic electrochemical transistors. Nat Rev Mater 3, 17086 (2018).[140]

These devices imbue two major advantages over traditional electrode-based sensors: 1) they are capable of orders of magnitude signal amplification, owing to their transistor nature and the high conductivities achieved with properly treated conductive polymers and 2) their amplification operation restricts the influence of external noise, making sensitive measurements feasible without electrical shielding.[142] As an exemplary demonstration of the capabilities of OECTs, a 2019 publication by Qing *et Al.* showed an OECT-based dopamine sensor which had a linear sensing range over the nano to micromolar range, enabling a wearable continuous monitor to achieve detection levels relevant to several media where dopamine is reachable non-invasively.[143]

5.2 Materials and Methods

Materials

Glucose oxidase from *Aspergillus niger* (Type VII, lyophilized powder, ≥100,000 units/g solid) and alcohol dehydrogenase were purchased from Sigma Aldrich and used as received. PEDOT:PSS (PH1000 formulation, Ossila, Sheffeld, UK) was purchased as a aqueous suspension (1-1.3wt% solids, high conductivity grade 1:2.5w/w PEDOT to PSS) , which was sonicated for 3 minutes and passed through a 10 μm PVDF filter prior to use. Film additives included imidazole (Fischer Scientific), polyethylene glycol (PEG) 400 and 1000 and a citric acid, polyvinyl alcohol, β-cyclodextrin mixture used for crosslinking with glutaraldehyde (25%) following a reported procedure.[144] All additives other than imidazole were from Sigma Aldrich and used as received.

Methods

- **Film preparation**

CPEHs were prepared on glass substrates (quartz or D263 borosilicate). For Xray scattering measurements, single side polished native silicone oxide wafers were used instead. Some substrates were modified with gold contacts to enable electrical characterization of the film. Gold contacts were achieved by thermal evaporation using an Angstrom Engineering system using a hard shadow mask. Under high vacuum (pressure < 1E-7 bar) a 5 nm layer of chromium (chromium rod from Lasker) was deposited at a rate of 3 Å/s, followed by a 100nm layer of gold (gold pellet from Lasker in a tungsten heating boat).

All substrates were cleaned by sonication in acetone, isopropyl alcohol, and DI H2O followed by UV-Ozone treatment. Mixtures for film casting were created in 200 μL

quantities to minimize enzyme usage. When additives were used, a homogeneous solution was created without the enzyme first by mixing via magnetic stir bar for at least 2 hours at room temperature. Imidazole was added at 0.1, 0.5 and 5 wt%, PEG was added at 0.04M final concentration. Glucose oxidase was added at 0.1 and 5mg/ml concentrations. Two methods were attempted to add the enzyme – via a PBS solution and directly from the dried form. PBS solutions proved to be completely detrimental to film conductivity and so the direct addition method was adopted. 25 μL of solution was dispensed on the center of a 15x15mm substrate, which was then spun at 2000 rpm for 45 seconds to create films which were 75-250 nm in thickness depending on the formulation. Films were left to dry overnight in a vacuum desiccator and stored there when not in use.

- Electrical characterization

4-point probe colinear measurements were used to measure the sheet resistance of the thin films. Custom lab-view and python scripts were used to set a voltage across the outer probes and to record the current flow between the inner probes as controlled and recorded by a Keithley 6200.

- Film thickness

Thickness was determined by contact profilometry using an Ambios XP-100 profilometer. In some instances, especially if the film was hydrated, even the lowest contact force (0.1mg) was too significant and deformed the film. In these instances, atomic force microscopy (Asylum AFM, crediting UCSB's microscopy facilities) was used in non-contact mode to measure the film thickness.

- Enzyme activity

Enzyme activity was measured using an absorbance method via a Tecan M220 plate reader. This method involved the use of ABTS dye and horseradish peroxidase, as described in the methods section 3.2. Analyte was added and pipetted up and down five times to ensure mixing just before starting the absorbance measurements. To reduce artifacts from the substrate, several locations were scanned per well.

- Spectroscopic characterization

A variety of spectroscopic methods were used to measure different film properties. UV-Vis-NIR absorbance data were collected using a Shimadzu UV3600. Circular dichroism spectra were collected using a JASCO J1500. Small angle Xray scattering (SAXS) was collected using the x-ray facilities in the Materials Research Laboratory. Grazing incidence wide angle Xray scattering (GIWAXS) was collected at the synchrotron beam line at Stanford SLAC National Accelerator Laboratory.

Acknowledgement for use of facilities:

"The MRL Shared Experimental Facilities are supported by the MRSEC Program of the NSF under Award No. DMR 2308708; a member of the NSF-funded Materials Research Facilities Network"

I acknowledge Phong Ngyuen of Professor Michael Chabinyc's Group for use of their thermal evaporation system for Phong's generous support in obtaining GI-WAXS measurements at the Stanford Linear Accelerator Center. Additionally, I acknowledge Tung Ngyuen of Professor Thuc-Quyen Nguyen's group, for teaching me how to fabricate OECTs and the research group of for use of their spin coater.

5.3 My Efforts and Results

Below are four claims that I make based upon my experiences working with CPEHs

1. **It is possible to add high amounts of enzyme to the film and retain the conductive properties.**

The charts below shows measured conductivities of PEDOT:PSS films containing 0.04M PEG or imidazole with varied amounts of GOx added directly to the solution for ~200nm thick films. Film conductivities on the order of 1000 S/cm are highly conductive for PEDOT:PSS. Interestingly for **Figure 5.1B**, in the presence of glucose oxidase, increases in film conductivity with imidazole occurred at a higher weight percentage than was reported in literature, albeit for a PEDOT:PSS formulation of a different conductivity grade.[145]

A)

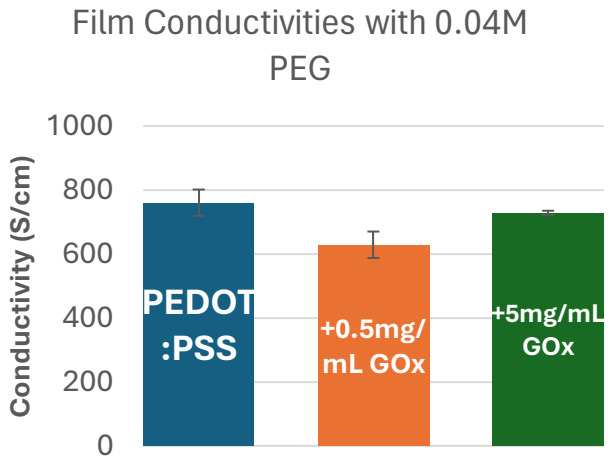

B)

Wt % midazole	pH	Conductivity (S/cm)
0	2.15	0.06
0.5	7.65	0.04
5	8.99	1061.5

Figure 5.3 Conductivity measurements of PEDOT:PSS films containing GOx and A) 0.04M PEG and B) 5mg/ml GOx and varying weight percents of imidazole.

2. **I was not able to spectroscopically measure indications of enzyme uniformity in the film and visual indications showed poor dispersion in PEDOT:PSS alone.**

Figure 5.4 Below offers visual evidence of potential pockets of enzyme, suggesting poor dispersion. I attempted several spectroscopies to try to measure any sort of dispersion of the enzyme, but the very thin nature of the films led to no resolvable signal in the case of circular dichroism, spectroscopic ellipsometry and Xray scattering. Of these methods, GIWAXS should ideally be able to resolve structures at the scale of enzymes, but at the time of experimentation access to this technique was highly limited to availability at Stanford's SLAC facilities when members of the Chabinyc group were visiting (approximately once or twice per year if they had extra space within their time). The developing capabilities in the BioPACFIC MIP to make such measurements are something which may aid any future efforts to make similar materials.

A) B) C)

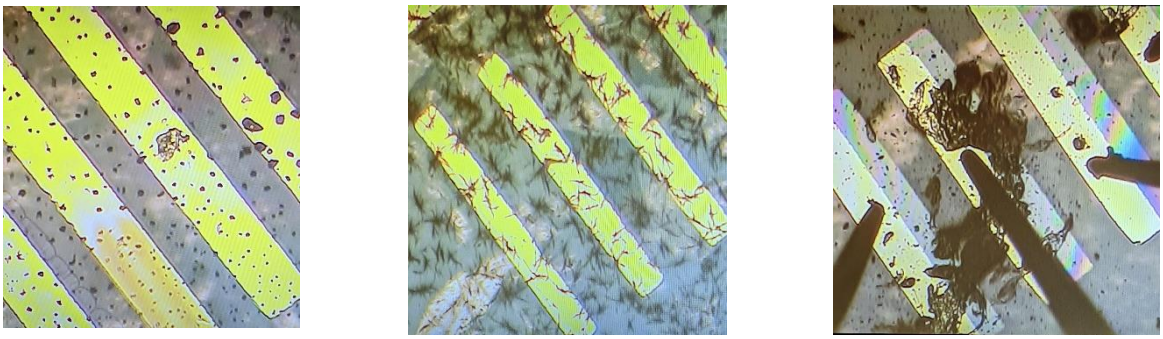

Figure 5.4 Visual inspection of PEDOT:PSS films with A) 5 mg/ml GOx or B) 5mg/ml GOx and 0.5 wt% PEG shows localized damage to the film following measurements of enzyme reactivity. Some films, such as one shown in C), showed large aggregation prior to exposure to aqueous environment.

3. **Glucose oxidase maintained activity, even when directly added to PEDOT:PSS films.**

UV-Vis based activity assay showed that films maintained the capability of reacting with glucose.

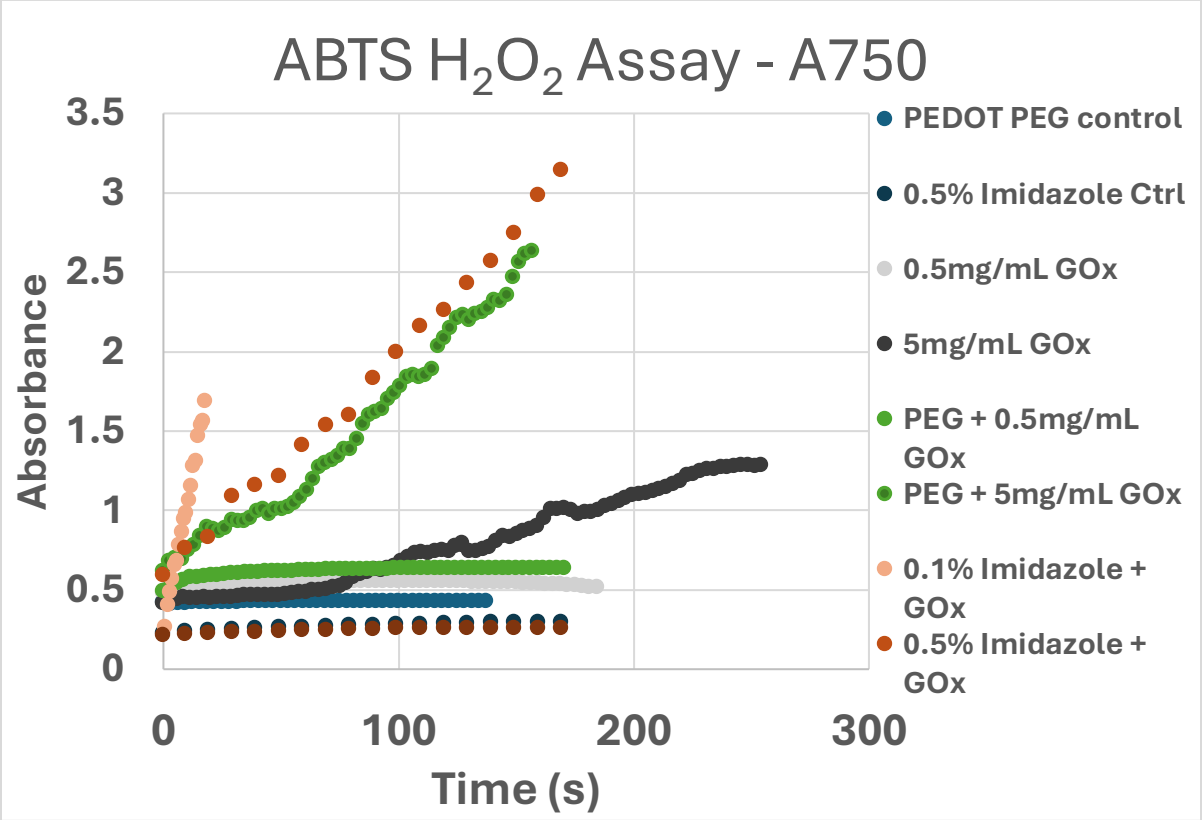

Figure 5.5 Reactivity of GOx incorporated into various PEDOT:PSS films as indicated in the legend. Higher activity is associated with higher GOx loading, but not necessarily optimal conductivity enhancement formulations (high imidazole shows better conductivity but poorer enzyme reactivity)

4. **Film stability is a major challenge. This presented as both loss of enzyme from the film, as well as delamination and film degradation when in an aqueous solution.**

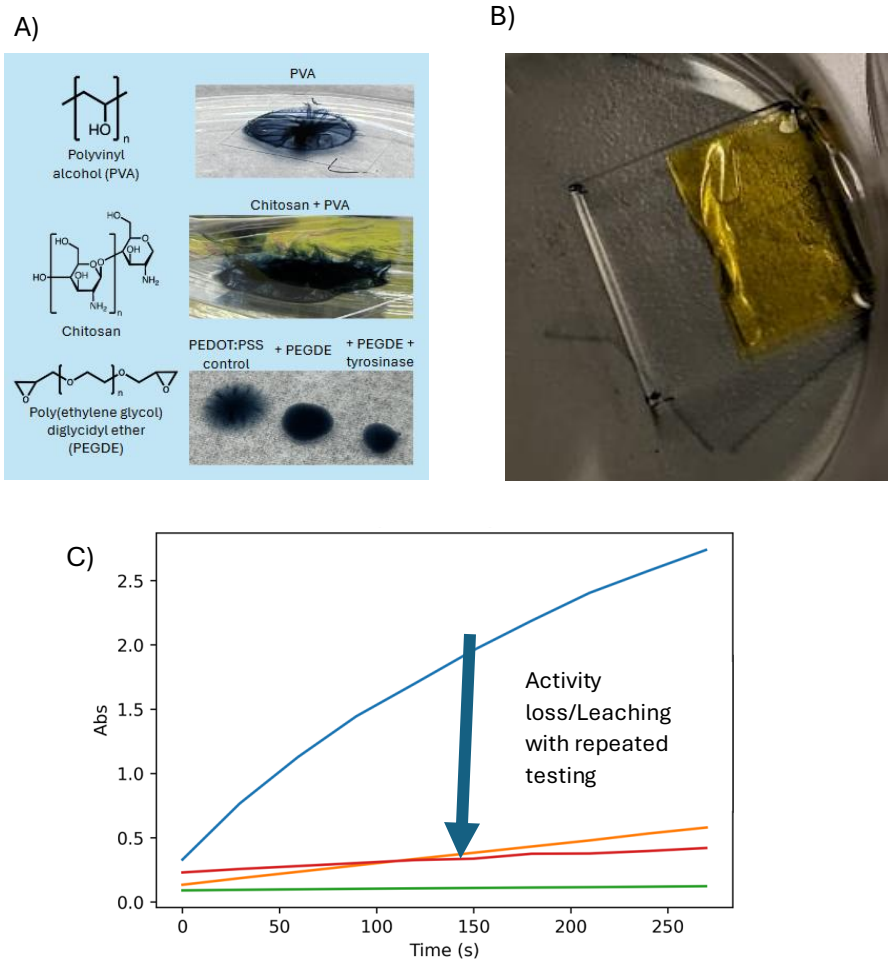

Figure 5.6 Film stability presents a major challenge in creating CPEHs. A) Different additives show varying success in keeping PEDOT:PSS CPEHs intact when in an aqueous environment. B) An example of delamination of a GOx-containing PEDOT:PSS film. C) Repeatedly testing the same GOx-containing film in new solutions shows repeatedly decreasing turnover of the reporter dye ABTS.

5.4 Conclusions and Next Steps

Although conductive polymers are neither a new material nor new to usage in biosensors, the scope of available polymers remains highly limited- the field is dominated by polyacetylene, polypyrrole, polyaniline, and polythiophene (of which PEDOT is a derivative) which have been in use since the 1980s. This author is not aware of any concerted effort to pair a bioelectrochemist and polymer chemist to design conductive polymers specifically for biosensor usage. This has largely resulted in a mismatch between the properties of the resulting thin films and the biosensing applications they are targeted for[146] – polyacetylene is insoluble in water, polyaniline is known to be sensitive to pH and PEDOT:PSS films swell significantly when hydrated, leading to loss of integrity and loss of enzymes. Further, the de facto operating mode of OECTs is to place the enzyme at the gate electrode, or at only the surface of the conductive polymer channel. Due to my own observations in the difficulty in dispersing enzymes into conductive polymer solutions, I hypothesize that there is likely a buried wealth of unpublished results from other's efforts to create similar materials.

Nevertheless, conductive polymers remain an exciting material for EEBs and electrochemical sensors broadly. Resent research has seen an expansion of conductive polymers as a component of hydrogels, crosslinked polymer networks with large water content, which are both biocompatible due to their matching mechanical properties, as well as viable in flexible electronics.[147] Hydrogels have seen some success as a host for enzymes, similarly owed to the beneficial mechanical properties; conductive polymer hydrogels may be the key linkage between thin film OECTs and CPEHs. The use of these hydrogels as a channel material in OECTs is still in a nascent stage, where differences in ionic and electronic conductivity in this medium differ from hydrated thin films, leading to differences in electrical performance.[148]

The potential for achievement in this field demands and deserve strong interdisciplinary effort. Just as the microelectrode underpinned the development of the modern CGM, so too might the OECT be the starting point of true next-generation diagnostics.

As an overall summary of this thesis, the individual fields represented in this work continue to fascinate me. Though the sci-fi future where a complete diagnosis is achieved with a simple full body "scan" still feels far off, the discussion of measuring singular enzymes and the capabilities of OECTs makes the goals of next generation medicine seem not so far off. I am proud to have contributed my mental and physical capabilities to these efforts and will continue to watch these fields with the strong belief that near-future sci fi precision medicine may be a reality and boon to humanity in my lifetime.

5.5 References for Chapter 5

1. da Silva, E. T. S. G. *et al.* Electrochemical Biosensors in Point-of-Care Devices: Recent Advances and Future Trends. *ChemElectroChem* **4**, 778–794 (2017).

2. Bartlett, P. N. & Al-Lolage, F. A. There is no evidence to support literature claims of direct electron transfer (DET) for native glucose oxidase (GOx) at carbon nanotubes or graphene. *Journal of Electroanalytical Chemistry* **819**, 26–37 (2018).

3. Ramanavicius, S. & Ramanavicius, A. Conducting Polymers in the Design of Biosensors and Biofuel Cells. *Polymers (Basel)* **13**, 49 (2020).

4. Yang, Y., Deng, H. & Fu, Q. Recent progress on PEDOT:PSS based polymer blends and composites for flexible electronics and thermoelectric devices. *Mater Chem Front* **4**, 3130–3152 (2020).

5. Shi, H., Liu, C., Jiang, Q. & Xu, J. Effective Approaches to Improve the Electrical Conductivity of PEDOT:PSS: A Review. *Adv Electron Mater* **1**, (2015).

6. Nezakati, T., Seifalian, A., Tan, A. & Seifalian, A. M. Conductive Polymers: Opportunities and Challenges in Biomedical Applications. *Chem Rev* **118**, 6766–6843 (2018).

7. Lakard, B. Electrochemical Biosensors Based on Conducting Polymers: A Review. *Applied Sciences* **10**, 6614 (2020).

8. Rivnay, J. *et al.* Organic electrochemical transistors. *Nat Rev Mater* **3**, 17086 (2018).

9. Friedlein, J. T., McLeod, R. R. & Rivnay, J. Device physics of organic electrochemical transistors. *Org Electron* **63**, 398–414 (2018).

10. Tybrandt, K., Kollipara, S. B. & Berggren, M. Organic electrochemical transistors for signal amplification in fast scan cyclic voltammetry. *Sens Actuators B Chem* **195**, 651–656 (2014).

11. Qing, X. *et al.* Wearable Fiber-Based Organic Electrochemical Transistors as a Platform for Highly Sensitive Dopamine Monitoring. *ACS Appl Mater Interfaces* **11**, 13105–13113 (2019).

12. Tan, P. *et al.* Solution-processable, soft, self-adhesive, and conductive polymer composites for soft electronics. *Nat Commun* **13**, 358 (2022).

13. Wang, Q., Chueh, C.-C., Eslamian, M. & Jen, A. K.-Y. Modulation of PEDOT:PSS pH for Efficient Inverted Perovskite Solar Cells with Reduced Potential Loss and Enhanced Stability. *ACS Appl Mater Interfaces* **8**, 32068–32076 (2016).

14. Thirumalai, D., Santhamoorthy, M., Kim, S.-C. & Lim, H.-R. Conductive Polymer-Based Hydrogels for Wearable Electrochemical Biosensors. *Gels* **10**, 459 (2024).

15. Tomczykowa, M. & Plonska-Brzezinska, M. Conducting Polymers, Hydrogels and Their Composites: Preparation, Properties and Bioapplications. *Polymers (Basel)* **11**, 350 (2019).

16. Gregorio, T., Mombrú, D., Romero, M., Faccio, R. & Mombrú, Á. W. Exploring Mixed Ionic–Electronic-Conducting PVA/PEDOT:PSS Hydrogels as Channel Materials for Organic Electrochemical Transistors. *Polymers (Basel)* **16**, 1478 (2024).

6.0 APPENDIX

6.1 Additional Work Regarding Single Entity Electrochemistry – Silver Nanoparticle Synthesis Mechanism Correction/Commentary and Characterization

6.1.1 Introduction

Using biomolecules as a reducing agent for nanoparticle synthesis is a fast-growing area of research. (1−4) The various biosynthetic routes applied so far have opened the possibility for developing an economical and environmentally friendly method compared with conventional hazardous inorganic reducing agents such as sodium borohydride. (5) Among the various types of biosynthesized nanoparticles reported, (6−10) silver nanoparticles (AgNPs) stand out for their antibacterial activity (11−13) and account for an integral part in next generation sensors, (14,15) optical devices, (16) and catalysis. (17) However, the majority of green synthesis works conducted so far have concentrated on a proof-of-concept for AgNP formation from plant extracts, (4,18) bacteria, (19) or fungi. (20) Furthermore, biosynthesized AgNPs usually require multiple isolation steps and result in polydispersed size distributions limiting their quality for industrial applications. (21,22) Consequently, this approach has demonstrated a discernible gap between methodology and mechanistic understanding of AgNP biosynthesis. From a mechanistic point of view, the central dogma supports a dominant reaction via a nitrate reductase enzyme, which is dependent on its natural cofactor nicotinamide adenine dinucleotide phosphate (NADPH) to reduce a silver nitrate salt. (23,24) In general, NADPH is known for its biological role as a coenzyme, mediating charge transfer between enzymes and its natural substrate. However, the formal potential of NADPH (−0.32 V vs NHE) suggests that it can act as an individual reducing entity in the case of charge transfer to an inorganic compound such as metal salts. The first examination of the ability to use NADPH as a reducing agent for nanoparticle formation was reported by Willner et al. (25) It was shown that NADPH

was able to act as part of the catalytic growth of gold nanoparticles. However, for this biomolecular synthetic route, the presence of gold seeds was essential for catalytic growth; hence, NADPH alone did not cause any noticeable effect. With respect to AgNP synthesis, the redox reaction between NADPH and silver ions are predicted to be a thermodynamically favorable process as shown in eq 1.

$$2Ag^{+} + NADPH \rightarrow 2Ag^{0} + NADP^{+} + 1H^{+} \quad E^{0} = 1.12V \tag{1}$$

Thus, NADPH was selected as a model reducing agent for two reasons: (a) it allowed the critical analysis of the suggested nitrate reductase mechanism prevalent in recent literature (b) it contains several ubiquitous chemical groups such as nicotinamide, ribose, phosphate, and adenosine, which may provide a suitable platform for NP synthesis. (26,27) Furthermore, by showing that the enzymatic route does not exist, the synthesis temperature range can be substantially extended. These insights shall stimulate and support the development of economic and sustainable methods of nanoparticle synthesis.

6.1.2 Results and Discussion

First, the possibility of forming AgNPs using solely NADPH without the aid of nitrate reductase was examined (see experimental conditions in the SI). This was achieved by introducing 0.2 mM of NADPH to a stirred solution containing 10 mM $AgNO_3$ and 50 mM 4-(2-hydroxyethyl)-1-piperazineethanesulfonic acid (HEPES) buffer (pH 7.2, 25 °C). It should be noted that HEPES was chosen as the buffer since it showed no interaction with the silver salt (**Figure S6.1**), in contrast to the commonly used phosphate buffer, (23) which is reactive toward silver to produce the insoluble $AgPO_4$. (28) **Figure 6.1A** shows the UV–vis absorption spectra of the solution at t = 0 (black curve) and after 24 h (red curve). As can be seen, the initial spectrum showed two absorption maxima at 340 and 260 nm, reflecting the classical

absorption features of NADPH. (29) With time, the solution changed color from transparent to yellow, manifested by the appearance of a new absorption maximum at 411 nm. Upon the reaction reaching completion, the growth of the new maximum at 411 nm ceased, and the peak at 340 nm completely vanished. The decrease in the 340 nm signal was ascribed to the consumption of NADPH, (30) while the high absorption at 411 nm corresponds to the surface plasmon resonance of AgNPs. (31)

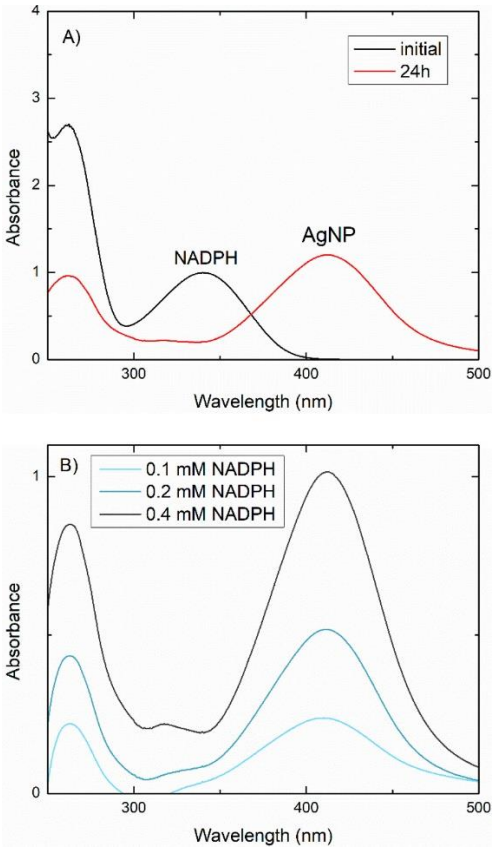

Figure 6.1 Absorbance of reductase free synthesized NPs. (A) UV–vis spectra of initial solution (t = 0) immediately after 0.2 mM NADPH was added (black, undiluted) and after 24 h (red, 1:3 dilution in HEPES). (B) UV–vis spectra of fully synthesized particles using 0.1, 0.2, and 0.4 mM NADPH. Samples were diluted by 1:9 in HEPES. All measurements were done under controlled temperature of 25 °C. All solutions contained 10 mM AgNO3 and 50 mM HEPES (pH 7.2).

NADPH was further confirmed to act as the sole reducing agent by varying the concentration of NADPH added into the solution. As evidenced in **Figure 6.1B**, the amplitude of the resulting

plasmonic peak was proportional to the concentration of NADPH. The position of the plasmonic peak remained constant, indicating that the size of the AgNPs formed does not depend on the NADPH concentration. In addition, the reaction was pH sensitive, which can be understood from the known 2e– and 1H+ oxidation process of NADPH to NADP+ (see *eq 1*). (32) We found that the ideal conditions for the synthesis were at physiological pH (**Figure S6.2**) using a HEPES buffer capacity of 50 mM (**Figure S6.3**).

The isolation of the nanoparticles was elegantly achieved by adding an equivalent amount of NaCl to react with the remaining Ag+ ions to form insoluble AgCl (e.g., for 0.2 mM NADPH particle synthesis, 9.6 mM NaCl was added into the solution). After the addition of NaCl, the resulting opaque solution was centrifuged at 4000 rpm for 30 min, and the precipitate was discarded to give a purified nanoparticle solution. After this centrifugation step, the solution still contained NADP+ as indicated by the high absorption at 260 nm (**Figure S6.4A**). To sediment and concentrate the cleaned particles, the solution was centrifuged at 15,000 rpm for 30 min. The liquid was decanted, and the particle pellet was diluted as necessary with water or 50 mM HEPES. After centrifugation at 15,000 rpm, the UV–vis absorption spectra of this solution still showed a small maximum at 260 nm reflecting a residue of NADP+ (**Figure 6.4B**). However, this does not directly provide evidence that NADP+ can be seen as the capping agent. In order to determine the chemical composition of the isolated NPs, high-angle annular dark-field (HAADF) imaging was performed and coupled with energy dispersive X-ray (EDX) spectroscopy. **Figure 6.2A** shows the HAADF image of a single isolated nanoparticle. The EDX elemental mapping of silver in Figure 2B confirms that the particle was indeed an AgNP. To identify the capping agent, a closer look was taken at sulfur and phosphorus, which are identifying components of the HEPES buffer and NADPH, respectively.

As can be seen from Figure 2C and D, the particle was covered by a mixture of P as well as S. We conclude that NADPH or its product NADP+ was capping the AgNPs, but there was a noticeable contribution of HEPES to the stabilization of the NP, which was also supported by the previously described buffer capacity experiments.

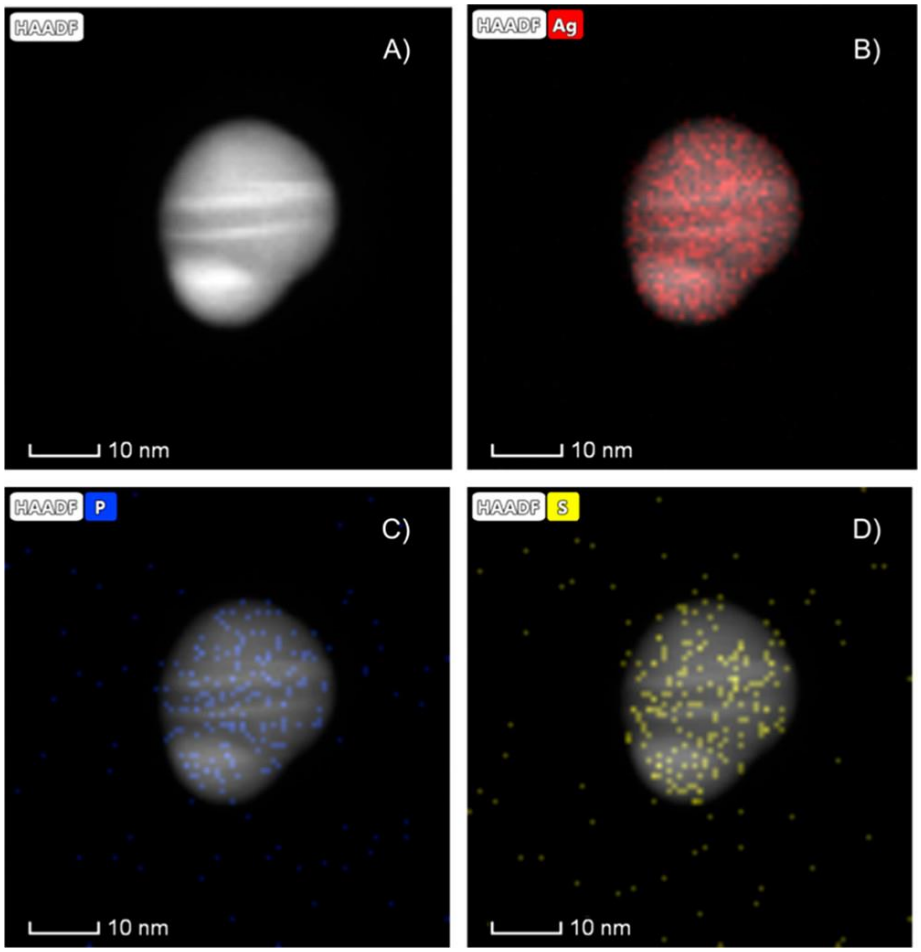

Figure 6.2. Elemental mapping of the capping agent. (A) HAADF-STEM image showing a single nanoparticle after the 25 °C synthesis route and the isolation steps. (B–D) Drift corrected EDX spectral mapping of the elements silver (red), phosphorus (blue), and sulfur (yellow), respectively, at the same location of the identified nanoparticle. Scale bar is 10 nm.

Next, the effect of adding nitrate reductase to the reaction was recorded. The UV–vis absorption spectra of particles synthesized without nitrate reductase were compared with particles synthesized in the presence of 33, 66, and 99 µg/mL of nitrate reductase. After the reactions had gone to completion, the UV–vis spectrum of each was taken as shown in **Figure 6.3A**. It was found that the amplitude of the plasmonic peak was inversely proportional to the concentration of nitrate reductase. Moreover, the full width at half-maximum (FWHM) of the plasmonic peak became larger as the enzyme concentration increased indicating a more dispersed population of particles. (33)

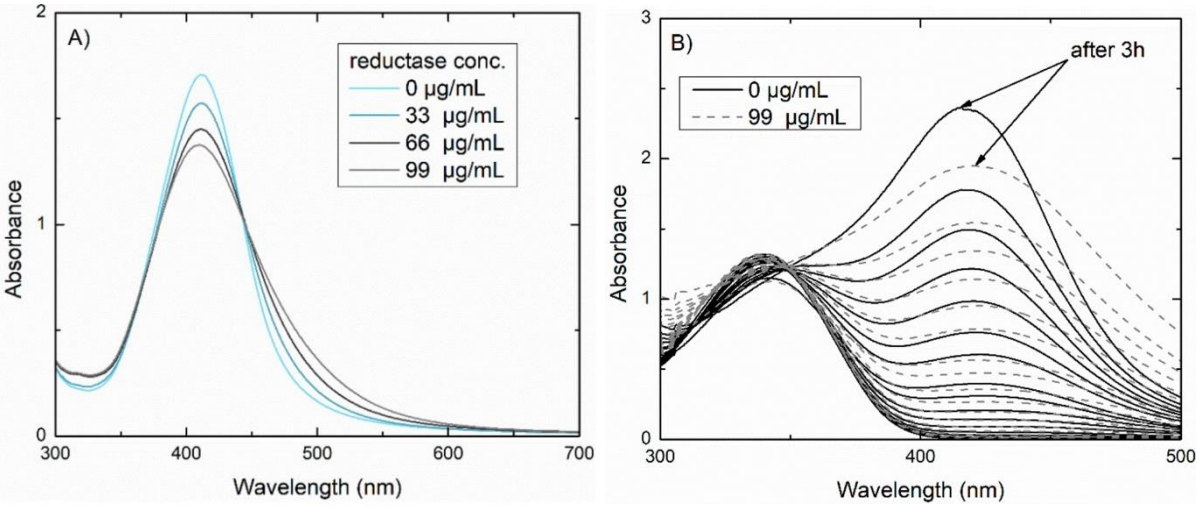

Figure 6.3. Absorbance of reductase added synthesized NPs. (A) UV–vis absorption spectra recorded 24 h after adding 0.2 mM NADPH into a solution of 10 mM AgNO3 (pH 7.2) and 0, 33, 66, and 99 µg/mL nitrate reductase. All solutions were diluted 1:2 with HEPES. (B) Time-dependent growth of the plasmonic peak over 3 h of an enzyme-free solution (solid line) and a solution with 99 µg/mL nitrate reductase enzyme (dashed line). Absorption spectra were taken for each sample every 10 min without dilution (every 15 min for the first hour). All measurements were done under a controlled temperature of 25 °C.

An in-depth comparison between enzyme and enzyme-free synthesis conditions was done using 0 and 99 µg/mL of nitrate reductase. These particles were synthesized in unison using the same stock of AgNO3, HEPES, and freshly prepared NADPH to omit any differences in

sample preparation. This test was done over 3 h to compare the propagation of the silver nanoparticle plasmonic peak for both types of synthesis. As shown **in Figure S6.3B**, the initial absorption spectra of the solution with (dashed line) and without (solid line) nitrate reductase were identical, and both exhibit the anticipated NADPH maximum at 340 nm. The plasmonic peak of enzyme and enzyme-free synthesized particles began to diverge after 1.5 h and differed drastically by 3 h, suggesting that nitrate reductase interfered with the reaction and influences the size dispersity. To further demonstrate the role of nitrate reductase, two additional control experiments were conducted in the absence of NADPH with (a) solely nitrate reductase and (b) denatured reductase at 25 °C. The resulting UV–vis spectra and experimental details are attached to **Figure S6.5**. Both spectra indicated no nanoparticle formation. We conclude that the enzyme not only interfered with the reaction but was completely unable to reduce the silver salt. Hence, NADPH was seen as the only entity responsible for the AgNPs synthesis.

In parallel to the spectroscopic characterization, we have made a comparison between AgNPs synthesized with and without nitrate reductase via transmission electron microscopy (TEM) imaging. **Figure 6.4A** shows typical images observed for the two synthesis methods. From the TEM images, it can be inferred that the NADPH-synthesized nanoparticles are monodispersed (**Figure 6.4A, left**), while in the presence of the enzyme the mean AgNP size appeared larger and more dispersed (**Figure 6.4A, right**). TEM size analysis of the cleaned AgNPs with and without nitrate reductase showed a clear discrepancy between the two reactions (**Figure 6.4B**). When NADPH was used solely in the solution, the TEM histogram displayed monodispersed NPs with a mean radius of 5.1 ± 1.0 nm. When nitrate reductase was present in the solution (99 μg/mL), the TEM histogram displayed NPs with a mean radius of 9.5 ± 5.7 nm. The results of the TEM images are in line with the previously shown increase in the FWHM of the

plasmonic mode when nitrate reductase is added. Moreover, the measured zeta potential of the AgNP solutions produced values of −29.9 ± 0.7 and −21.3 ± 0.7 mV when synthesized without and with the enzyme, respectively (**Figure 6.6** and **Table 6.1**). The observations above point out that nitrate reductase interferes with the redox reaction of NADPH and the silver salt, leading to a higher dispersion and lower stability of the synthesized AgNPs.

Figure 6.4 Size determination of the synthesized AgNPs. (A) Brightfield TEM images of silver nanoparticles synthesized with 99 µg/mL nitrate reductase (right) and with NADPH alone

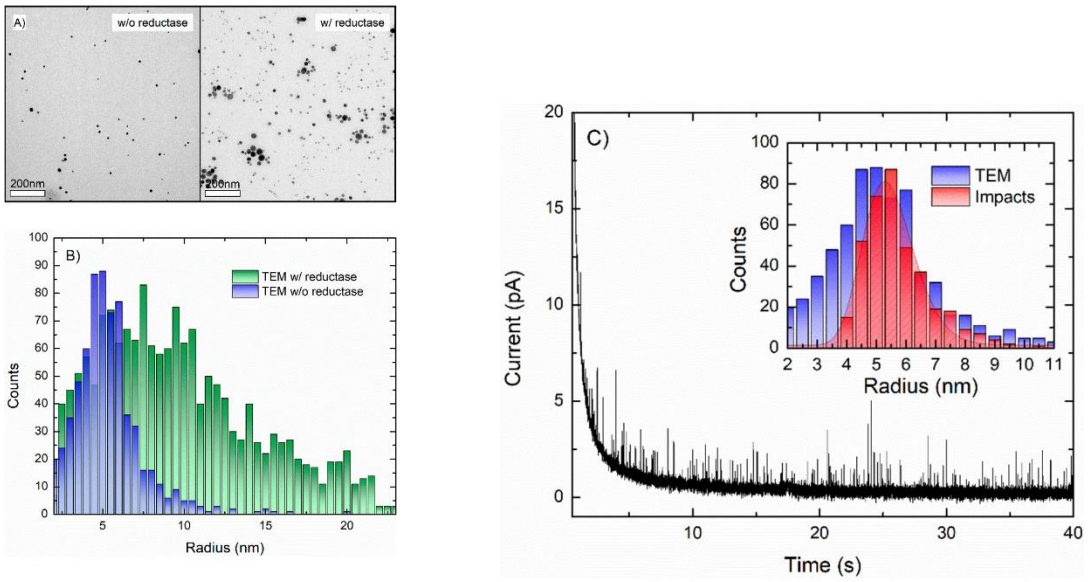

without the enzyme (left). (B) Size distribution extracted from TEM imaging of the AgNPs synthesized with and without nitrate reductase (each histogram contains >500 NPs). (C) Single entity chronoamperogram of the NADPH synthesized AgNPs showing individual current spikes arising from a single AgNP oxidation. Inset: Compiled histogram from the single entity measurements overlaid with the TEM histogram.

To confirm the results obtained by TEM imaging, particles were further characterized via electrochemical experiments. First, a volume of 4 µL of the purified and concentrated

nanoparticle solution was dropcast onto a glassy carbon electrode (r = 1.5 mm, see further experimental details in the SI). Next, the NPs were stripped using anodic stripping voltammetry. The voltammogram showed a clear oxidative peak at 94 mV vs SCE (**Figure S6.7**), which agrees with previously reported values for the AgNP oxidation potential under these conditions. (34) Last, state-of-the-art characterization of individual NADPH synthesized AgNPs was done via single entity electrochemistry (see details in the SI). (35−39) The strength of the complementary single entity electrochemistry method arises from its ease of use, the fact that it is an in situ method, and also the rapid data acquisition that enabled us to acquire a substantial amount of data for seizing a large quantity of nanoparticles in a very short period of time (e.g., a single 40 s recording can produce sufficient statistical data at high nanoparticle concentrations). For the single entity experiments, a gold microelectrode (r = 6.25 μm, CHI), an Ag/AgCl (3 M) reference electrode, and a Pt wire counter electrode were introduced into a freely diffusing clean AgNP solution. The solution was supported by 20 mM NaCl in order to ensure a fast oxidation process while keeping the AgNPs stable. (40) The microelectrode was held at a sufficient oxidative overpotential (0.4 V vs SCE) while the current–time plots were recorded at a filtering frequency of 0.14 kHz. (41) As can be seen from Figure 4C, the observed chronoamperograms showed individual stochastic current spikes, which were attributed to oxidation of a single AgNP randomly colliding with the electrode (additional recordings are shown in the **Figure S6.8**). Using Igor Pro software, each spike was analyzed, and the charge was extracted (SI). The calculated charges were compiled to give the size distribution of the nanoparticles. The mean charge was found to be in agreement with the TEM imaging as can be seen from the histogram in the Figure 4C inset.

The minimal components present in the solution enabled us to learn about the rate of the reaction by simply varying the concentration of NADPH in the solution or by varying the reaction temperature. **Figure 6.5A** shows an example of the observed changes in the UV–vis spectra over the first 2 h at 25 °C, taken with a time interval of 3 min, using 0.2 mM NADPH. With time, the 340 nm signal decreased, while the 260 nm peak increased. Both observations indicate that NADPH was oxidized to NADP+ during the reaction (extinction coefficient of the product NADP+ is higher than of NADPH at 260 nm). (42) We repeated the same analysis with NADPH concentrations of 0.1, 0.2, and 0.4 mM (see full spectra in **Figure S6.9**). From these spectra, the kinetics analysis via the 340 nm absorption decay within the regime of the nanoparticle nucleation phase demonstrated a linear correlation between the rate constant and the NADPH concentration (Figure 5A, inset). This indicates that the reaction rate is a pseudo-first-order reaction with respect to NADPH with a rate constant of 6.6 × 10–3 ± 2 × 10–4 s–1. Additionally, we were able to increase the reaction rate substantially by increasing both the NADPH concentration and the reaction temperature. Since the reaction was enzyme-free, denaturing temperature limitations were alleviated. The time dependence of the plasmonic peak formation was recorded in order to learn the time scale needed to complete the reaction. As shown in **Figure 6.5B**, when using 1 mM NADPH and a reaction temperature of 50 °C, the reaction was 90% completed within 35 min. The kinetics data shown are similar to the classical kinetics of NP formation which is initiated by a lag time of the nucleation phase followed by a rapid NP growth until the reducing agent is depleted. Increasing the reaction temperature to 80 °C permitted a rapid reaction that was 90% completed within 7 min, while the plasmonic peak location appeared to be constant as a function of temperature (**Figure S6.10**). The monodispersity of the particles was not altered through the increased reaction temperature

(**Figure S6.11**). Interestingly, the completion of the biomolecular synthesized AgNPs at 80 °C was faster than most conventional methods using the same concentration of an inorganic reducing agent and similar temperature, which qualifies the here suggested pathway as a competitive but sustainable approach.

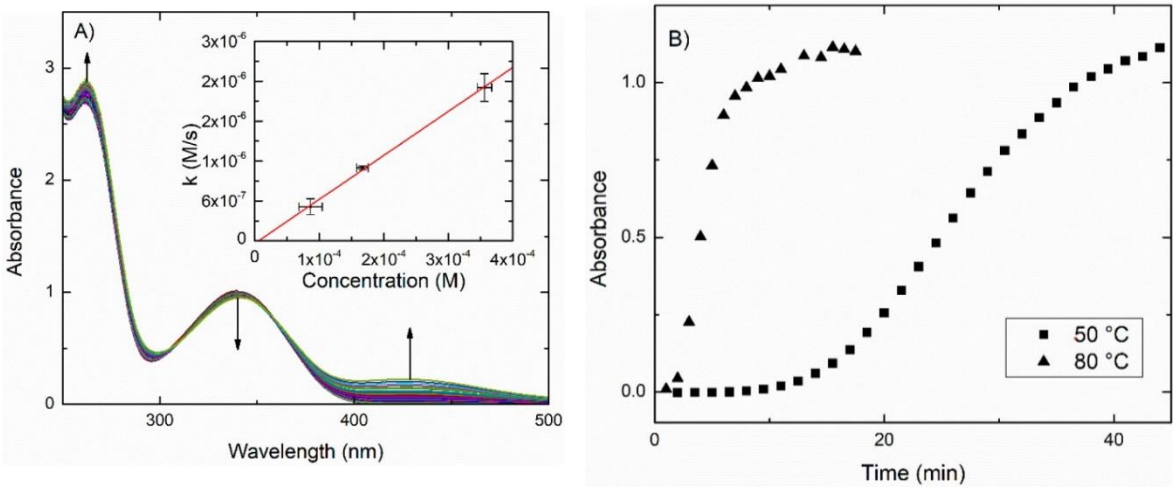

Figure 6.5. Kinetics and duration of NP synthesis. (A) Absorption spectra of 50 mM HEPES, 10 mM AgNO3, and 0.2 mM NADPH solutions with each spectrum taken every 3 min for 2 h. Inset: Compiled data of NADPH reduction rate as a function of NADPH concentration, monitored at 340 nm. NADPH concentrations were 0.1, 0.2, and 0.4 mM. (B) Kinetics data of the plasmonic peak formation at 50 and 80 °C, with 1 mM NADPH and 10 mM AgNO3 (pH 7.2).

6.1.3 Conclusions

The bottom-up approach used here showed that NADPH can serve as the sole reducing agent for AgNP formation. It was found that the reaction did not require the use of nitrate reductase, and instead, the particles formed in the enzyme-free reaction were smaller, monodispersed, and more stable than those synthesized with the addition of nitrate reductase. The reaction between only AgNO3 and NADPH enabled us to unravel the kinetics of the reaction and showed that it is of pseudo-first-order with respect to NADPH. Since the reaction was observed to be more efficient in enzyme free conditions, the overall reaction temperature range could be

substantially extended. Elevating it to 80 °C increased the reaction rate to the point that particles were fully synthesized within 7 minutes. Future systematic comparison between a single biological reducing component and metal salts holds a promising potential for both a deeper mechanistic understanding of nanoparticle formation and an applicative, cost-effective, and environmentally friendly way for industrial-scale production of nanoparticles.

6.1.4 References

(1) Keat, C. L.; Aziz, A.; Eid, A. M.; Elmarzugi, N. A. Biosynthesis of Nanoparticles and Silver Nanoparticles. *Bioresour. Bioprocess*. **2015**, 2, 47.

(2) Hulkoti, N. I.; Taranath, T. C. Biosynthesis of Nanoparticles Using Microbes - A Review. *Colloids Surf., B* **2014**, 121, 474−483.

(3) Li, X.; Xu, H.; Chen, Z.-S.; Chen, G. Biosynthesis of Nanoparticles by Microorganisms and Their Applications. *J. Nanomater.* **2011**, 16, 1.

(4) Ahmed, S.; Ahmad, M.; Swami, B. L.; Ikram, S. A Review on Plants Extract Mediated Synthesis of Silver Nanoparticles for Antimicrobial Applications: A Green Expertise. *J. Adv. Res.* **2016**, 7 (1), 17−28.

(5) Agnihotri, S.; Mukherji, S.; Mukherji, S. Size-Controlled Silver Nanoparticles Synthesized over the Range 5−100 Nm Using the Same Protocol and Their Antibacterial Efficacy. *RSC Adv.* **2014**, 4 (8), 3974−3983.

(6) Jha, A. K.; Prasad, K. Ferroelectric BaTiO3 Nanoparticles: Biosynthesis and Characterization. *Colloids Surf., B* **2010**, 75 (1), 330−334.

(7) Ahmad, A.; Mukherjee, P.; Senapati, S.; Mandal, D.; Khan, M. I.; Kumar, R.; Sastry, M. Extracellular Biosynthesis of Silver Nanoparticles Using the Fungus Fusarium Oxysporum. *Colloids Surf., B* **2003**, 28 (4), 313−318.

(8) Huang, J.; Li, Q.; Sun, D.; Lu, Y.; Su, Y.; Yang, X.; Wang, H.; Wang, Y.; Shao, W.; He, N.; et al. Biosynthesis of Silver and Gold Nanoparticles by Novel Sundried Cinnamomum Camphora Leaf. *Nanotechnology* **2007**, 18 (10), 105104.

(9) Raliya, R.; Tarafdar, J. C.; Singh, S. K.; Gautam, R.; Choudhary, K.; Maurino, V. G.; Saharan, V. MgO Nanoparticles Biosynthesis and Its Effect on Chlorophyll Contents in the Leaves of Clusterbean (Cyamopsis Tetragonoloba L.). *Adv. Sci., Eng. Med.* **2014**, 6 (5), 538−545.

(10) Azizi, S.; Ahmad, M. B.; Namvar, F.; Mohamad, R. Green Biosynthesis and Characterization of Zinc Oxide Nanoparticles Using Brown Marine Macroalga Sargassum Muticum Aqueous Extract. *Mater. Lett.* **2014**, 116, 275−277.

(11) Lok, C.-N.; Ho, C.-M.; Chen, R.; He, Q.-Y.; Yu, W.-Y.; Sun, H.; Tam, P. K.-H.; Chiu, J.-F.; Che, C.-M. Proteomic Analysis of the Mode of Antibacterial Action of Silver anoparticles. *J. Proteome Res.* **2006**, 5 (4), 916−924.

(12) Batchelor-McAuley, C.; Tschulik, K.; Neumann, C. C. M.; Laborda, E.; Compton, R. G. Why Are Silver Nanoparticles More Toxic Than Bulk Silver? Towards Understanding the Dissolution and Toxicity of Silver Nanoparticles. *Int. J. Electrochem Sci.* **2014**, 9 (3), 1132−1138.

(13) Xiu, Z.; Zhang, Q.; Puppala, H. L.; Colvin, V. L.; Alvarez, P. J. J. Negligible Particle Specific Antibacterial Activity of Silver Nanoparticles. *Nano Lett.* **2012**, 12 (8), 4271−4275.

(14) Lin, J.; He, C.; Zhao, Y.; Zhang, S. One-Step Synthesis of Silver Nanoparticles/Carbon Nanotubes/Chitosan Film and Its Application in Glucose Biosensor. *Sens. Actuators, B* **2009**, 137 (2), 768−773.

(15) Maduraiveeran, G.; Ramaraj, R. Enhanced Sensing of Mercuric Ions Based on Dinucleotide-Functionalized Silver Nanoparticles. *Anal. Methods* **2016**, 8 (44), 7966−7971.

(16) Haes, A. J.; Van Duyne, R. P. A Nanoscale Optical Biosensor: Sensitivity and Selectivity of an Approach Based on the Localized Surface Plasmon Resonance Spectroscopy of Triangular Silver Nanoparticles. *J. Am. Chem. Soc.* **2002**, 124 (35), 10596−10604.

(17) Jiang, Z.-J.; Liu, C.-Y.; Sun, L.-W. Catalytic Properties of Silver Nanoparticles Supported on Silica Spheres. *J. Phys. Chem. B* **2005**, 109 (5), 1730−1735.

(18) Song, J. Y.; Kim, B. S. Rapid Biological Synthesis of Silver Nanoparticles Using Plant Leaf Extracts. *Bioprocess Biosyst. Eng.* **2009**, 32 (1), 79.

(19) Nanda, A.; Saravanan, M. Biosynthesis of Silver Nanoparticles from Staphylococcus Aureus and Its Antimicrobial Activity against MRSA and MRSE. *Nanomedicine* **2009**, 5 (4), 452−456.

(20) Bhainsa, K. C.; D'Souza, S. F. Extracellular Biosynthesis of Silver Nanoparticles Using the Fungus Aspergillus Fumigatus. *Colloids Surf., B* **2006**, 47 (2), 160−164.

(21) Govindarajan, M.; Nicoletti, M.; Benelli, G. Bio-Physical Characterization of Poly-Dispersed Silver Nanocrystals Fabricated Using Carissa Spinarum: A Potent Tool Against Mosquito Vectors. *J. Cluster Sci.* **2016**, 27 (2), 745−761.

(22) Yilmaz, M.; Turkdemir, H.; Kilic, M. A.; Bayram, E.; Cicek, A.; Mete, A.; Ulug, B.

Biosynthesis of Silver Nanoparticles Using Leaves of Stevia Rebaudiana. *Mater. Chem. Phys.* **2011**, 130 (3), 1195−1202.

(23) Kumar, S. A.; Abyaneh, M. K.; Gosavi, S. W.; Kulkarni, S. K.; Pasricha, R.; Ahmad, A.; Khan, M. I. Nitrate Reductase-Mediated Synthesis of Silver Nanoparticles from $AgNO_3$. *Biotechnol. Lett.* **2007**, 29 (3), 439−445.

(24) Durá n, N.; Marcato, P. D.; Alves, O. L.; De Souza, G. I.; Esposito, E. Mechanistic Aspects of Biosynthesis of Silver Nanoparticles by Several Fusarium Oxysporum Strains. *J. Nanobiotechnol.* **2005**, 3, 8.

(25) Xiao, Y.; Pavlov, V.; Levine, S.; Niazov, T.; Markovitch, G.; Willner, I. Catalytic Growth of Au Nanoparticles by NAD(P)H Cofactors: Optical Sensors for NAD(P)+-Dependent Biocatalyzed Transformations. *Angew. Chem., Int. Ed.* **2004**, 43 (34), 4519−4522.

(26) Berti, L.; Burley, G. A. Nucleic Acid and Nucleotide-Mediated Synthesis of Inorganic Nanoparticles. *Nat. Nanotechnol.* **2008**, 3 (2), 81−87.

(27) Hinds, S.; Taft, B. J.; Levina, L.; Sukhovatkin, V.; Dooley, C. J.; Roy, M. D.; MacNeil, D. D.; Sargent, E. H.; Kelley, S. O. Nucleotide- Directed Growth of Semiconductor Nanocrystals. *J. Am. Chem. Soc.* **2006**, 128 (1), 64−65.

(28) Williams, W. J. Handbook of Anion Determination; Butterworth-Heinemann, **2013**.

(29) Data for Biochemical Research, Third ed.; Oxford University Press: Oxford, NY, **1989**.

(30) Fruscione, F.; Sturla, L.; Duncan, G.; Van Etten, J. L.; Valbuzzi, P.; De Flora, A.; DiZanni, E.; Tonetti, M. Differential Role of NADP+ and NADPH in the Activity and Structure of GDP-D-Mannose 4,6-Dehydratase from Two Chlorella Viruses. *J. Biol. Chem.* **2008**, 283(1), 184−193.

(31) Saion, E.; Gharibshahi, E.; Naghavi, K. Size-Controlled and Optical Properties of Monodispersed Silver Nanoparticles Synthesized by the Radiolytic Reduction Method. *Int. J. Mol. Sci.* **2013**, 14 (4), 7880−7896.

(32) Walsh, C. Flavin Coenzymes: At the Crossroads of Biological Redox *Chemistry. Acc. Chem. Res.* **1980**, 13 (5), 148−155.

(33) Orbaek, A. W.; McHale, M. M.; Barron, A. R. Synthesis andCharacterization of Silver Nanoparticles for an Undergraduate Laboratory. *J. Chem. Educ.* **2015**, 92 (2), 339−344.
(34) Ellison, J.; Tschulik, K.; Stuart, E. J. E.; Jurkschat, K.; Omanović , D.; Uhlemann, M.; Crossley, A.; Compton, R. G. Get More out of Your Data: A New Approach to Agglomeration and Aggregation Studies Using Nanoparticle Impact Experiments. *ChemistryOpen* **2013**, 2 (2), 69−75.

(35) Anderson, T. J.; Zhang, B. Single-Nanoparticle Electrochemistry through

Immobilization and Collision. *Acc. Chem. Res.* **2016**, 49 (11), 2625−2631.

(36) Ustarroz, J.; Kang, M.; Bullions, E.; Unwin, P. R. Impact and Oxidation of Single Silver Nanoparticles at Electrode Surfaces: One Shot versus Multiple Events. *Chem. Sci.* **2017**, 8 (3), 1841−1853.

(37) Ellison, J.; Batchelor-McAuley, C.; Tschulik, K.; Compton, R. G. The Use of Cylindrical Micro-Wire Electrodes for Nano-Impact Experiments; Facilitating the Sub-Picomolar Detection of Single Nanoparticles. *Sens. Actuators, B* **2014**, 200, 47−52.

(38) Wonner, K.; Evers, M. V.; Tschulik, K. Simultaneous Opto- and Spectro-Electrochemistry: Reactions of Individual Nanoparticles Uncovered by Dark-Field Microscopy. *J. Am. Chem. Soc.* **2018**, 140, 12658.

(39) Sun, T.; Wang, D.; Mirkin, M. V. Electrochemistry at a Single Nanoparticle: From Bipolar Regime to Tunnelling. *Faraday Discuss*. **2018**, 210, 173.

(40) Huynh, K. A.; Chen, K. L. Aggregation Kinetics of Citrate and Polyvinylpyrrolidone Coated Silver Nanoparticles in Monovalent and Divalent Electrolyte Solutions. *Environ. Sci. Technol*. **2011**, 45 (13), 5564−5571.

(41) Little, C. A.; Xie, R.; Batchelor-McAuley, C.; Kätelhö n, E.; Li, X.; Young, N. P.; Compton, R. G. Quantitative Methodology for the Study of Particle−Electrode Impacts. *Phys. Chem. Chem. Phys*. **2018**, 20 (19), 13537−13546.

(42) Murray, R. K.; Bender, D. A.; Botham, K. M.; Kennelly, P. J.; Rodwell, V. W.; Weil, P. A. Harpers Illustrated Biochemistry, 29 ed.; McGraw-Hill Medical: New York, **2012**.

6.2 Supplemental Figures and Methods

6.2.1 Materials

Sodium chloride (NaCl, ≥99.5%), sodium hydroxide (NaOH, ≥98%), β-nicotinamide adenine dinucleotide 2'-phosphate reduced tetrasodium salt (NADPH, ≥ 97%), β-nicotinamide adenine dinucleotide 2'-phosphate hydrate (NADP+, ≥95%) and nitrate reductase from *Aspergillus niger* (≥300 units/g) were purchased from Sigma Aldrich, silver nitrate (AgNO3, ≥99.7%) was purchased from Fisher Chemical and free acid ULTROL grade 1M HEPES buffer was purchased from EMD Millipore. DI water was filtered using a WaterPro BT purification system. pH measurements were done using an Accumet AB150 pH Benchtop Meter which was calibrated with Orion pH buffers 4.01, 7 and 10.01 purchased from Sigma Aldrich. All data excluding single entity electrochemical data was analyzed using Origin Pro 8.5.1.

6.2.2 Synthesis and purification

At the start of the synthesis, the silver solution (excluding NADPH) was placed into a 25°C water bath and stirred until full temperature equilibrium was achieved. Silver nanoparticles were synthesized in batch volumes between 30 mL and 100 mL. Each solution contained 50 mM HEPES (excluding Fig. S3) and 10 mM AgNO3 along with NaOH to raise the pH to 7.2. Next, between 0.1-0.4 mM NADPH was added into the solution and the absorption spectrum at each individual time interval was recorded by UV-Vis. Particles were also synthesized using the same procedure with an addition of 100 - 300 μg of enzyme in the solution prior to NADPH injection. UV-Vis measurements were taken as is from the reaction or at dilutions ranging from 1:3 to 1:9 in water, as stated in the paper. Once the synthesis was complete, the vials were wrapped in aluminum foil and stored at room temperature until further purification. Fully

synthesized silver nanoparticles were isolated through centrifugation. First, a UV-Vis spectrum of the unpurified nanoparticle solution was taken against a 50 mM HEPES and 10 mM $AgNO_3$ reference. The remaining concentration of Ag+ ions were neutralized with the equivalent concentration of NaCl to form AgCl precipitate. This solution was then centrifuged at 4000 rpm at 4°C for 30 minutes, the resulting supernatant was collected and another UV-Vis was taken at a 1:3 dilution. The new solution was then ultra-centrifuged at 15,000 rpm for 30 minutes at room temperature. Centrifugation was done using an Eppendorf 5424 and a Sorvall Discovery 90. The resulting solution was decanted off and the remaining silver nanoparticle pellet was re-suspended with 15 mL of 50 mM HEPES and a UV-Vis was taken again.

6.2.3 Kinetics

UV-Vis spectroscopy was done on a Shimidzu UV 1800. UV-Vis measurements were scanned from 700 or 500 to 200 nm in a 1 cm path length quartz cuvette. Note that in order to get the most accurate concentration of NADPH, the UV-Vis of freshly prepared NADPH solution was taken and the absorbance at 340 nm was correlated to its concentration using its known extinction coefficient of 6.3 mM^{-1} cm^{-1}.1 Particles were synthesized using the same procedure as previously stated and UV-Vis measurements were taken to measure kinetics of nanoparticle formation. A 100 mL solution of 50 mM HEPES, 10 mM $AgNO_3$,and varying concentrations of NADPH were reacted in a 150 mL Erlenmeyer flask. The flask was placed into a 25°C water bath and stirred continuously. 2mL of solution was placed into the cuvette at designated time intervals since the time NADPH was added (t=0). UV-Vis absorption measurements were done against a 50 mM HEPES and 10 mM $AgNO_3$ reference. Absorbance data for NADPH at 340 nm was extracted from each spectrum and plotted as a function of time. The slope of this graph was correlated to the rate of NADPH disappearance and plotted against multiple trials of 0.1,

0.2 and 0.4 mM NADPH solutions to form a plot of the reaction rate as a function of NADPH concentration.

6.2.4 Macroelectrode anodic stripping voltammetry

For stripping voltammetry, a 5 mL solution of 20 mM NaCl was made and purged with N_2 for 20 minutes. A glassy carbon working electrode (r = 1.5 mm) was polished for 6 minutes (2 min per alumina size) using 1 μm, 0.3 μm, 0.05 μm alumina oxide slurry on a microcloth polishing pad. Next, the glassy carbon electrode was sonicated in water for 2 min and 4 μl of concentrated purified silver nanoparticles was drop cast onto the freshly polished working electrode and allowed to dry under a gentle stream of N_2 for 20 minutes. A platinum wire counter electrode and SCE reference electrode were used to run a single sweep over the range of 0V to 0.3 V at a scan rate of 0.1 V s^{-1} at steps size of 2.4 mV. A Metrohm PGSTAT 128N potentiostat was used for these electrochemical measurements.

6.2.5 Single entity electrochemistry

Chronoamperograms were measured using a computer-controlled HEKA EPC 10 USB patch clamp amplifier with a 3-electrode mode head stage. The scaling of the current monitor output was set to 1mV/pA implying a feedback resistor of 50 MΩ. The current signal was filtered in two serial stages: first with an analog 3-pole low-pass Bessel filter at 10 kHz and second with an analog 4-pole low-pass Bessel filter at 0.14 kHz. Data points were acquired at a sampling rate of 10 kHz equivalent to each 100 μs time interval. The recorded current traces (see Figure S7) were exported from HEKA Patchmaster (version 2x90.3) to Igor Pro (version 8.0.0.10) as waves. A custom macro was coded in Igor to identify and fit the current spikes. By integration

the peak area was obtained to receive the amount of charge transferred in every single event. The value of the charge was then used to calculate the particle radius, r, following *eq S6.2*.

$$r_{np} = \sqrt[3]{\frac{3QA}{4\pi F\rho}} \tag{S6.2}$$

where Q is the charge, F the Faraday constant, A the relative atomic mass (A_{Ag} = 108 u), and ρ the bulk density of the impeding particles (ρ_{Ag} = 10.5 g/cm^3)

6.2.6 Transmission Electron Microscopy

Nanoparticles were imaged using a FEI Tecnai G2 20 TEM operating at 200 kV. TEM was performed using purified non-diluted particles. The samples were prepared by drop-casting 4µl of solution onto freshly plasma-cleaned pure-carbon film coated copper grids (Ted Pella Inc.). The grids were allowed to air dry before being loaded into a single-tilt TEM holder and being inserted into the microscope. Bright field TEM (BFTEM) was performed on the samples to capture images with 5.77 µA filament (LaB6) current. Images were captured at 19.5kX, 39kX, and 71kX magnification using a Gatan Ultrascan CCD camera. The magnification of the microscope is regularly calibrated using a MAG*I*CAL calibration standard. Images were taken until at least 800 particles were captured and particle sizes were analyzed using ImageJ software. Size distribution histograms were created with Origin Pro (version 8.5.1.) High-angle annular dark field (HAADF) scanning transmission electron microscopy (STEM) was performed with a ThermoFisher Talos G2 200X TEM/STEM w/ChemiSTEM EDS operating at 200 kV. The AgNP sample was deposited onto an ultra-thin carbon film on a lacey carbon film support (Ted Pella Inc.) by drop-casting a small volume of NP solution on the grid and let it dry. The grid was then mounted on a single-tilt holder and loaded into a Pfeiffer HiVac cube

to pre-evacuate the sample overnight before loading it into the TEM column. Energy dispersive X-ray spectroscopy was conducted with four SuperXG2 detectors. 200 frames were acquired for each EDX map with a dwell time of 20.00 μs.

6.2.7 Zeta Potential

Dilutants for zeta potential measurements were filtered through a 0.2 μm filter and then used to dilute the concentrated purified particles at a ratio of 1:9. The diluted particles were placed into a folded capillary zeta cell and analyzed. Each analysis consisted of 10 measurements with a minimum of 35 runs per measurement. Zeta potential parameters were as follows: equilibrium time 120 seconds, at 25°C, minimum of 12 trials done.

6.3 Supplemental Figures and Tables

Figure 6.S1 HEPES and $AgNO_3$ UV-Vis spectrum without NADPH

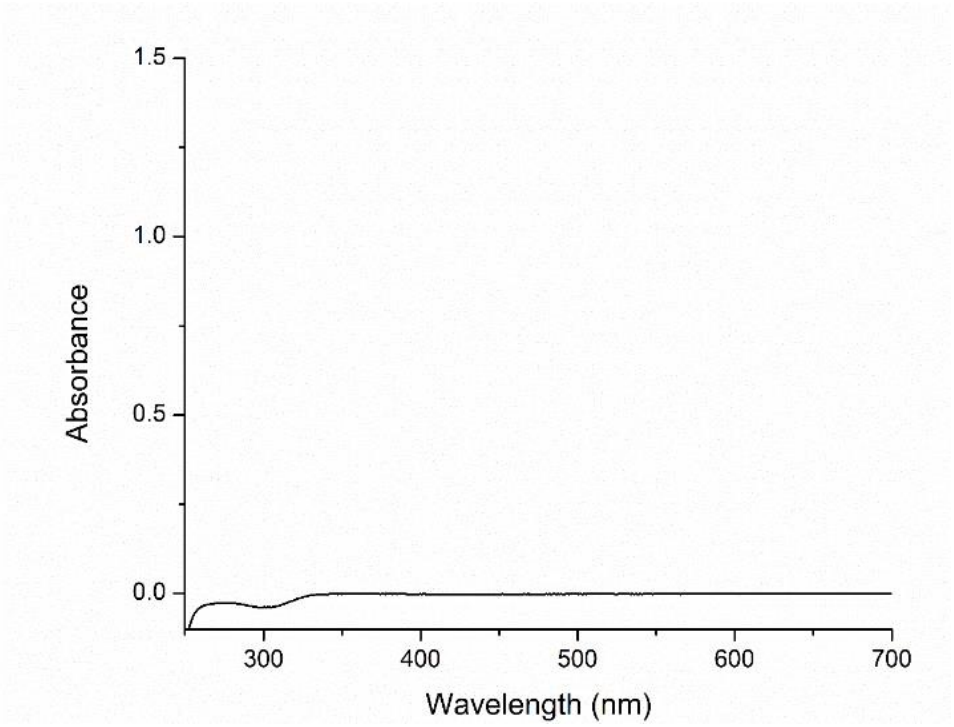

Figure 6.S1 Control test of 24 hours incubated 50 mM HEPES and 10 mM $AgNO_3$ against freshly made 50mM HEPES and 10 mM $AgNO_3$ reference.

Figure 6.S2 Comparing the plasmonic peak of AgNPs synthesized at different pHs

In order to compare and find the optimal pH to synthesize particles using NADPH alone, 1 pH above and below physiological conditions were used. As seen in **Fig. 6.S2**, the most prominent peak corresponding to nanoparticle formation (410nm) is that of pH 7.2. The broader peaks for pH 6.2 and 8.2 are indicative of polydispersed nanoparticle populations. It should also be noted that pH 6.2 gave particles that were unstable and sedemented out of solution.

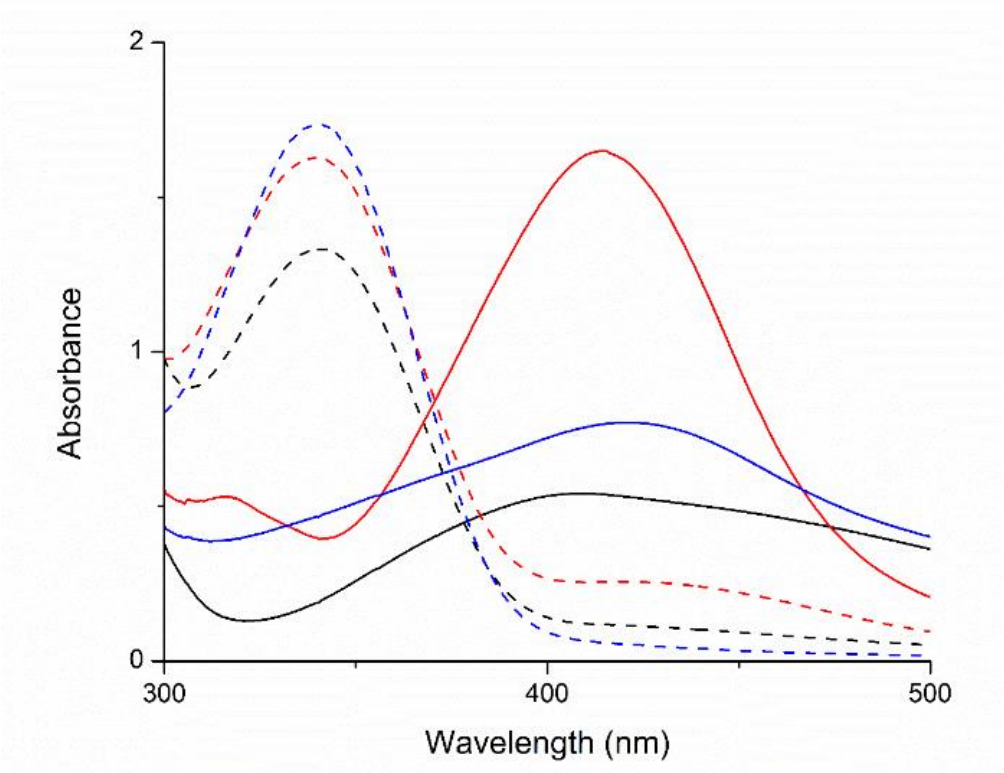

Figure 6.S2 Comparison of initial (t=1 h, dashed lines) and final spectra (t=24 h, solid lines) of particles synthesized using NADPH alone at pH 6.2 (black), 7.2 (red) and 8.2 (blue).

Figure 6.S3 Buffer Capacity Effect on Particle Synthesis

As seen in **Fig. 6.S3** the peak with the thinnest FWHM was observed using 50 mM HEPES solution. In 10 mM HEPES, the silver nanoparticle peak is red shifted indicating larger sized particles, while the 100 mM HEPES solution produced a lower plasmonic peak amplitude together with a broad tail which indicates a wider size distribution. **Fig. 6.S3** inset shows the respective colors of solutions after 24 hours. None are the same which indicates that the buffer concentration plays a role in the final particle formation. Note that the particles synthesized in water have already begun to agglomerate and sediment out. As 50 mM HEPES gave the thinnest and highest plasmonic peak, it was used in all future synthesis.

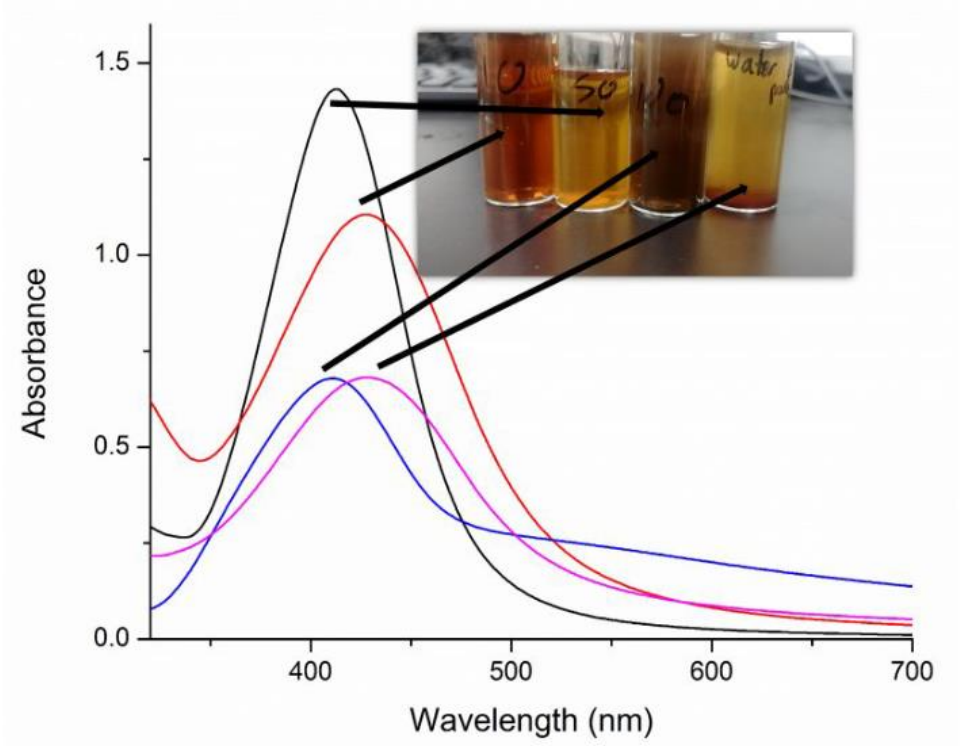

Figure 6.S3 Comparison between 0 (pink), 10 (red), 50 (black) and 100 (blue) mM HEPES buffer used during synthesis and final spectra of silver nanoparticles. All solutions were diluted 1:3 with water.

Figure 6.S4 Absorption Spectra of Purified Silver Nanoparticles Synthesized with and without Nitrate Reductase

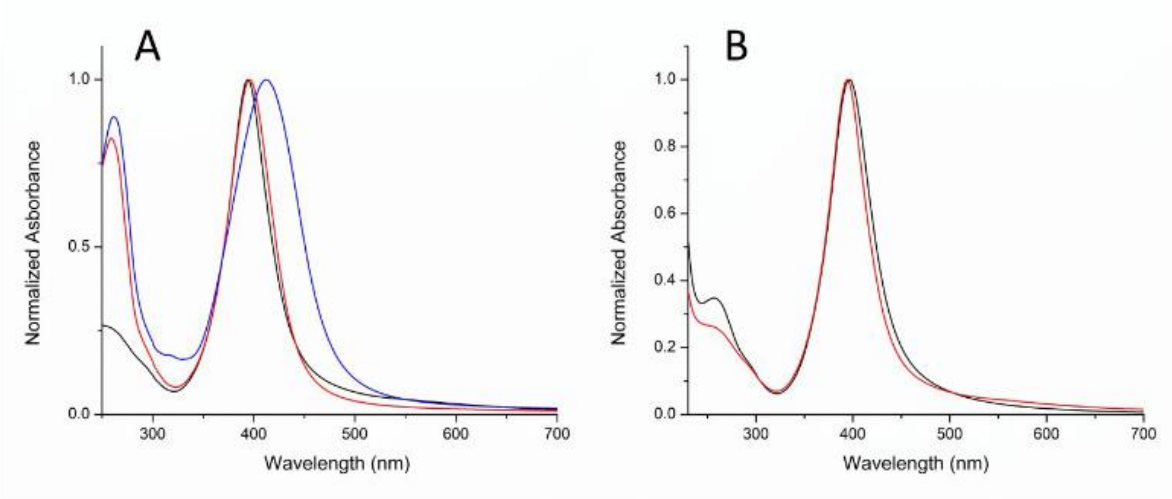

Figure 6.S4 (A) Particles before (blue) and after purification through centrifuging at 4000 rpm (red) and 15,000 rpm (black). (B) Purified NADPH synthesized AgNPs with (black) and without (red) nitrate reductase enzyme.

Figure 6.S5 Nitrate Reductase Control Experiments

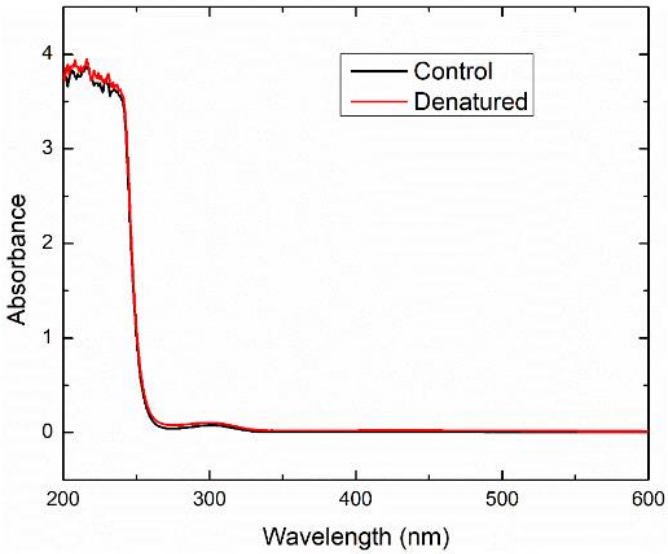

Figure 6.S5 UV-Vis absorbance spectrum comparing the synthesis pathway of solely nitrate reductase at 25°C to the route with pre-boiled nitrate reductase at 80 °C. Both syntheses did not contain NADPH. While an absorption of nitrate reductase can be seen below 300 nm, there is no evidence for nanoparticle formation in both cases.

Experimental details

a) The control synthesis to show the sole role of nitrate reductase was run with the same components and concentrations as described in the paragraph “Synthesis and purification” but without NADPH at 25°C.

b) For the second experiment the nitrate reductase was denatured by heating the enzyme in a solution of water, HEPES buffer and NaOH to 80 0C for 30 minutes. Concentrations were the same as in the original experiment with NADPH. Afterwards, the solution was cooled in a water bath to 25 °C and $AgNO_3$ was added as described above.

Figure 6.S6 Testing the Stability of Particles Synthesized With and Without Nitrate Reductase

The stability of silver nanoparticles synthesized with and without nitrate reductase was compared using zeta potential. Zeta potential measurements were taken using a Malvern Zetasizer Nano ZS and a He-Ne, 4 mW, 633 nm red laser. The zeta potential for the enzyme free synthesized particles was -29.9 mV while particles synthesized with nitrate reductase had a potential of -21.3 mV.

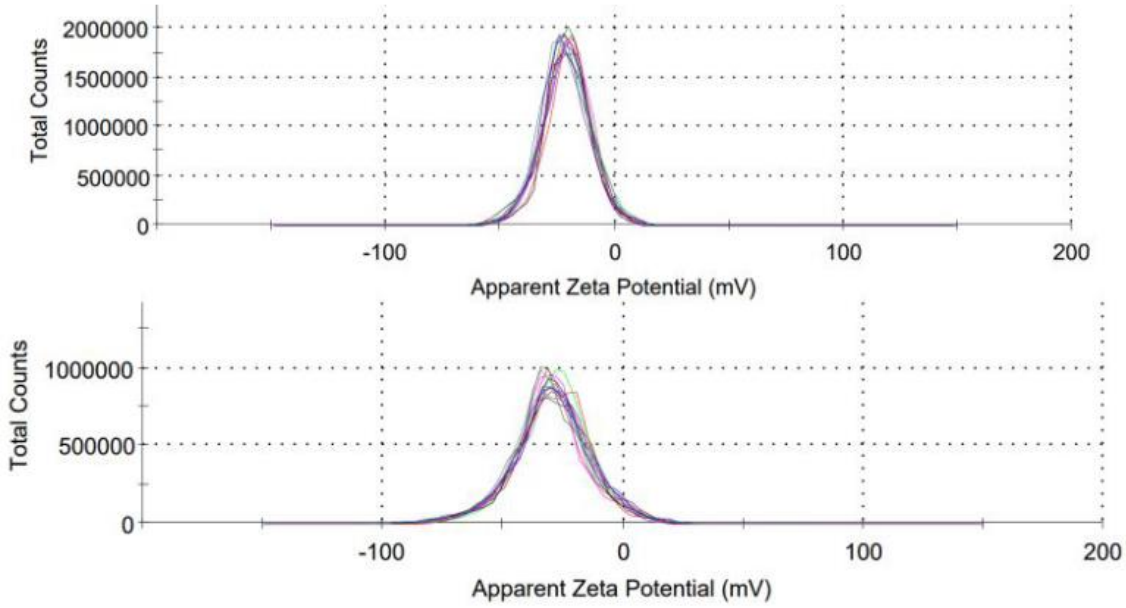

Figure 6.S6 Zeta potential values of particles synthesized with (top) and without (bottom) nitrate reductase.

Table 6.S1. Zeta potential measurements for each run along with statistics of all runs for both NADPH synthesized AgNPs and for NADPH with the enzyme nitrate reductase.

Run Number	NADPH AgNPs ζ Potential (mV)	NADPH AgNPs + Enzyme ζ Potential (mV)
Run 1	-29.3	-20.3
Run 2	-28.4	-21.1
Run 3	-29.9	-20.7
Run 4	-29.7	-20.9
Run 5	-30.6	-20.9
Run 6	-30.8	-20.7
Run 7	-29.6	-20.9
Run 8	-30.7	-21.2
Run 9	-29.0	-21.8
Run 10	-30.7	-21.8
Run 11	-29.7	-22.2
Run 12	-30.0	-22.7
mean	-29.9	-21.3
std	0.744	0.708
RSD %	2.49	3.33

Figure 6.S7 Anodic Stripping Voltammetry of Biosynthesized Nanoparticles

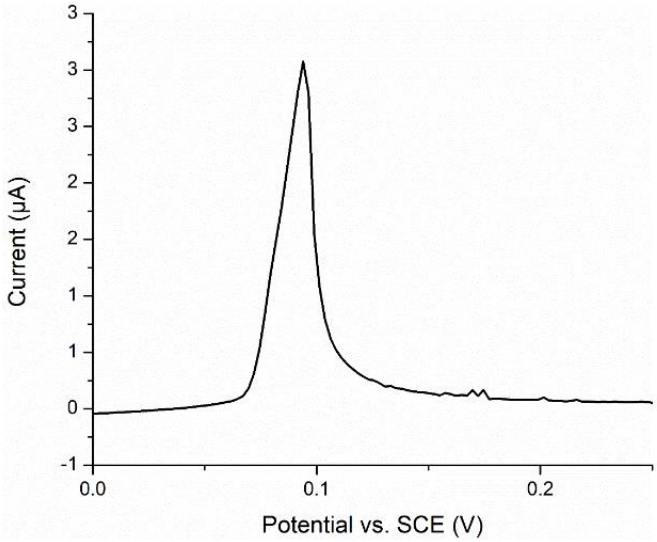

Figure 6.S7 Anodic Stripping voltammetry of NADPH synthesized nanoparticles. Glassy carbon working was used as a working electrode, saturated calomel electrode as a reference and Pt wire as a counter electrode. Scan was done at 25 °C. Scan rate of 100 mV/s.

Figure 6.S8 Single Entity Electrochemistry Data

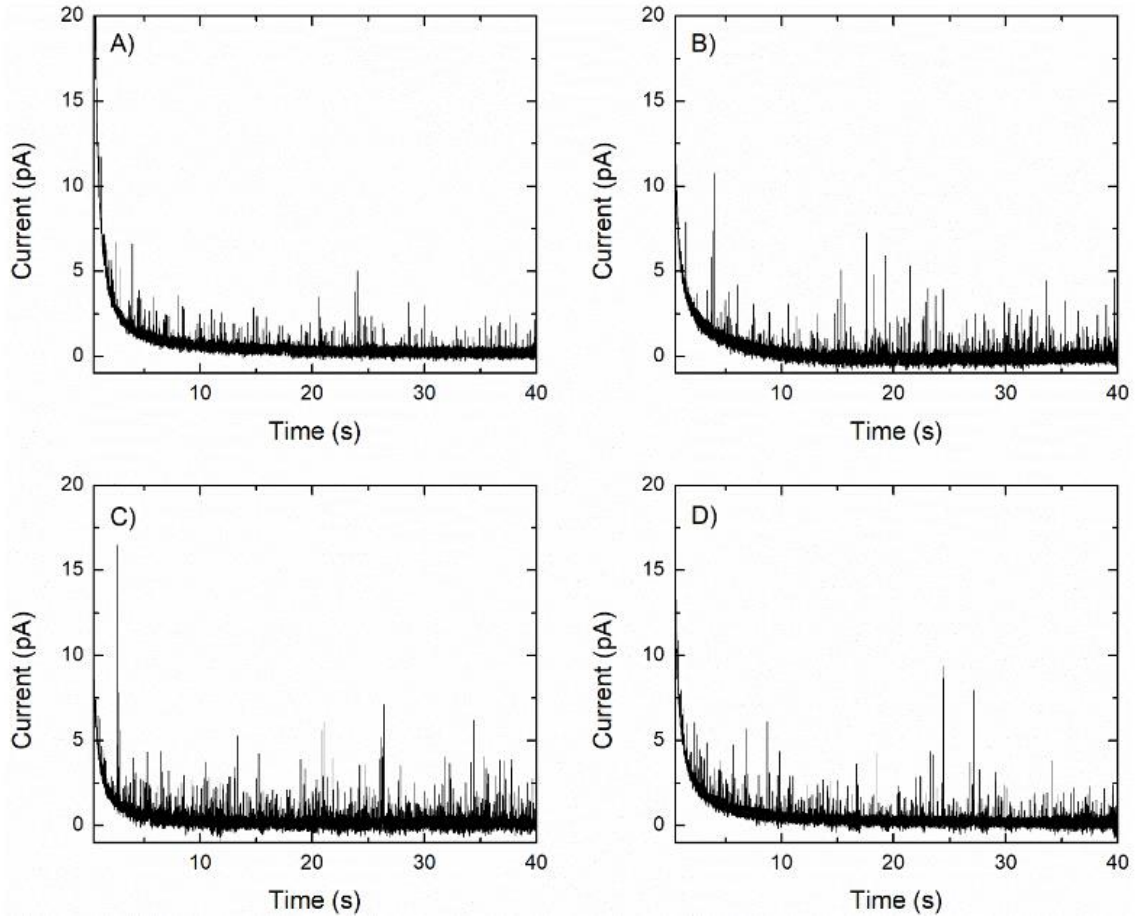

Figure 6.S8 Four exemplary chronoamperograms exhibiting nano-impacts were recorded in concentrated silver nanoparticle solutions (20 mM NaCl and 50 mM HEPES buffer). The AgNPs were synthesized in 50mM HEPES, 10 mM AgNO3 and 0.2 mM NADPH. A gold microelectrode (r = 6.25 μm, CHI), Ag/AgCl (3M) reference and Pt wire counter electrode were introduced into a freely diffusing clean AgNP solution. To record a single trace the cell was biased with a holding potential of 0 mV for 1 s and then at + 400 mV for 40 s. Fig. S8 A) is the result presented in the main text while Fig. S8 B-D) are additions, all showing similar current spike (and hence charge) magnitude

Figure 6.S9 Full Kinetics Spectra of Particles Synthesized at Different Concentrations of NADPH

The full kinetic spectra for nanoparticles synthesized with 0.1, 0.2 and 0.4 mM NADPH are shown. Each graph contains the spectrum taken every 2 minutes for 2 hours used to measure the kinetics of silver nanoparticle formation.

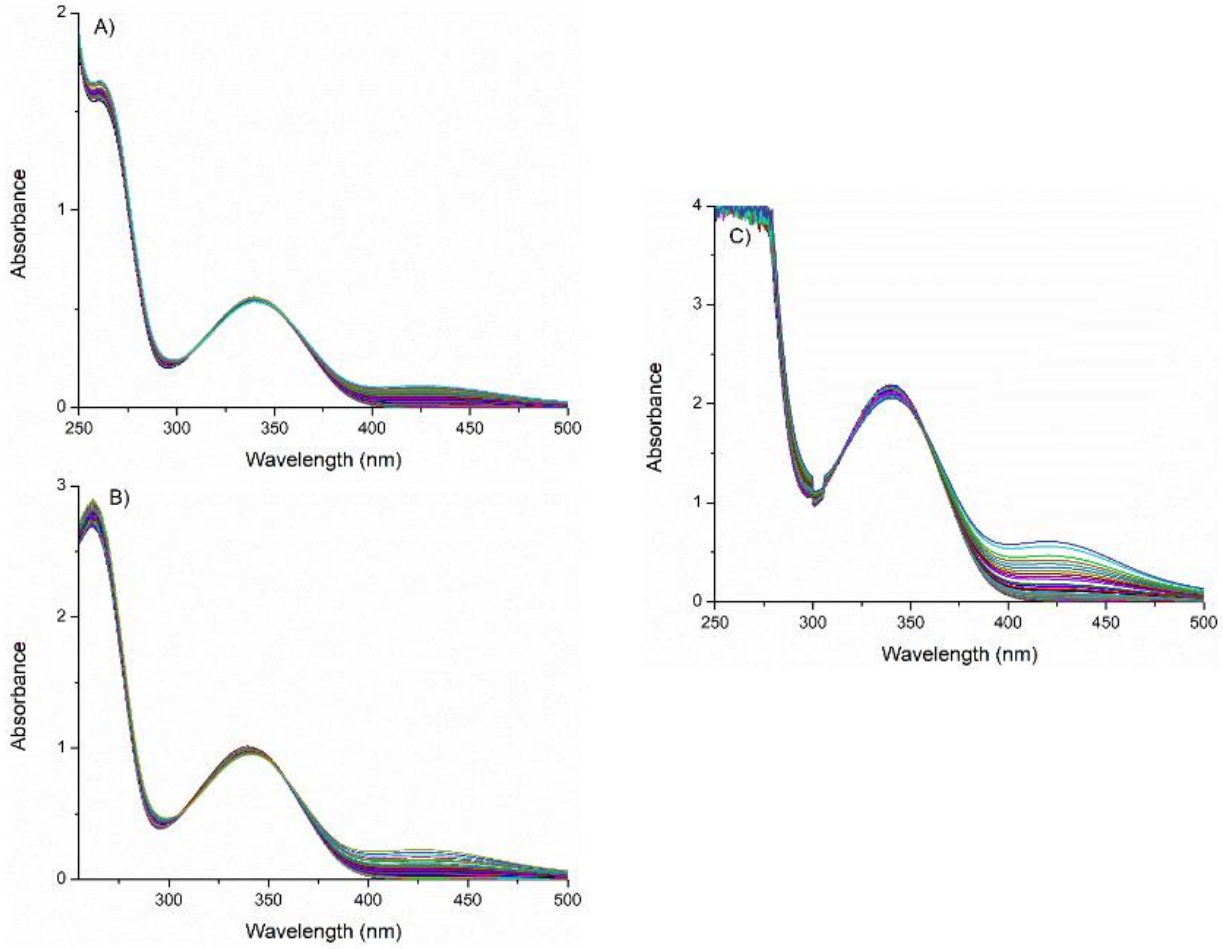

Figure 6.S2 Full kinetics data of 0.1 (A), 0.2 (B) and 0.4 (C) mM NADPH solution taken every 3 minutes for 2 hours.

Figure 6.S10 Final Spectra for Different Synthesis Temperatures

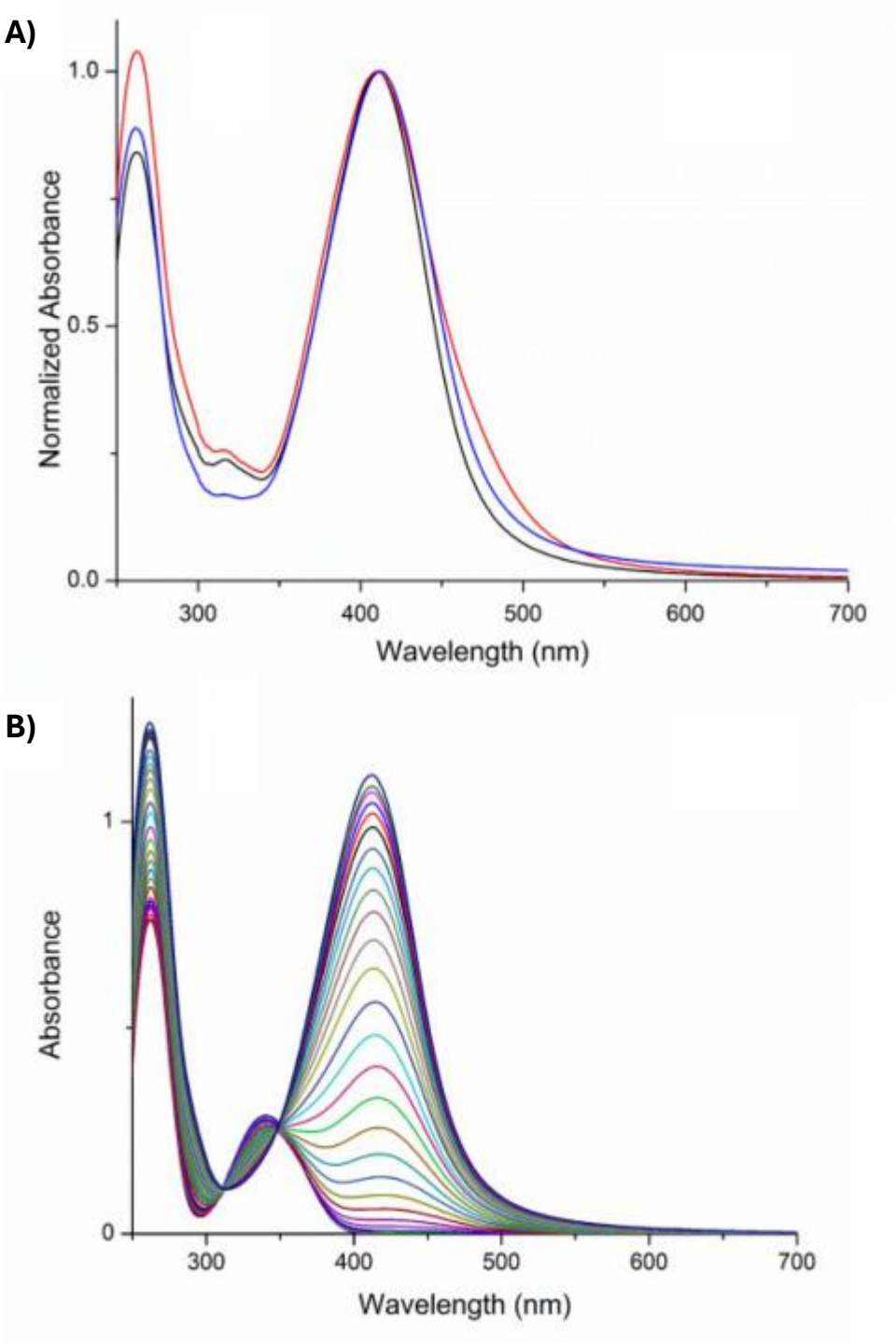

Figure 6.S10 (A) Overlaid spectra of particles synthesized at 25 °C (blue), 50 °C (black) and 80 °C (red). Note the plasmonic peak stays the same within ± 2 nm. (B) Spectra of particles taken every 2 minutes while synthesizing at 50 °C.

Figure 6.S11 Size Distribution of AgNPs Synthesized at 80°C

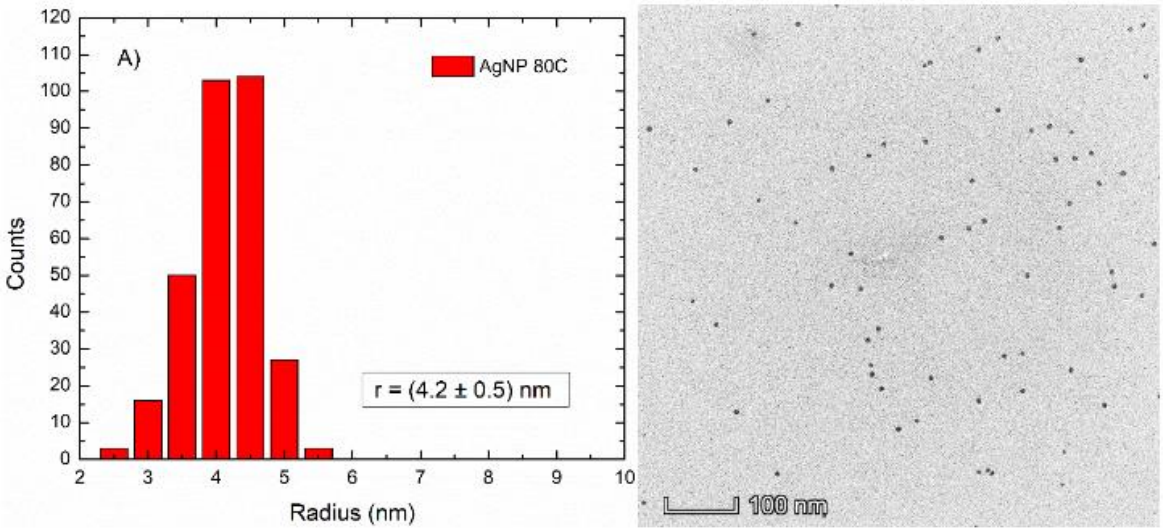

Figure 6.S11 A) Size histogram of AgNPs synthesized at 80 °C. Statistics were acquired over a series of 9 bright-field TEM images at different sample locations. B) Bright-field TEM image showing homogenously sized nanoparticles synthesized at 80 °C.

6.4 Supplemental References

(1) H. U. Bergmeyer, Z. *Klin. Chem. Klin. Biochem.*, **1975**, 13, 507–508.

(2) Y.-G. Zhou, N. V. Rees and R. G. Compton, *Angew. Chem.*, **2011**, 123, 4305–4307.